OCEAN RENEWABLE POWER COMPANY
FINAL TECHNICAL REPORT, DE-EE0008386.000
Design of High-deflection Foils for Marine Hydrokinetic Applications

PRINCIPAL INVESTIGATORS:

- *JARLATH MCENTEE, VICE PRESIDENT – ENGINEERING & CHIEF TECHNOLOGY OFFICER*
- *MARTIN WOSNIK, DIRECTOR - CENTER FOR OCEAN RENEWABLE ENERGY, UNIVERSITY OF NEW HAMPSHIRE*
- *BUDI GUNAWAN, PRINCIPAL ENGINEER, SANDIA NATIONAL LABORATORIES*

March 31, 2022

Ocean Renewable Power Company, LLC
254 Commercial St. Suite 119B
Portland, ME 04101
Phone (207) 772-7707
www.orpc.co

Acknowledgment:
This material is based upon work supported by the U.S. Department of Energy's Office of Energy Efficiency and Renewable Energy (EERE) under the Water Power Technologies Office (WPTO) Award Number DE-EE0008386.

Contents

List of Acronyms

AEP	annual energy production
ASCII	American Standard Code for Information Interchange
CFD	computational fluid dynamics
Cp	coefficient of performance
DAQ	data acquisition system
DOE	Department of Energy
FEA	finite element analysis
FLS	fatigue limit state
FORJ	fiber optic rotary joint
FSI	fluid structure interaction
HD-FOS	high-definition fiber optic sensing
HPC	high performance computing
LCOE	levelized cost of energy
LRFD	load and resistance factor design
MHK	marine hydrokinetic
MHKDR	Marine Hydrokinetic Data Repository
NaN	not a number
ODiSI	Optical Distributed Sensor Interrogator
ORPC	Ocean Renewable Power Company
RANS	Reynolds Averaged Navier Stokes methods
Re	Reynolds number
RMS	root mean square
SA	Spalart-Almaras turbulence model
TSR	tip speed ratio
ULS	ultimate limit state
UNH	University of New Hampshire

List of Figures

List of Tables

Executive Summary

This project used model-scale tank testing and fluid-structure-interaction (FSI) simulations to investigate the behavior of foils with large deflections and the effect of these deflections on crossflow turbine performance with the goal of determining the maximum allowable deflections consonant with efficiency and a robust, durable structure. A validated modeling and simulation approach was used in the design of an Ocean Renewable Power Company (ORPC) full-scale turbine. The methodology is applicable to the design of other marine hydrokinetic (MHK) devices, and to hydrokinetic turbines which experience significant deflections during operation.

Foils for model scale turbines were designed and built by ORPC and tested at Jere A. Chase Ocean Engineering Laboratory at the University of New Hampshire (UNH). Numerous foils exhibiting different deflection behaviors were investigated. The external profile of the test foils was maintained constant, and stiffness of the foils varied using different construction materials. Both straight and helical turbines were tested. The foil materials included solid carbon composite, solid glass composite, hollow glass composite, silicon bronze and titanium. Turbine foils were supported by a pair of turbine struts, one of which was movable along the turbine foil. This provides a means of varying foil stiffness for a given foil material. These turbines were instrumented to collect data characterizing turbine performance and foil strain. Sandia National Laboratories (Sandia) assisted with the selection of the strain measurement methodology and provided the fiber optic interrogator, slip ring, and distributed strain sensors used in the testing. Sandia aided assistance in installation, testing, and integration of the fiber optic sensor system. Sandia reviewed strain data from the calibration tests and in-tank tests and confirmed that strain data was being measured appropriately.

Simulation and validation work focused on developing engineering tools for predicting the effect of high deflection on performance and structural longevity. The tank tests were modeled using computational fluid dynamics (CFD) and finite element analysis (FEA) simulations. Methodologies were investigated and refined to allow for load transfer between the CFD and FEA models. A fluid structure interaction (FSI) methodology was validated using the tank test data.

Data and analysis show that:

- As the struts are moved, the strain range experienced by the foil changes significantly, with high strains experienced in cases with low level of structural support for the foil. Strain reflects patterns generally expected from distributed loads on beams. Strain is symmetric between inner and outer surfaces, indicating a pure bending loading.
- The hydrodynamic performance reduction from carbon to glass composite foils is very small and may well be within the error bounds of the test. This indicates that while stiffness is important from a structural viewpoint, its impact on hydrodynamic performance may be less than expected.
- The helical turbine is hydrodynamically very different from the straight foil turbines. The helical turbine tested is a highly twisted turbine and may as a result be introducing additional hydrodynamic effects when compared with the straight foil turbines.
- Testing of the titanium helical turbine indicates that surface roughness is a critical parameter for testing at the model scale.

Using the analytical methodologies developed in this work, a new high-deflection rotor for ORPC's turbines was designed, making use of the lessons learned in model testing and analytical methods explored in the project. This improved rotor design implements improvements in foil geometry which lead to improved turbine performance and reduced structural loading, using alternative turbine strut

placement and design. This updated rotor design provides a 24 percent increase in energy efficiency over the baseline efficiency. This represents a 24 percent increase in annual energy production (AEP) and a 19 percent reduction in levelized cost of energy (LCOE) for a representative ORPC Power System. LCOE values for an array of four TidGen® Power System are shown in Table 1.

Table 1: Predicted AEP increases and LCOE reductions for an array of four TidGen® Power Systems

	Array of four Baseline TidGen TGUs	**Array of four High Deflection Foil TidGen TGUs**	**% Change**
Turbine Efficiency	42.0%	52.2%	24.3%
AEP (MWhr)	538.5	669.2	24.3%
LCOE ($/kWhr)	0.67	0.54	-19.5%

Summary of Project Activities

The project had four tasks each with separate milestones. The tasks were:

- Task 1: Model Scale Testing of High-deflection Foils
- Task 2: Fluidic and Structural Modeling of Hydrokinetic Turbines
- Task 3: System Integration
- Task 4: Project Reporting & Management

Model scale testing of flexible crossflow turbines was carried out for multiple turbine and foil designs at the UNH's Jere A. Chase Ocean Engineering Laboratory using a crossflow turbine test bed installed in the towing tank. Turbine performance and strain data were collected and analyzed. The data sets for the testing conducted by the UNH team are being curated and will be made available by UNH on a publicly accessible data hosting service or website, as well as on the Department of Energy (DOE) Marine Hydrokinetic Data Repository (MHKDR).

ORPC developed fluid and structural modeling methods to be used to design and analyze high-deflection foils. At the beginning of the project, the intent was to focus on using low order computational methods such as momentum models, panel and vortex models, and simple beam-element structural models for FSI modelling, based on the assumption that these modelling techniques would provide sufficiently accurate results with much lower computational effort. ORPC worked to develop such low-order analytical methods however, none of low-order methods are fully capable of taking the structural deflections as inputs to hydrodynamic models, and these methods suffer from inaccuracies inherent in their formulation. ORPC determined that the project should focus on computational fluid dynamics methods, which were expected to provide more accurate results, although at a higher computational cost. ORPC developed one-way and two-way FSI modelling approaches and validated the one-way FSI methodology using test data. One-way FSI modelling proved accurate. Two-way FSI modelling was attempted but not completed in this work due to issues encountered with parallelization of the problem on High Performance Computing systems. While it is expected that two-way FSI would be preferred, this project determined that one-way FSI was sufficient for a large class of problems and preferred in some cases due to the lower computational effort required.

ORPC applied the FSI tools to a commercial ORPC turbine design. As the basis for design exploration, ORPC selected the RivGen 2.1 turbine variant. This turbine has been previously deployed in multiple

applications, and while there are differences in mechanical joint design between the variants, the basic hydrodynamic shape has been well established, and operational experience with the design obtained in open-water tests. Using the tools developed in this work the efficiency of the baseline turbine is predicted to increase in efficiency by 24 percent which in turn is predicted to lead to an increase in AEP of 24 percent. These improvements will lead to a reduction in LCOE of 19 percent.

Cost, schedule, and technical performance was managed throughout the Project. Quarterly reports were submitted during the performance periods. Project management plans and intellectual property management plans were developed. Risk management for project and technical risks were performed and risk management strategies were executed and updated throughout the Project.

Dissemination of technical work will occur in the form of conference papers to be authored by UNH as part of a Ph.D. program. Up to three papers are expected to be published within the next two years related to the work conducted in this project. Component and LCOE content models are uploaded to the DOE MHKDR.

This final report describes project progress, system/component performance, lessons learned, opportunities identified for further improvement of LCOE, and next steps in technology development.

The project provided an excellent opportunity to develop analytical approaches for assessing performance of hydrokinetic turbines, and for validating these approaches with a high-quality data set from scale model testing. Some key lessons learned include:

- The strain data collection methodology used in this work is an excellent technique for collecting in-situ strain measurements for hydrokinetic turbine testing.
- Hydrodynamic performance reduction from carbon to glass composite foils is small and may well be within the error bounds of the test. This indicates that while stiffness is important from a structural viewpoint, its impact on hydrodynamic performance may be less than expected.
- ORPC worked to develop low-order analytical methods to guide design of high deflection foils. These were deemed inadequate to the task or were assessed to be computationally intense with insufficient benefit. None of low-order methods are fully capable of taking the structural deflections as inputs to hydrodynamic models.
- A comparison of CFD analysis and test data finds that agreement between the 3D CFD results and the test data for the straight carbon and glass foil turbine is very good.
- This one-way FSI methodology developed in this project is relatively easy to implement, with an easy to replicate workflow, and is sufficiently accurate for design of hydrokinetic turbines.

Based on the findings of the test work, increased deflection should not adversely affect turbine efficiency significantly. A more detailed program of structural optimization should be carried out by ORPC to further refine the turbine design. The methodologies developed here will be carried over to more complex geometries to include ducting, fairings, and other incidental support structures that often exist within crossflow turbines.

1.0 Task 1: Model Scale Testing of High-Deflection Foils

1.1 Task Summary

Model scale testing of flexible crossflow turbines was carried out for multiple turbine and foil designs at the UNH's Jere A. Chase Ocean Engineering Laboratory using a crossflow turbine test bed installed in the towing tank. Turbine performance and strain data were collected and analyzed. The data sets for the testing conducted by the UNH team are being curated and will be made available by UNH on a publicly accessible data hosting service or website.

1.2 Test Plan

ORPC, UNH and Sandia developed a test plan for the project. The test plan was completed and outlines best practices for tank testing crossflow turbines and specifically addresses difficulties previously encountered with in situ strain measurements during crossflow turbine testing[1].

1.3 Model Turbine Design

ORPC designed and constructed scale-model turbines for use in the towing tank at UNH (Figure 1).

Two configurations of turbine were selected for testing: 1) a straight foil turbine and 2) a turbine with helically twisted foils. Parameters for each turbine are provided in Table 2.

For each turbine, multiple materials sets were used for construction of turbine foils (Table 3). This provided the opportunity to test turbines with the same external shape but with differing torsional and flexural rigidity. This results in a wide range of stiffness between test turbines.

Radial turbine struts were provided for each turbine. One radial strut was affixed at one end of the test turbine, while the second strut was moved to different locations spanwise along the turbine foils, thus creating different lengths of the "free ends" of the turbine foils. This provides variation in stiffness between turbine foils of the same materials.

Within each series of turbines, the external geometry remained constant, while the torsional and flexural rigidity changed. Due to the different materials and structural support locations used, a wide range of stiffness between the test turbines resulted.

Simplified analysis tools were used to design the foils, including momentum stream tube analysis techniques, and simple beam bending structural models.

While the helical turbine design uses the same foil profile as the straight turbine, the performance characteristics of the helical design were expected to be different from the straight foil turbine. The length of each foil is increased due to the helical twist and hence the solidity of the turbine changes. The degree of helical twist used in the model turbines is much higher than would be used in a full-scale turbine as a full "wrap" of the turbine is achieved in a shortened spanwise length for the model turbine. This helical scale model turbine represents an extreme of design that provides a test case at the edge of the expected design space.

[1] Gunawan B; Bachant P; Neary VS; Wosnik M (2016) Fiber Optic Instrumentation for Measuring Rotor Strain on MHK Turbines, Proceedings of the 4th Marine Energy Technology Symposium, METS2016, April 25-27, 2016, Washington, DC.

ITEM NO.	PART NUMBER	DESCRIPTION	QTY.	MATERIAL
1	V0042-89955K419	Drive Shaft	1	Carbon Steel
2	P-ATGU-10694	Shaft Coupling Star Plate_Top	2	ALUMINIUM
3	V0042-9684T340	Flange Mount Shaft Collar - 2"	2	Carbon Steel
4	V0042-91102A755	Split Lock Washer	6	Carbon Steel
5	V0042-91255A583	Button Head Cap Screw - 5/16-18 x 1	6	Carbon Steel
6	P-xHDF-10714	Strut	2	Aluminium 6061 T6
7	P-xHDF-10715	Strut Extension_75mm	6	Aluminium 6061-T6
8	P-xHDF-10717	Straight Foil Clamp_Lower	6	Aluminium 6061-T6
9	P-xHDF-10718	Straight Foil Clamp_Upper	6	Aluminium 6061-T6
10	V0042-9684T340	Flange Mount Shaft Collar - 2"	4	Carbon Steel
11	V0042-93501A029	Belleville Spring Lock Washer	12	Carbon Steel
12	V0042-93332A276	Helical Insert	12	Steel
13	V0042-90665A158	Low-Profile Socket Head Cap Screw	12	Alloy Steel
14	V0042-91595A408	Dowel Pin_5mm	24	Alloy Steel
15	V0042-90835A200	Barrel Nut	6	Carbon Steel
16	V0042-94365A390	Hex Thumb Nut W/ Flange	6	18-8 Stainless Steel
17	V0042-91074A129	Wedge Lock Washer	6	Zinc Coated Steel
18	V0042-98750A437	Threaded Rod	6	Grade B - Mid Strength Steel
19	V0042-91255A587	Button Head - Socket Cap Screw	12	Alloy Steel
20	V0042-91102A755	Split Lock Washer	12	Zinc Plated Steel
21	P-xHDF-10734	Foil	3	E-Glass/Carbon

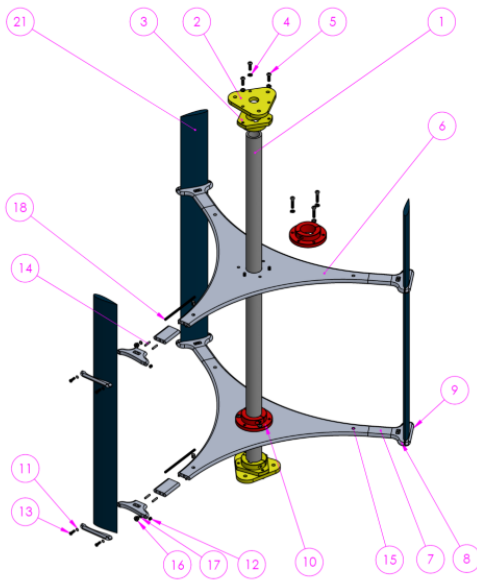

REV.	DESCRIPTION	DATE	DRAWN	CHK	APP
-		-TBD-	-TBD-	-TBD-	-TBD-

REVISIONS

UNLESS OTHERWISE SPECIFIED:
LINEAR DIMENSIONS ARE IN MM
MASS UNITS ARE IN KG
TOLERANCES:
ANGULAR: ±1°
X.X ±3
X.XX ±1
X.XXX ±0.5
WEIGHT [KG] 15
MATERIAL VARIOUS
FINISH N/A
DO NOT SCALE DRAWING

	NAME	DATE
DRAWN	MEB	1/29/2020
CHECKED	-TBD-	
ENG APPR.	-TBD-	

PROPRIETARY AND CONFIDENTIAL
This drawing represents details and design features as elements of a design prepared by and for **Ocean Renewable Power Company, Inc.** (ORPC). ORPC retains exclusive ownership of the drawing, details and designs and are not to be used by any person, unless prior written consent is obtained. This plan is to be returned upon completion of said work.

ORPC
254 COMMERCIAL ST. SUITE 119B PORTLAND, ME 04101 USA (207) 772-7707

TITLE: HIGH DEFLECTION TURBINE

SIZE	DWG. NO.	REV
B	A-xHDF-10733	A

SCALE: 1:20 SHEET 1 OF 1

Figure 1: Scale Model Turbine Geometry

1.4 Model Turbine Construction Details

Different materials and methods of manufacturing were used for the foils.

Due to testing constraints, not all these combinations were tested in the tow tank during this project. Additional testing is expected to occur later.

Details of the turbine shapes are provided in Table 2.

Details of turbine materials are provided in Table 3.

Details of strut locations are provided in Table 4.

1.4.1 Carbon Composite Foil

Carbon composite foils were constructed from carbon fiber prepreg. The ply schedule is provided in Table 5. The plies were laid up in a closed mold and oven cured. This provided a solid carbon fiber laminate. The laminate is symmetric and anisotropic, with higher stiffness in the spanwise direction.

1.4.2 Glass Composite Foil

Glass composite foils were constructed in the same manner as the carbon foils, with glass fiber prepreg used instead of carbon fiber prepreg and using a similar layup schedule and process.

1.4.3 Rubber-filled Glass Composite Foil

A set of foils was constructed comprised of a skin of glass composite with seven plies of glass fabric. This was vacuum infused with an epoxy resin. The internal void space inside the foil was filled with a Shore D, urethane casting resin.

1.4.4 Silicon Bronze Foil

To evaluate alternative manufacturing processes, ORPC determined to make a set of foils by casting silicon bronze, which is a material well-suited to marine applications. A sand-casting mold was made using a carbon fiber foil as a template and three foils cast in solid silicon bronze.

1.4.5 3D-printed Titanium Foil

To evaluate alternative manufacturing processes, ORPC determined to make a set of foils using additive manufacturing. Metal 3D printing was used to print segments of foils which were then fixtured together to form a complete foil span.

The 3D printed material comprises sintered titanium particles and the as-printed part has a relatively rough surface finish of 20 to 22 µm Sa. The turbine was tested in the as-printed condition and after surface finish was improved by buffing, where the average surface roughness decreased to 6 to 13 µm Sa.

Figure 2: Straight foil turbine and helical foil turbine, showing different positioning of movable strut.

Table 2: Turbine Configuration

	Straight Foil Turbine	***Helical Foil Turbine***
Turbine radius	0.5m	0.5m
Number of Foils	3	3
Foil span	0.9m	0.9m
Foil chord	0.095m	0.095m

Foil mounting position	1/2 chord position	1/2 chord position
Foil pitch	0 degree	0 degree
Twist per meter	0 degree	135 degrees
Foil profile	NACA0018	NACA0018

Table 3: Turbine Materials

Description	***Material***	***Straight Foil***	***Helical Foil***	***Struts***
Carbon Prepreg - Solid	Gurit Carbon SparPreg	x		
Fiberglass Prepreg - Solid	Gurit Glass SparPreg	x	x	
Fiberglass Prepreg - hollow with rubber	Glass fiber skin with Shore D urethane casting resin fill	x		
Silicon bronze - solid	CDA 875	x		
3D Printed Titanium	Ti-6Al-4V, 98% solid		x	
Aluminum struts	6061-T6			x
Shaft	Carbon steel	x	x	x

Table 4: Turbine Strut Locations:

Strut location positions
0.900m
0.675m
0.450m
0.225m
0.123m

Table 5: Symmetric Laminate schedule for Carbon and Glass composite foils

Layer No.	Orientation (deg)	Ply thickness (mm)	Width (mm)
1	0	0.586	98
2	0	0.586	95
3	45	0.586	91
4	-45	0.586	87
5	0	0.586	84
6	0	0.586	80
7	90	0.586	21
8	45	0.586	33
9	-45	0.586	40
10	90	0.586	47
11	0	0.586	53
12	0	0.586	58
13	45	0.586	63
14	-45	0.586	67
15	0	0.586	70

16	0	0.586	74
Note: The laminate is symmetric and consists of an additional 16 plies for a total of 32 plies.			

1.5 Instrumentation

In addition to the standard crossflow turbine tow test instrumentation used at UNH, fiber optic strain sensors were embedded along the length of the foils. For the straight foils, both sides of two of the three foils were instrumented. Each of the two foils were permanently connected via the fiber cable. Due to the increased length in the helical foils, only two sides of a single foil were instrumented. Sandia National Laboratories assisted with the selection of the strain measurement methodology and provided the fiber optic interrogator, slip ring, and distributed strain sensors used in the testing. Sandia also aided assistance in installation, testing, and integration of the fiber optic sensor system. Sandia reviewed strain data from the calibration tests and in-tank tests and confirmed that strain data was being measured appropriately.

The fiber optic strain measurement instrumentation consisted of:

- Distributed fiber optic sensors:
  For the experiments conducted at UNH, fiber length was approximately 5.2 m and a sampling rate of 100 Hz, and a gage pitch of 2.6 mm was selected during testing. Gage pitch is the fiber distance between the centers of two neighboring gages. This setting produces approximately 2000 data points for a 5.2 m length fiber (it varied slightly with the exact length of each fiber), with 50 percent overlap.
- Fiber optic slip ring:
  A pressure-compensated Princetel fiber optic rotary joint (FORJ) RPCA-155-28A-FA was used throughout the testing. This is the same model that was used by Sandia and UNH on a prior WPTO-funded Reference Model Project (RM2 at 1:6 scale). The FORJ is rated for 10,000 psi (6 km water depth).
- Luna Odisi 6100 Optical Distributed Sensor Interrogator (ODiSI):
  The ODiSI 6000 Series products are multichannel high-definition fiber optic sensing (HD-FOS) interrogators. Working with sensors based on low-cost unaltered optical fiber and operating on the principle of measuring Rayleigh backscatter, the ODiSI system can measure and acquire strain and temperature with a high spatial resolution.

Figure 3: Fiber Optic sensors being embedded in two structural fiberglass composition straight turbine foils

Typically, a groove was routed into both sides of two foils, and the fiber laid into and potted into the groove (Figure 3). Potting materials were sanded flush with the foil surface.

Each fiber optic element could report strain measurement at 2.6mm intervals along the fiber and allowed for real time strain measurement along both sides of each length of foil during tow tank testing. The fiber optic strand was delicate and extreme care was required when installing and routing the cable for testing.

1.6 Structural Calibration

Prior to tow tank testing each turbine configuration was subject to a structural calibration test whereby known loads were applied at specified positions along the span of one foil in a turbine. Measurements of deflection were taken at known locations. Strain data was collected for each of the calibration tests. These data were used to calibrate structural model material properties used in Task 2.

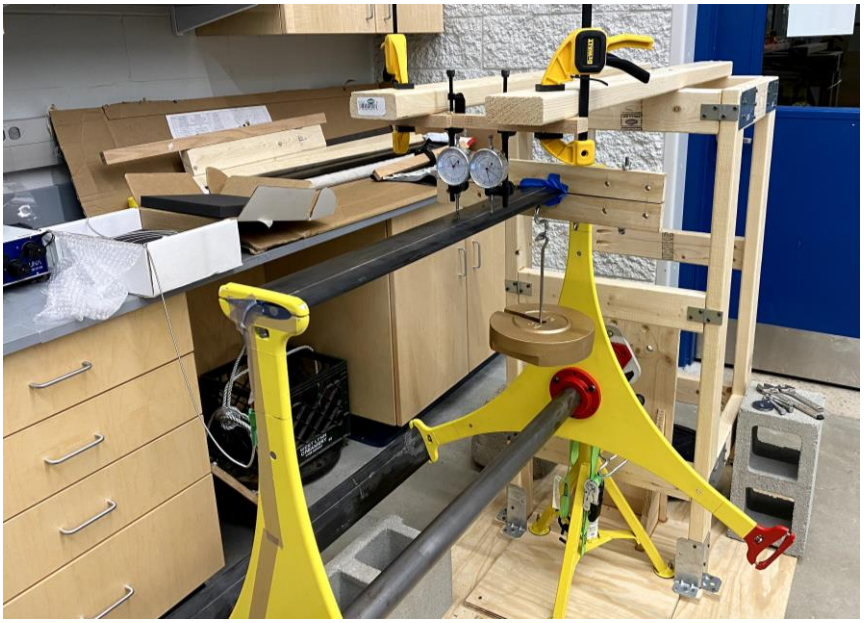

Figure 4: Calibration testing for carbon foil turbine with strut separation = 0.900m

Figure 5: Calibration testing for carbon foil turbines with strut separation = 0.123m

An example of the tabular data for deflection is shown in Table 6.

Table 6: Exemplar table of deflection results for structural calibration test

Test #	Weight Location (m)	Weight (kg)	Test 1 (mm)		Test 2 (mm)		Test 3 (mm)		Mean	Std Deviation	Mean	Std Deviation
			Trailing Edge	Leading Edge	Trailing Edge	Leading Edge	Trailing Edge	Leading Edge	Trailing Edge	Leading Edge	Trailing Edge	Leading Edge
1a	0.3	5.520	-0.403	-0.383	-0.409	-0.385	-0.401	-0.380	-0.404	0.004	-0.383	0.003
1b	0.3	10.545	-0.763	-0.726	-0.751	-0.714	-0.771	-0.730	-0.762	0.010	-0.723	0.008
1c	0.3	15.565	-1.134	-1.082	-1.139	-1.085	-1.137	-1.086	-1.137	0.003	-1.084	0.002
2a	0.4	5.520	-0.680	-0.652	-0.672	-0.640	-0.682	-0.650	-0.678	0.005	-0.647	0.006
2b	0.4	10.545	-1.308	-1.259	-1.294	-1.250	-1.289	-1.243	-1.297	0.010	-1.251	0.008
2c	0.4	15.565	-1.938	-1.868	-1.941	-1.871	-1.937	-1.875	-1.939	0.002	-1.871	0.004
3a	0.6	5.520	-1.329	-1.297	-1.315	-1.283	-1.310	-1.284	-1.318	0.010	-1.288	0.008
3b	0.6	10.545	-2.552	-2.489	-2.548	-2.483	-2.559	-2.498	-2.553	0.006	-2.490	0.008
3c	0.6	15.565	-3.760	-3.665	-3.750	-3.658	-3.760	-3.665	-3.757	0.006	-3.663	0.004

4a	0.7	5.520	-1.661	-1.619	-1.658	-1.614	-1.647	-1.610	-1.655	0.007	-1.614	0.005
4b	0.7	10.545	-3.185	-3.109	-3.168	-3.092	-3.161	-3.090	-3.171	0.012	-3.097	0.010
4c	0.7	15.565	-4.685	-4.560	-4.690	-4.569	-4.676	-4.559	-4.684	0.007	-4.563	0.006
5a	0.8	5.520	-1.920	-1.869	-1.913	-1.865	-1.911	-1.863	-1.915	0.005	-1.866	0.003
5b	0.8	10.545	-3.660	-3.580	-3.639	-3.560	-3.641	-3.565	-3.647	0.012	-3.568	0.010
5c	0.8	15.565	-5.412	-5.225	-5.391	-5.248	-5.395	-5.250	-5.399	0.011	-5.241	0.014

Notes: Carbon fiber foils
0.123m strut separation
Indicator location at 0.512m along span
Leading edge measurement @ 14.72mm from leading edge of foil
Training edge measurement @ 14.89mm from trailing edge of foil

An example of the strain data from the structural test is shown in Figure 6. There are some data dropouts along the span, recorded as not a number (NaN).

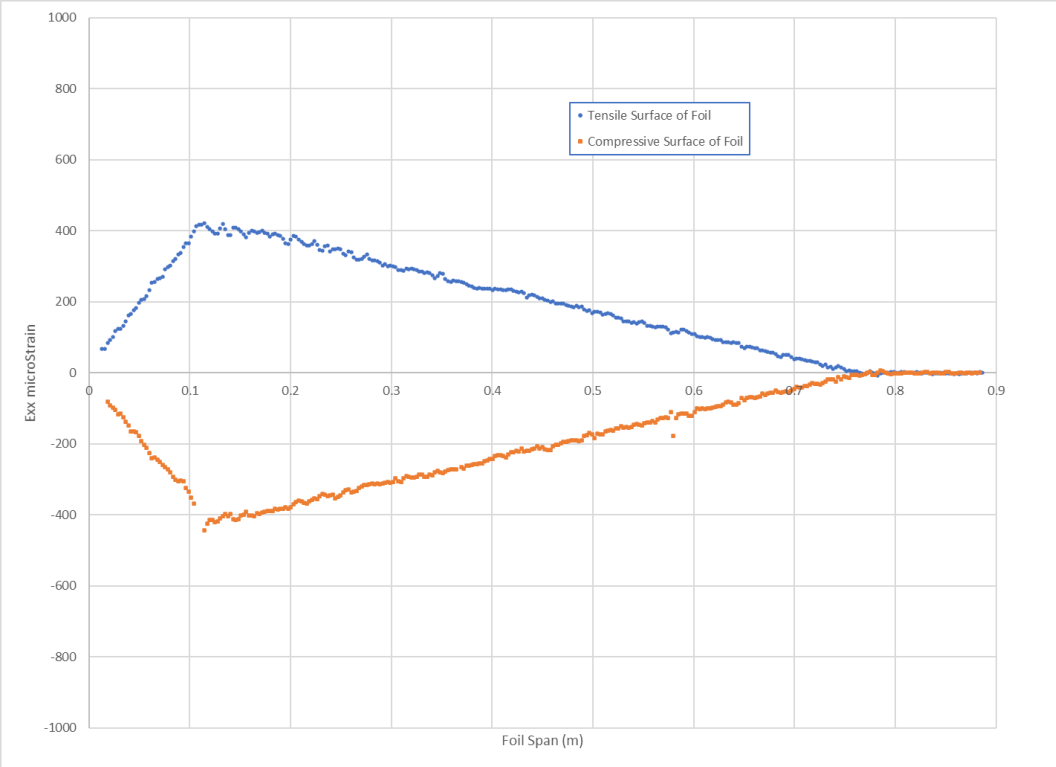

Figure 6: Example strain data from structural calibration test.
Carbon foil, with weight of 15.565kg applied at 0.800m along the span.
Fixed strut located at span = 0m and extending for 0.0127m.
Movable strut located at span = 0.123m and extending from 0.110m to 0.123m

The influence of the struts is seen in the plot. For the case shown the presence of the fixed strut at span = 0m is clearly indicated. The width of the struts is 0.0127mm and strain measurements do not register until this side of the strut is passed. The second movable strut is located between 0.110m and 0.123m along the strut. Again, this location is clearly defined in the strain plots. The applied weight is at 0.800m. There is some ambiguity as to the location of the weight due to the blocking used to transfer load to the

foil (Figure 4). This test is equivalent to a beam bending test, with the beam supported as a cantilever and with load applied at a discrete point.

Another example of strain data from the calibration testing is provided in Figure 7. In contrast to the previous example, this case represents beam bending with a support at each end with struts at their maximum separation of 0.900m. The calibration weight was applied near the center of the foil. Maximum stain occurs at the load application point. Strain transitions from compressive to tensile moving from left to right along the span indicating the localized effects of the strut joint, as well as the end effects on the strain gauge as it wraps around the foil from the upper to the lower surface of the foil (Figure 3).

Multiple such calibration sets were obtained for the straight foil turbines.

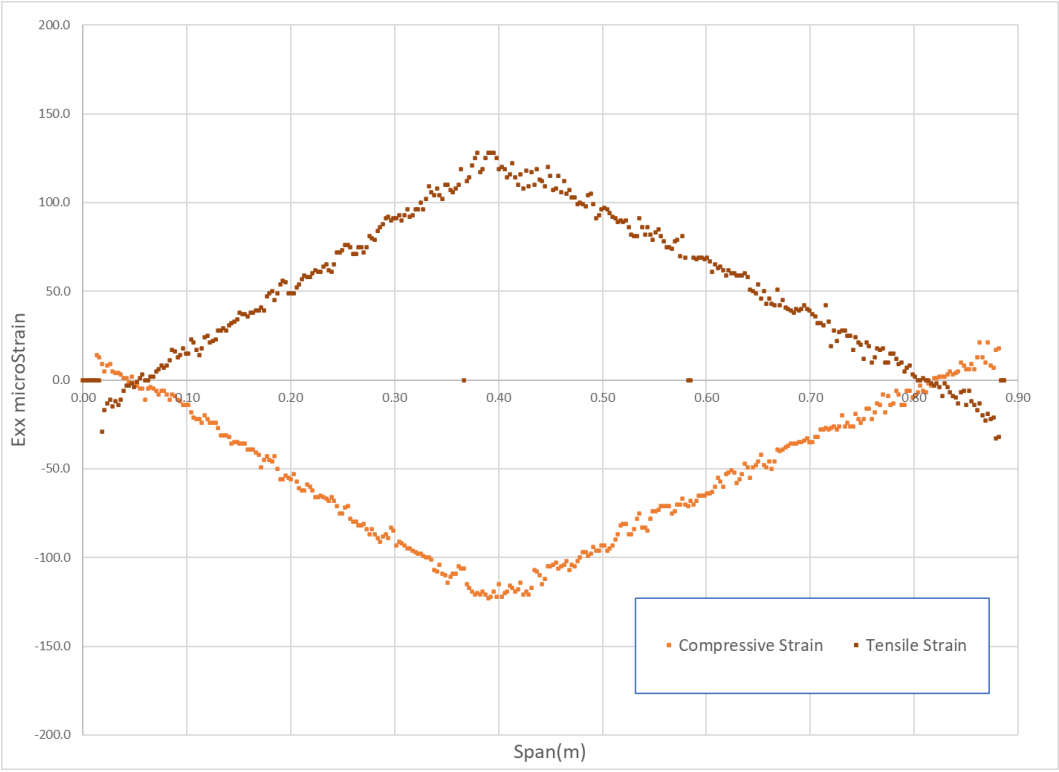

Figure 7: Example strain data from structural calibration test.
Carbon foil, with weight of 15.565kg applied at 0.400m along the span.
Fixed strut located at span = 0m and extending for 0.0127m.
Movable strut located at span = 0.900m and extending from 0.887m to 0.900m

For the helical foil turbines, it proved difficult to manage the run of fiber optic strand between two foils and so only one of the foils for each helical turbine test was outfitted with a strain gauge.

For the additive manufactured titanium model, it was not possible to inset the fiber optic strand within the body of the material, and testing was conducted without strain measurements.

1.7 Tow Tank Geometry

Testing of the various model turbines was conducted at UNH.

Tank parameters are as follows:

- Length: 36 m
- Width: 3.66 m
- Depth: 2.44 m
- Fresh water
- Temperature ~ 23°C

The turbines were mounted in a vertical orientation (Figure 8) in a streamlined test frame. A servo motor/generator was used to control the rotational speed of the turbine and torque was measured with an inline rotatory torque cell, mounted between the turbine and the motor/generator, with a secondary torque measurement from a moment arm and a load cell where the motor is mounted to the tow frame. The test frame rides on linear bearings and is connected to the tow carriage via two S-beam load cells which provide an overall thrust measurement, from which tare thrust measurements was subtracted. Tow speeds ranged from 0.6 to 1.3 m/s. The turbine center is located at a depth of 1.200m. Tow speed and turbine rotational speed were fixed for each test run, controlling turbine tip speed ratio (TSR).

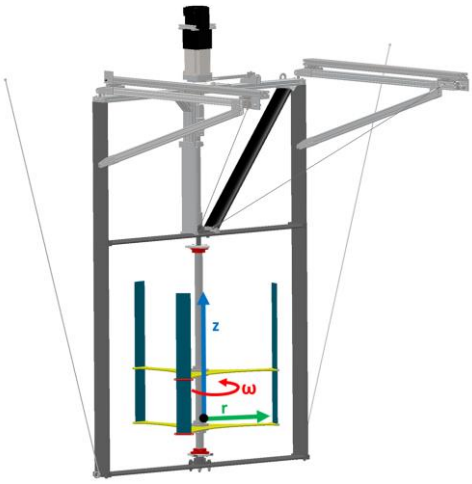

Figure 8: Coordinate system for turbine test. Rotation is positive around Z.

1.8 Straight Foil Carbon Composite Turbine Test

Test data will first be presented and commentary on the data and test findings will be provided later in this report.

1.8.1 Straight Foil Carbon Composite Turbine Hydrodynamic Results

Initial tank testing focused on the carbon straight foil turbine. Multiple tests were performed to establish the testing speed at which the performance results became Reynolds Number independent.

For a given strut location and turbine type, the turbine was spun up to a preset rotational speed and then then towed along the tank. Testing resulted in data which was then processed and presented as turbine efficiency, and non-dimensional turbine forces. Standard definitions of Coefficient of Performance (Cp) and Coefficients of Drag were used. The testing was repeated three times for each test condition.

The movable strut was then repositioned along the span, and the turbine retested for the new strut position (Table 4). The fixed strut was always located nearest the bottom of the tank.

Test results were Reynolds number independent at a tow speed of 1.1 m/s.

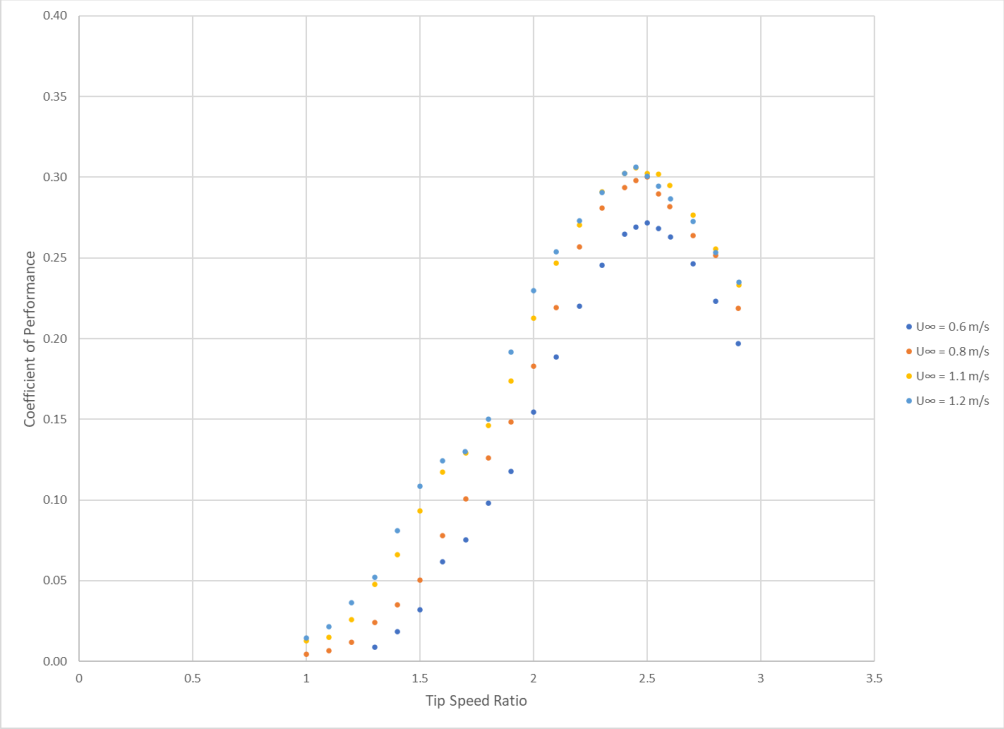

Figure 9: Average Coefficient of Performance vs. Tip Speed Ratio for carbon straight foil turbine. Testing performed at different tow speeds. Movable strut is located at 0.900m position.

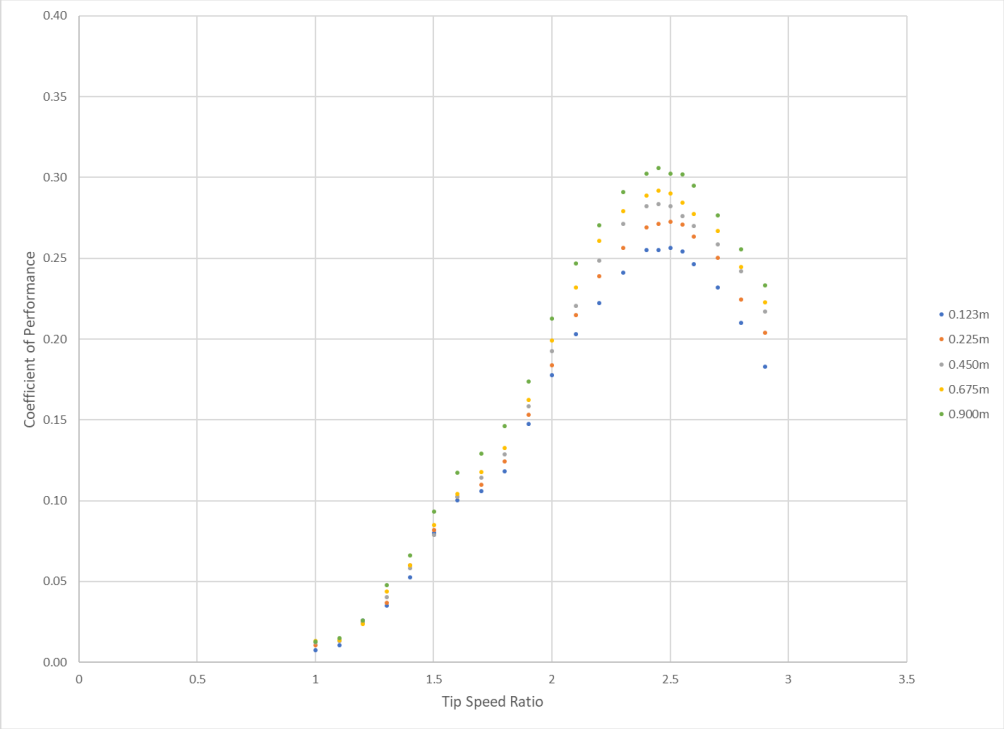

Figure 10: Average Coefficient of Performance vs. Tip Speed Ratio for carbon straight foil turbine, tow speed of 1.1 m/s, and strut positions from 0.123 to 0.900 m.

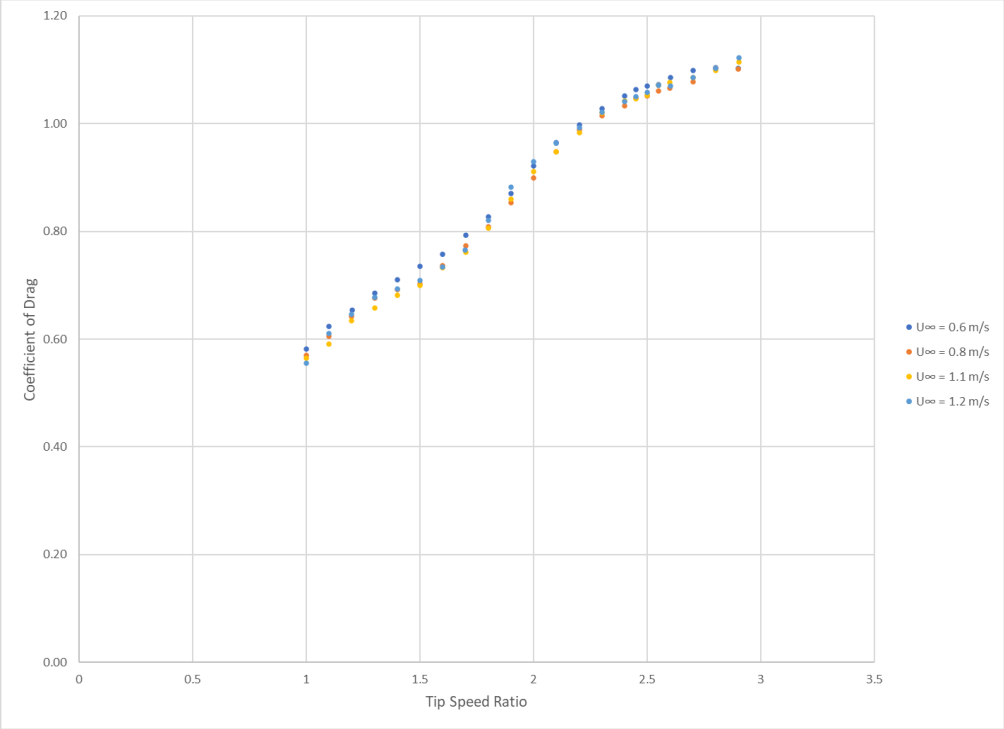

Figure 11: Average Coefficient of Drag vs. Tip Speed Ratio for carbon straight foil turbine. Testing performed at different tow speeds. Movable strut is located at 0.900m position.

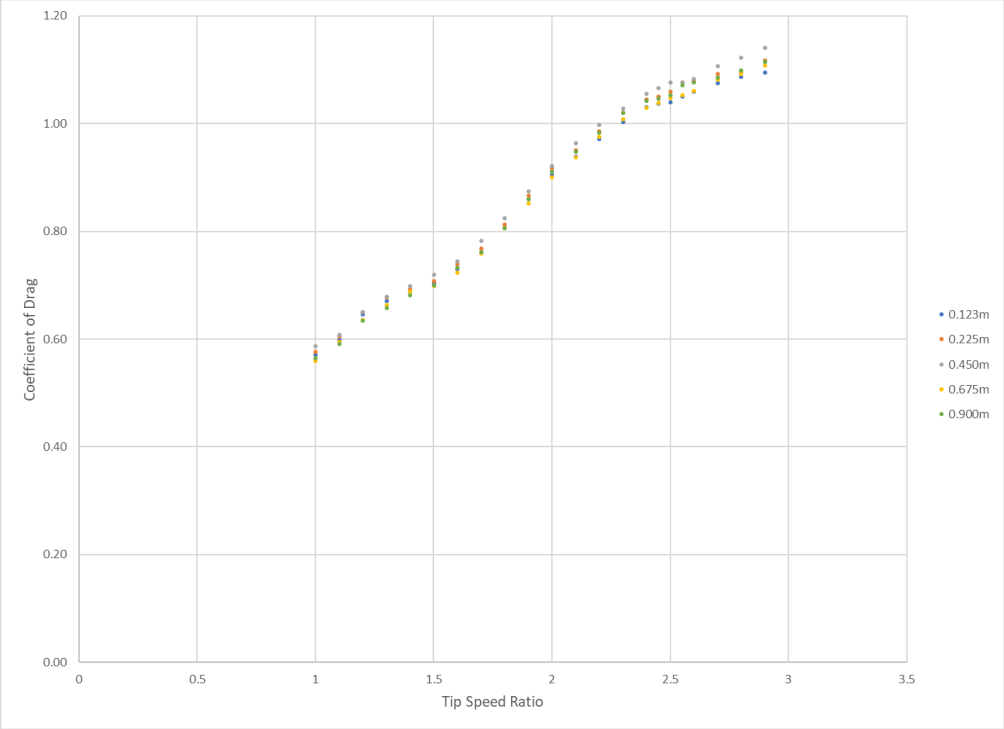

Figure 12: Average Coefficient of Drag vs. Tip Speed Ratio for carbon straight foil turbine, for a tow speed of 1.1 m/s, and strut positions from 0.123 to 0.900 m.

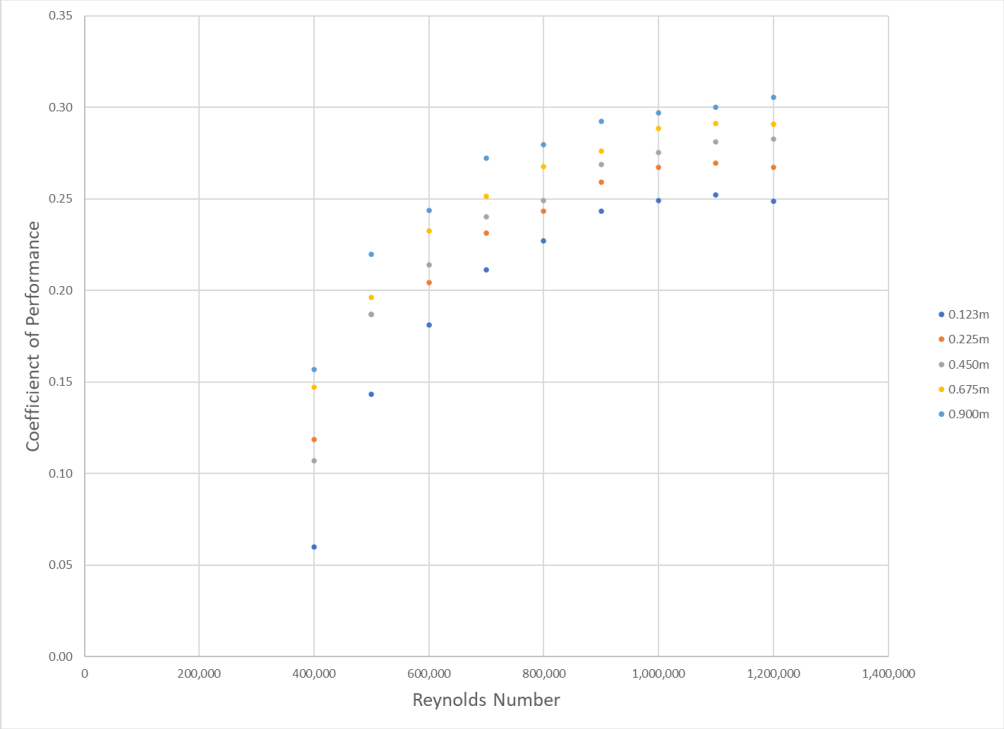

Figure 13: Average Coefficient of Performance at a Tip Ratio of 2.50 for carbon straight foil turbine for different Reynolds Number (different tow speeds).

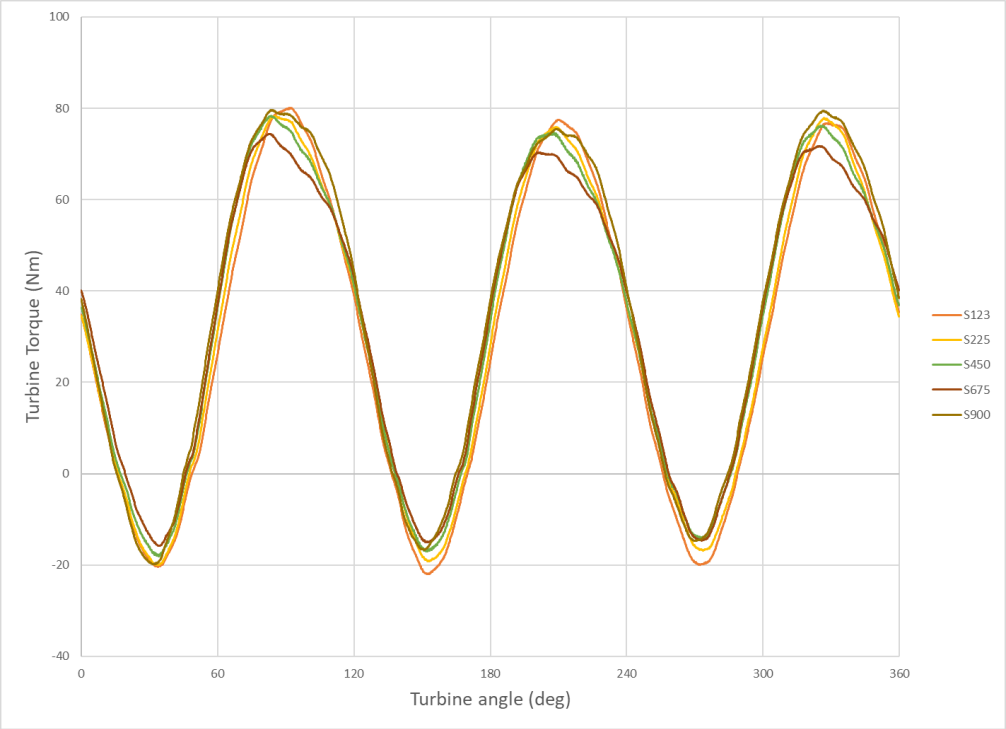

Figure 14: Turbine torque as a function of turbine rotational position for carbon straight foil turbines for different strut positions. Turbine tow speed = 1.1m/s, and tip speed ratio = 2.40.

1.8.2 Straight Foil Carbon Composite Turbine Structural Results

Strain data for the straight carbon composite foil turbine for various struts locations is shown in the following figures. The data are presented in two charts. The leftmost chart shows the strain on the outside surface of the foil along the foil span as a function of turbine angular position. The rightmost chart shows the strain on the outside surface and the inside surface at a stated spanwise location on the foil as a function of turbine angular position. The pattern of strain at any given point along the span can be inferred from these two plots.

Strain measurements near the end of the foils are not aligned with the spanwise direction as the fiber sensing element changed direction to wrap onto the other side of the foil (Figure 2).

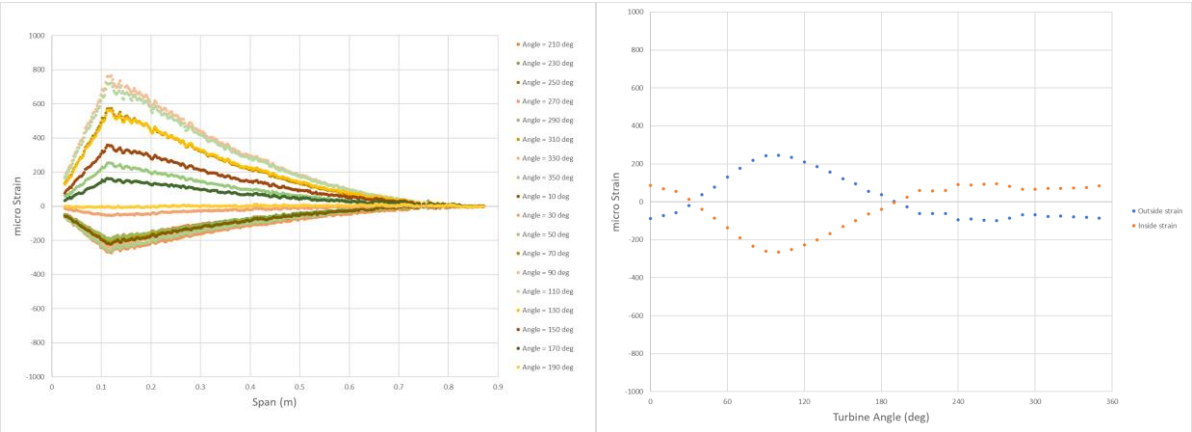

Figure 15: Strut location of 0.123m. Major strain in outermost ply of the outside surface for the straight carbon composite foil along the foil span, for different turbine rotational positions (left). Major strain for the outermost plies on the outer and inner surface of the same foil as a function of turbine rotational position at spanwise location of 0.440m (right). Tip speed ratio is 2.40.

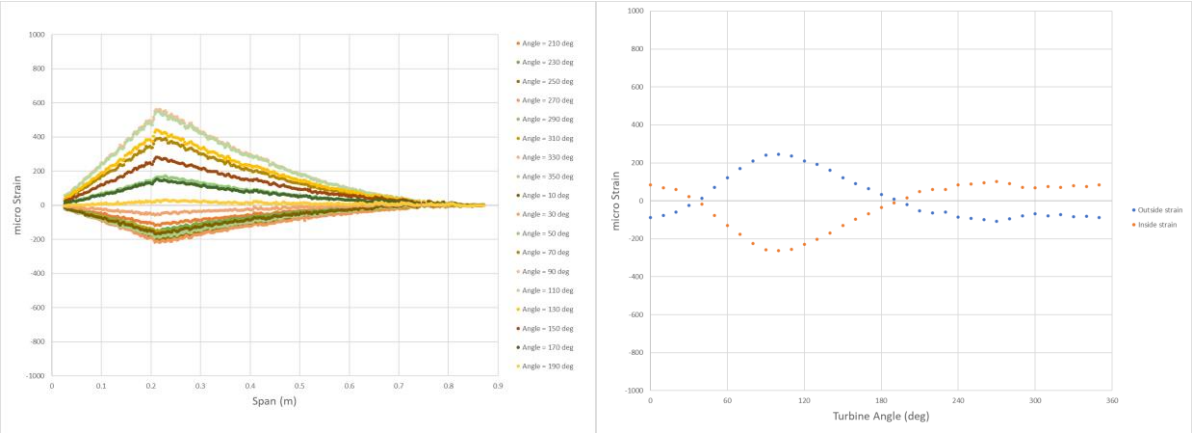

Figure 16: Strut location of 0.225m. Major strain in outermost ply of the outside surface for the straight carbon composite foil along the foil span, for different turbine rotational positions (left). Major strain for the outermost plies on the outer and inner surface of the same foil as a function of turbine rotational position at spanwise location of 0.440m (right). Tip speed ratio is 2.40.

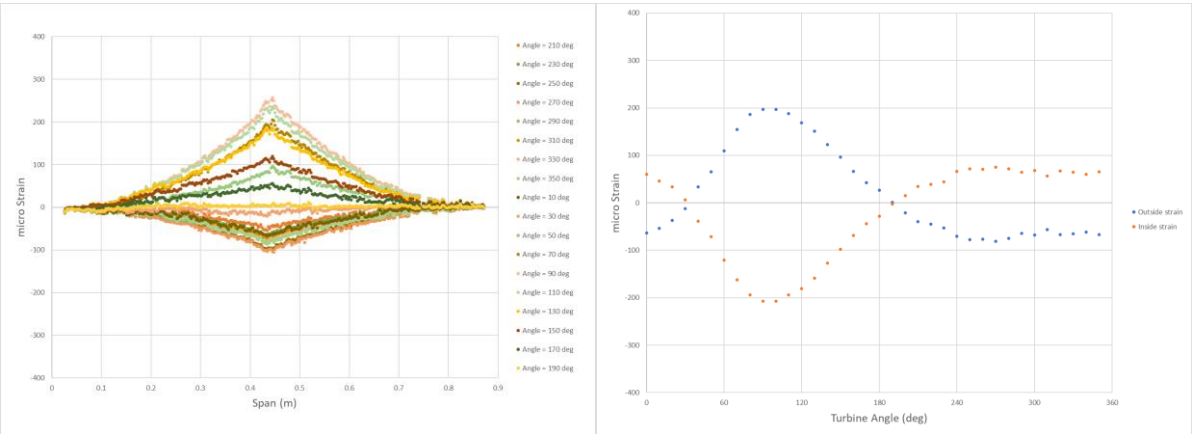

Figure 17: Strut location of 0.450m. Major strain in outermost ply of the outside surface for the straight carbon composite foil along the foil span, for different turbine rotational positions (left). Major strain for the outermost plies on the outer and inner surface of the same foil as a function of turbine rotational position at spanwise location of 0.400m (right). Note change in strain scale from prior plots. Tip speed ratio is 2.40.

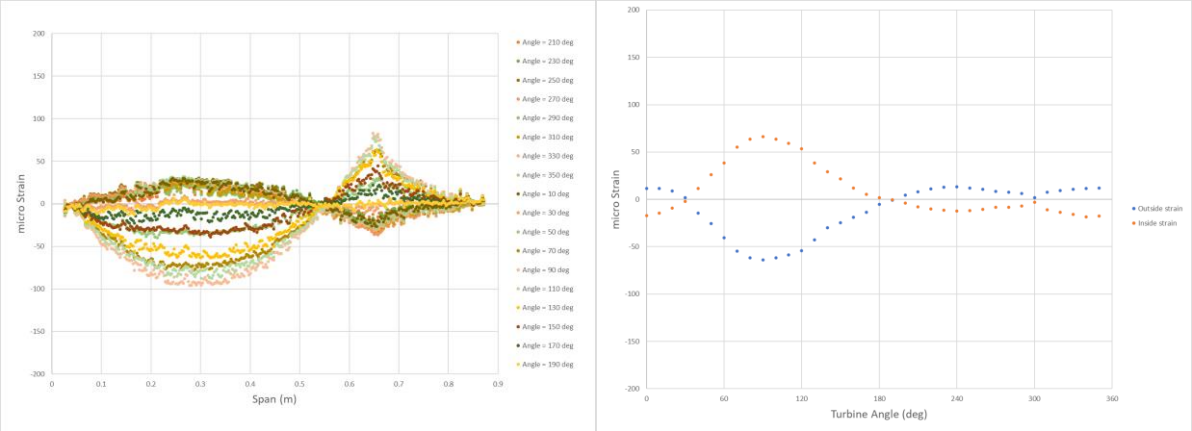

Figure 18: Strut location of 0.675m. Major strain in outermost ply of the outside surface for the straight carbon composite foil along the foil span, for different turbine rotational positions (left). Major strain for the outermost plies on the outer and inner surface of the same foil as a function of turbine rotational position at spanwise location of 0.440m (right). Note the change in scales compared with prior plots. Tip speed ratio is 2.40.

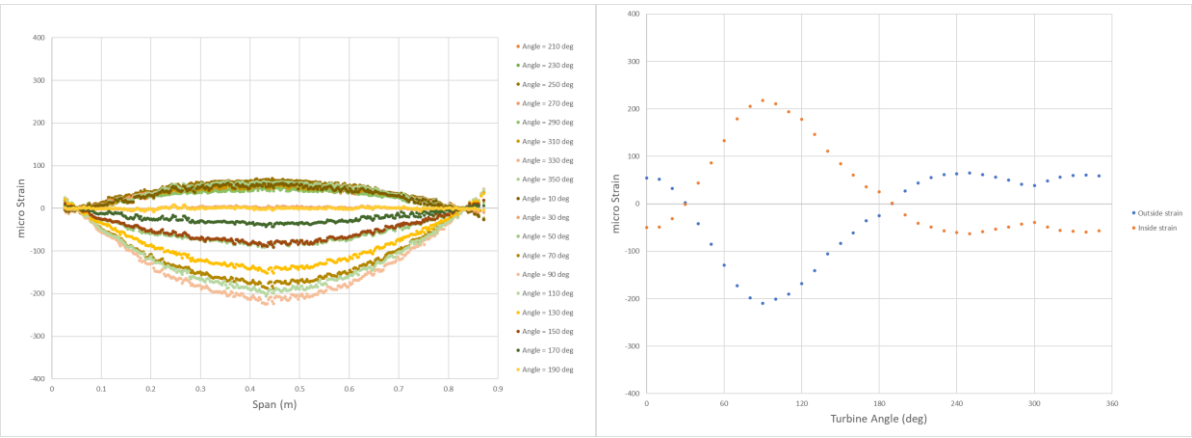

Figure 19: Strut location of 0.900m. Major strain in outermost ply of the outside surface for the straight carbon composite foil along the foil span, for different turbine rotational positions (left). Major strain for the outermost plies on the outer and inner surface of the same foil as a function of turbine rotational position at spanwise location of 0.440m (right). Note the change in scales compared with prior plots. Tip speed ratio is 2.40.

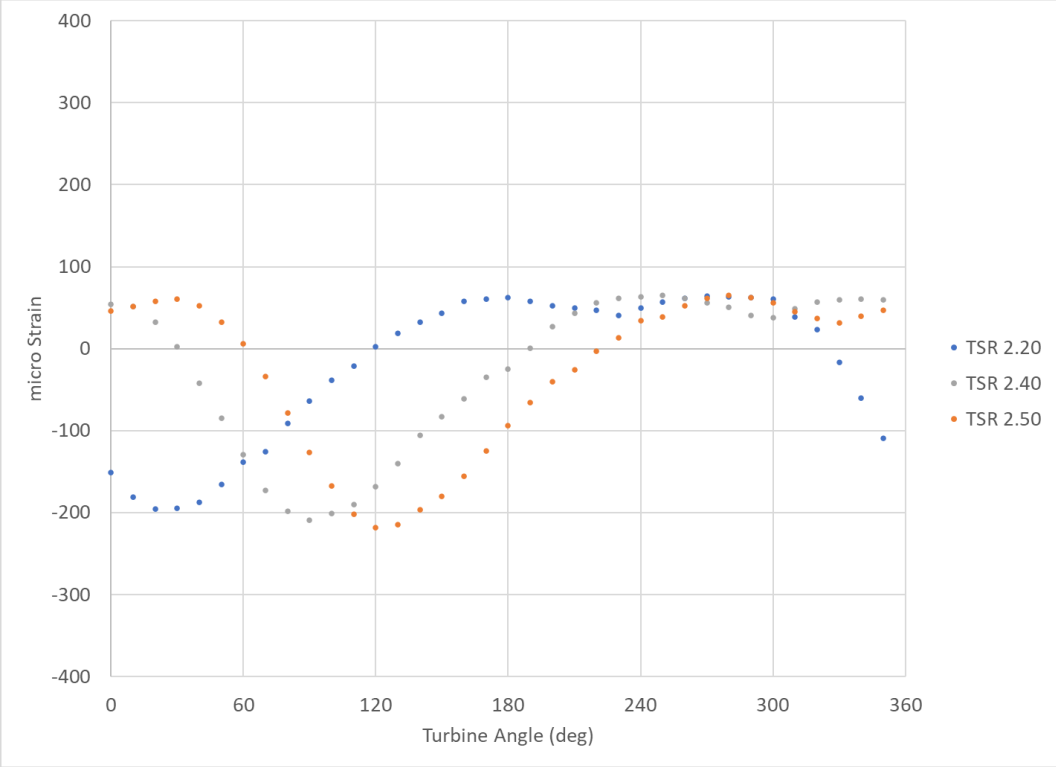

Figure 20: Strut location of 0.900m. Major strain in outermost ply of the outside surface for the straight carbon composite for different turbine angles, for different tip speed ratios. The angular position of maximum compressive strain changes with tip speed ratio, advancing as TSR increases. The spanwise location for this strain measurement is 0.440m.

1.9 Straight Foil Glass Composite Turbine Test

Test data will first be presented and commentary on the data and test findings will be provided later in this report.

1.9.1 Straight Foil Glass Composite Turbine Hydrodynamic Results

The same test methodology was used as for straight carbon foil turbines.

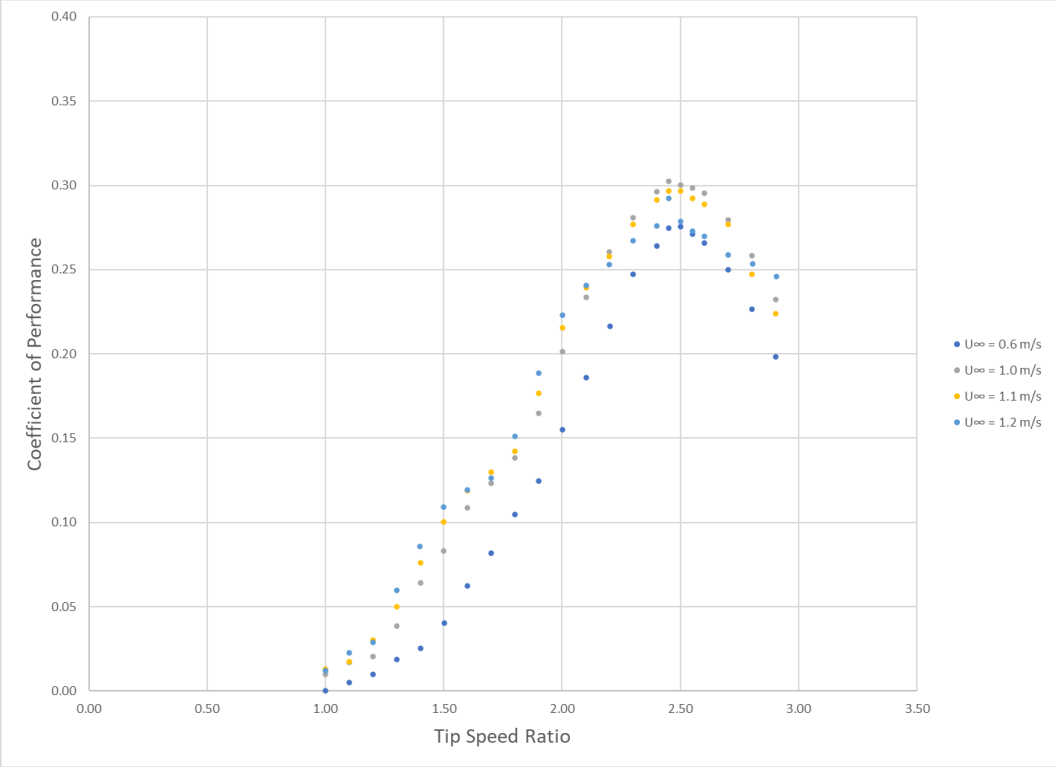

Figure 21: Average Coefficient of Performance vs. Tip Speed Ratio for glass composite straight foil turbine. Testing performed at different tow speeds. Movable strut is located at 0.900m position.

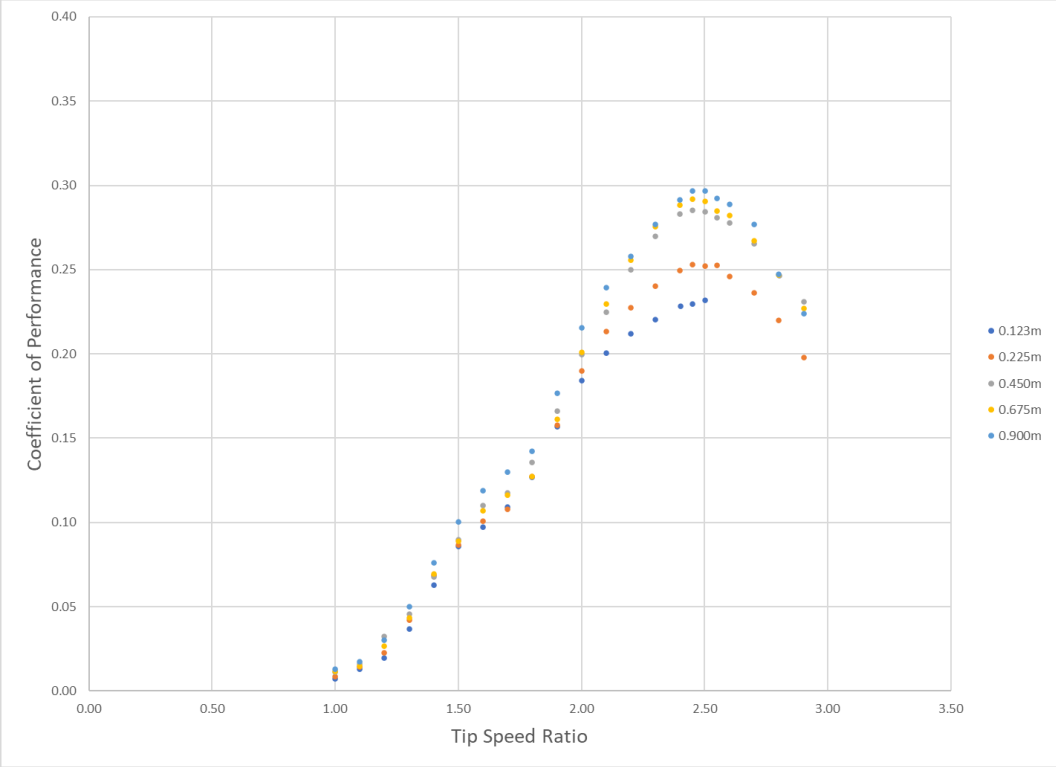

Figure 22: Average Coefficient of Performance vs. Tip Speed Ratio for glass composite straight foil turbine for a tow speed of 1.1 m/s, and strut positions from 0.123 to 0.900 m.

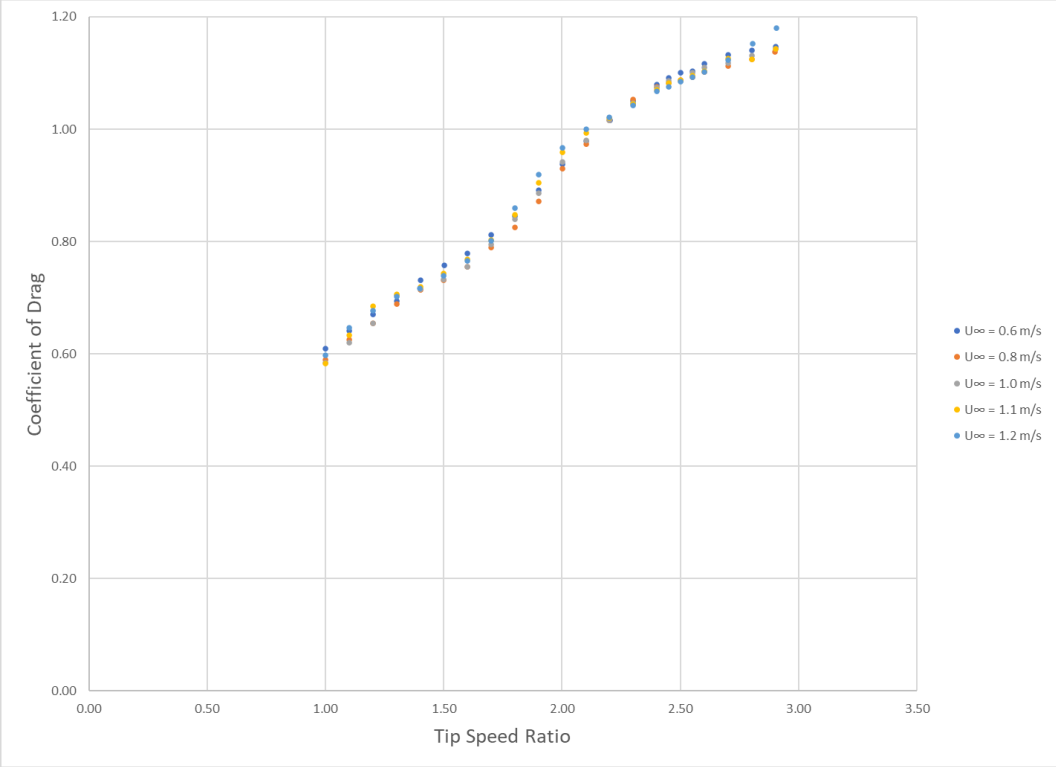

Figure 23: Average Coefficient of Drag vs. Tip Speed Ratio for glass composite straight foil turbine. Testing performed at different tow speeds. Movable strut is located at 0.900m position.

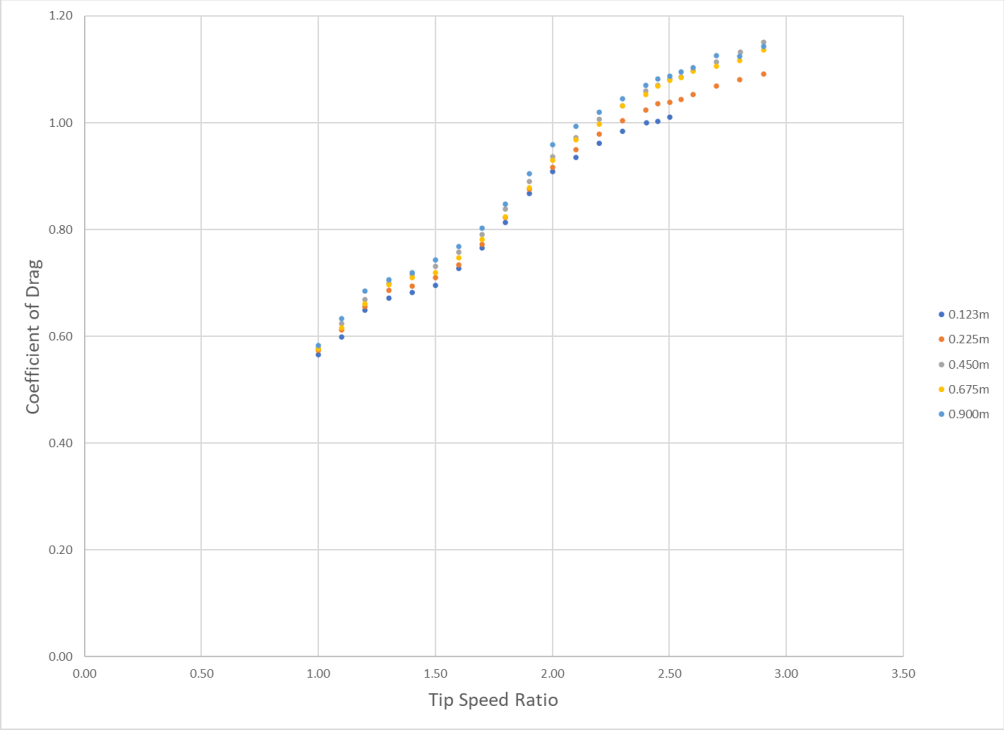

Figure 24: Average Coefficient of Drag vs. Tip Speed Ratio for glass composite straight foil turbine, for a tow speed of 1.1 m/s, and strut positions from 0.123 to 0.900 m.

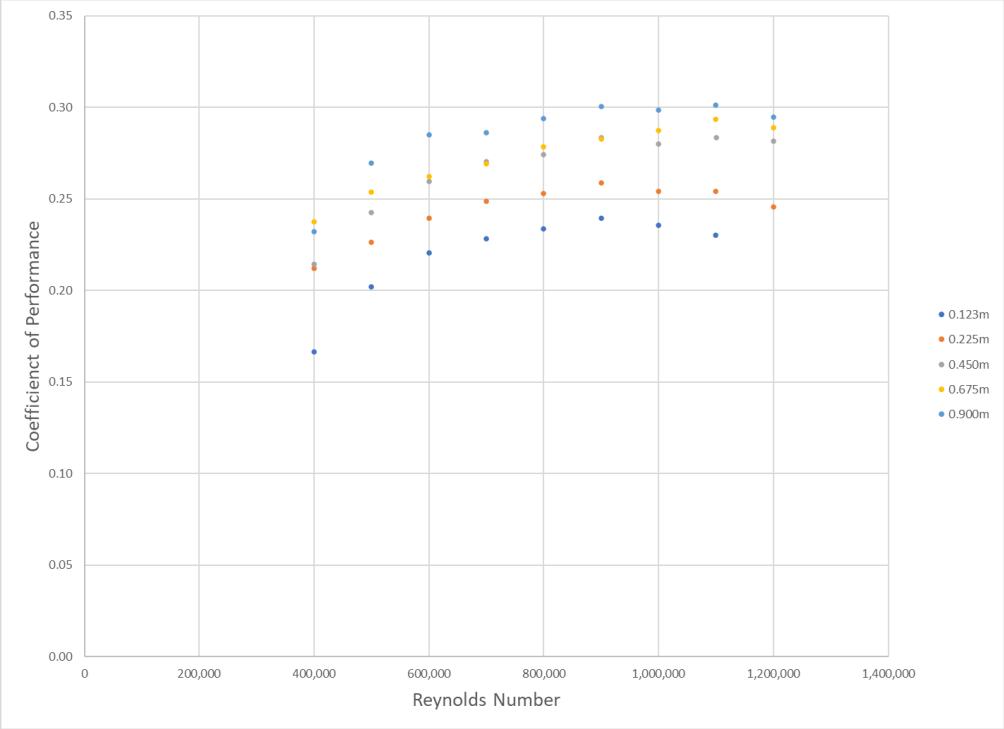

Figure 25: Average Coefficient of Performance at a Tip Ratio of 2.50 for glass composite straight foil turbine for different Reynolds Number (different tow speeds).

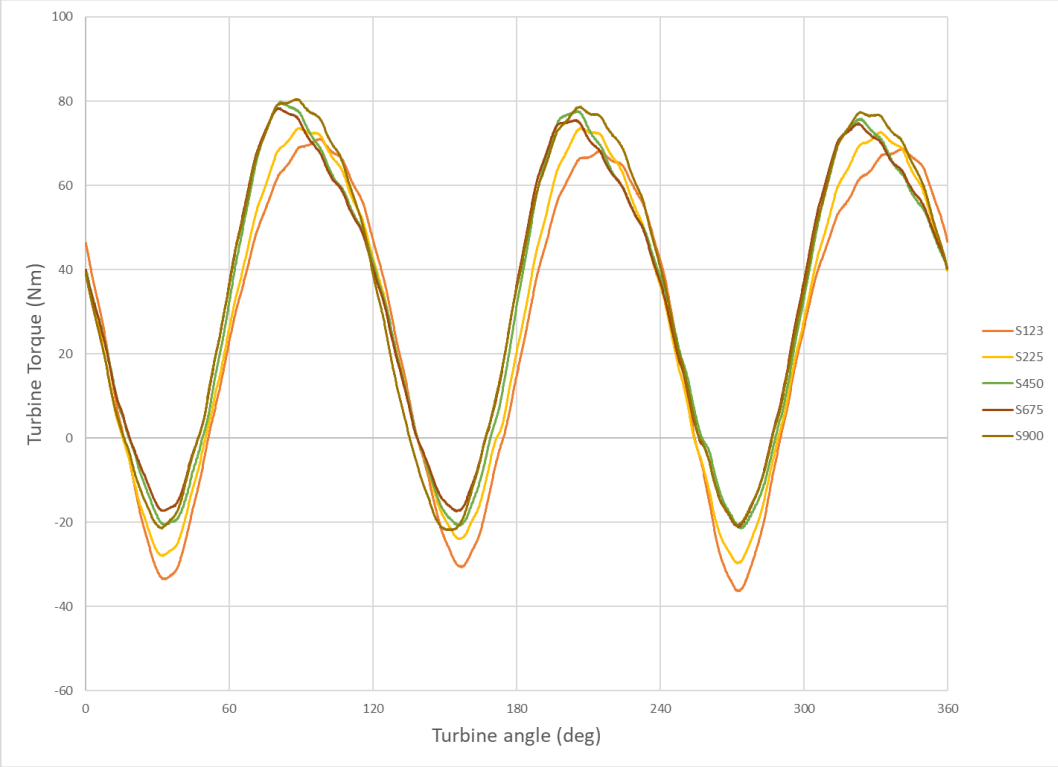

Figure 26: Turbine torque as a function of turbine angle for glass composite straight foil turbine for different strut positions. TSR 2.40, Tow speed = 1.1m/s.

1.9.2 Straight Foil Glass Composite Turbine Structural Results

Strain data for the straight glass composite foil turbine for various struts locations is shown in the following figures. The data is presented in two charts. The leftmost chart shows the strain on the outside surface of the foil along the foil span as a function of turbine angular position. The rightmost chart shows the strain on the outside surface and the inside surface at a stated spanwise location on the foil as a function of turbine angular position. The pattern of strain at any given point along the span can be inferred from these two plots. Note that when compared with the carbon foil test, the strains are higher, and that the strain sensing seems less capable with significant amount of data dropouts.

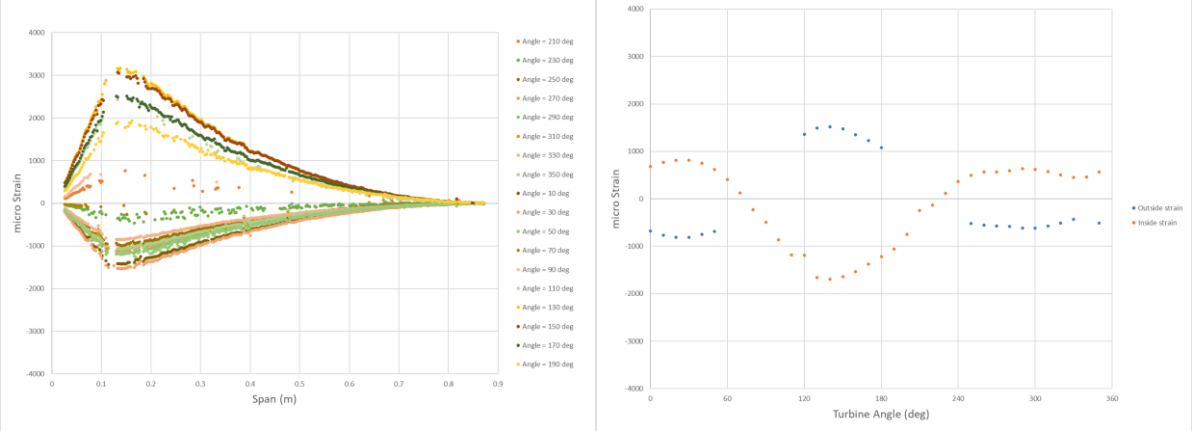

Figure 27: Strut location of 0.123m. Major strain in outermost ply of the outside surface for the straight glass composite foil along the foil span, for different turbine rotational positions (left). Major strain for the outermost plies on the outer and inner surface of the same foil as a function of turbine rotational position at spanwise location of 0.351m (right). Note that for higher strain measurements data quality decreases and data dropouts increase. Tip speed ratio is 2.40.

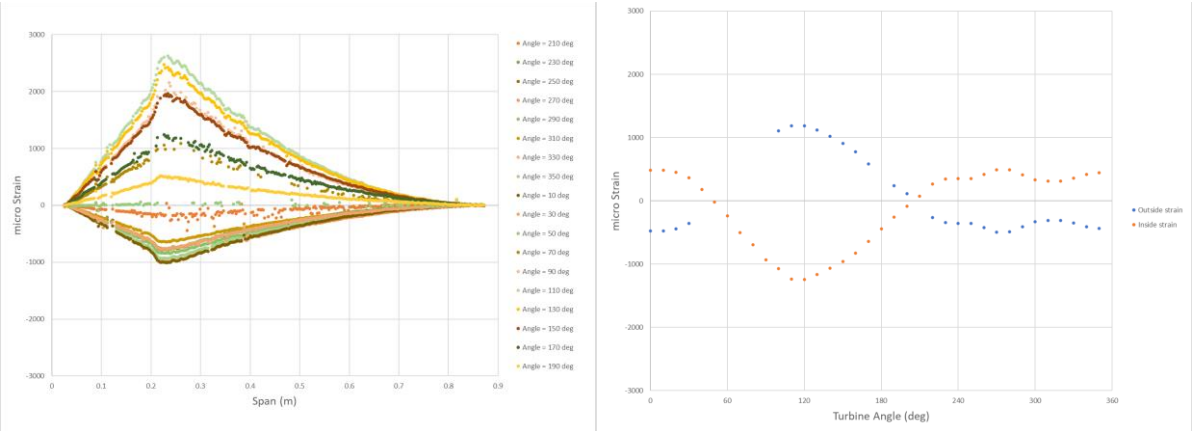

Figure 28: Strut location of 0.225m. Major strain in outermost ply of the outside surface for the straight glass composite foil along the foil span, for different turbine rotational positions (left). Major strain for the outermost plies on the outer and inner surface of the same foil as a function of turbine rotational position at spanwise location of 0.442m (right). Note change in scale from prior plot. Tip speed ratio is 2.40.

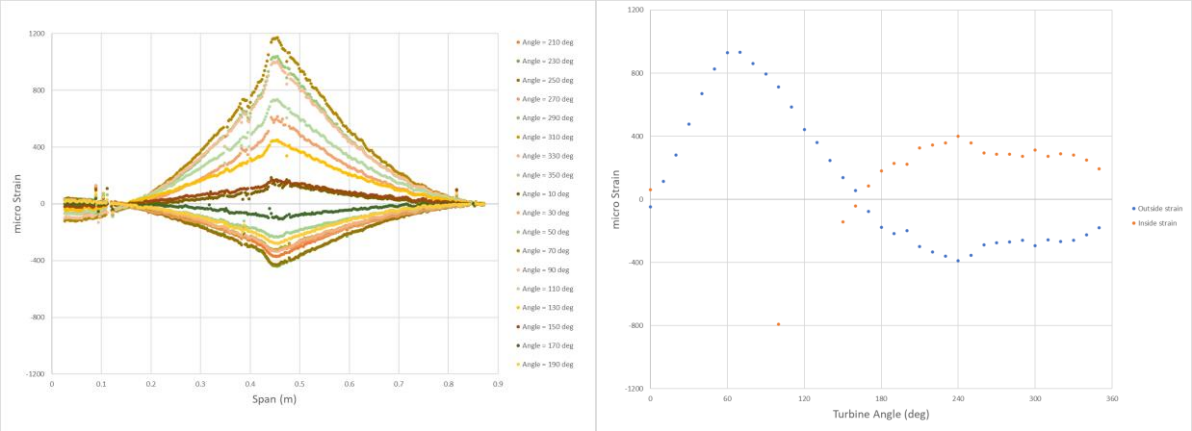

Figure 29: Strut location of 0.450m. Major strain in outermost ply of the outside surface for the straight glass composite foil along the foil span, for different turbine rotational positions (left). Major strain for the outermost plies on the outer and inner surface of the same foil as a function of turbine rotational position at spanwise location of 0.502m (right). Note the change in scales compared with prior plots. Tip speed ratio is 2.40.

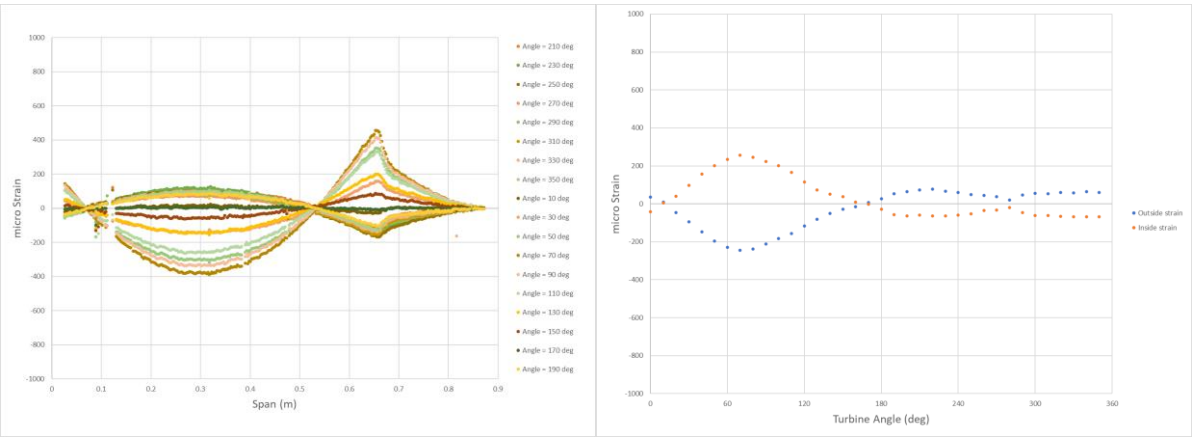

Figure 30: Strut location of 0.675m. Major strain in outermost ply of the outside surface for the straight glass composite foil along the foil span, for different turbine rotational positions (left). Major strain for the outermost plies on the outer and inner surface of the same foil as a function of turbine rotational position at spanwise location of 0.440m (right). Note the change in scales compared with prior plots. Tip speed ratio is 2.40.

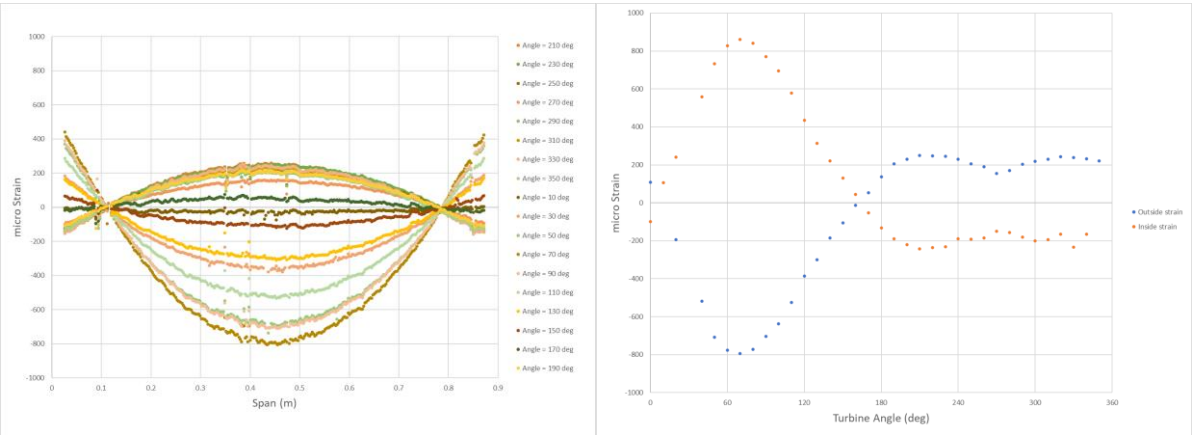

Figure 31: Strut location of 0.900m. Major strain in outermost ply of the outside surface for the straight glass composite foil along the foil span, for different turbine rotational positions (left). Major strain for the outermost plies on the outer and inner surface of the same foil as a function of turbine rotational position at spanwise location of 0.440m (right). Tip speed ratio is 2.40.

1.10 Helical Foil Glass Composite Turbine Test

Test data will be presented first. Commentary on the data and test findings will be provided later in this report.

1.10.1 Helical Foil Glass Composite Turbine Hydrodynamic Results

For the helical foil glass composite turbine, testing was not conducted at a strut location of 0.123m as the strains were potentially large enough to cause damage to the composite.

Initial testing showed that the performance of the helical turbine to be significantly different from the straight foil. The maximum obtainable Cp value was lower and occurred at a higher-than-expected tip speed ratio. It was possible to test at a higher tow carriage speed than for the straight foil.

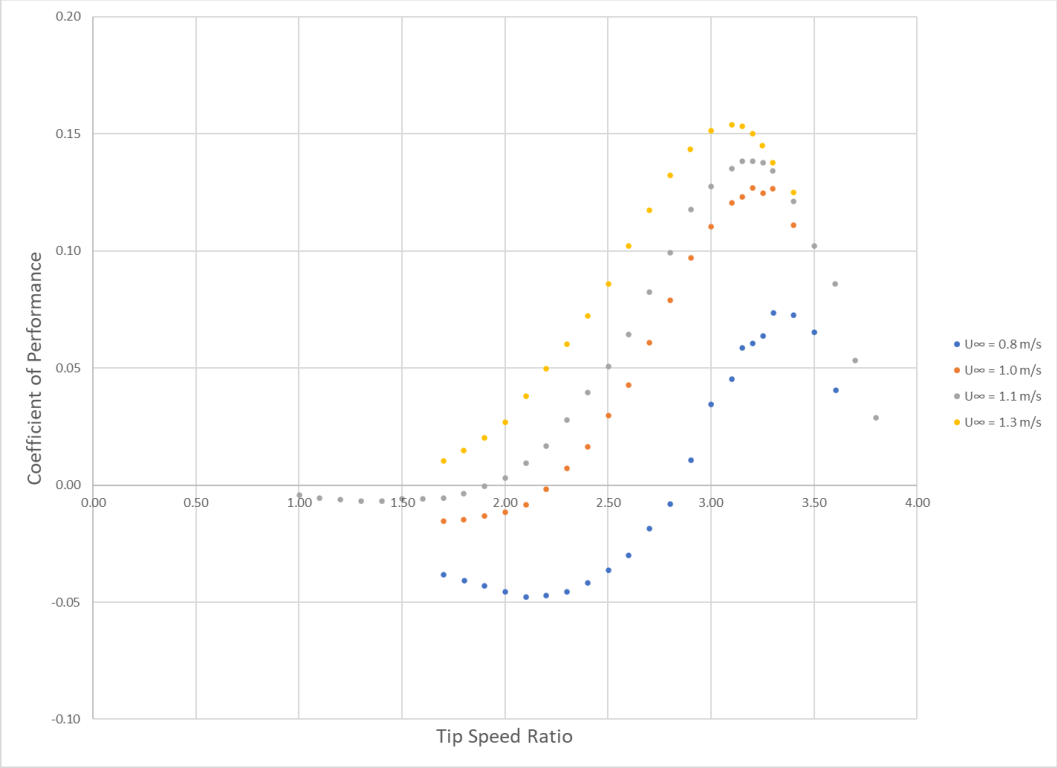

Figure 32: Average Coefficient of Performance vs. Tip Speed Ratio for glass composite helical foil turbine. Testing performed at different tow speeds. Movable strut is located at 0.900m position.

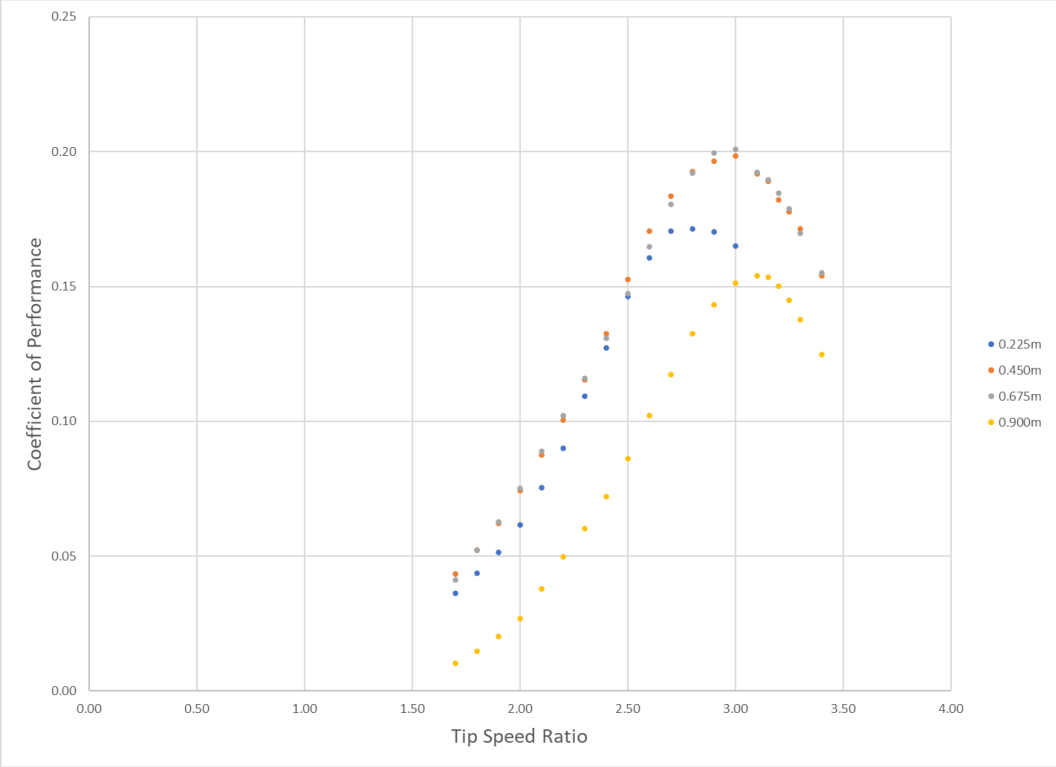

Figure 33: Average Coefficient of Performance vs. Tip Speed Ratio for glass composite helical foil turbine for a tow speed of 1.3 m/s, and strut positions from 0.225 to 0.900 m.

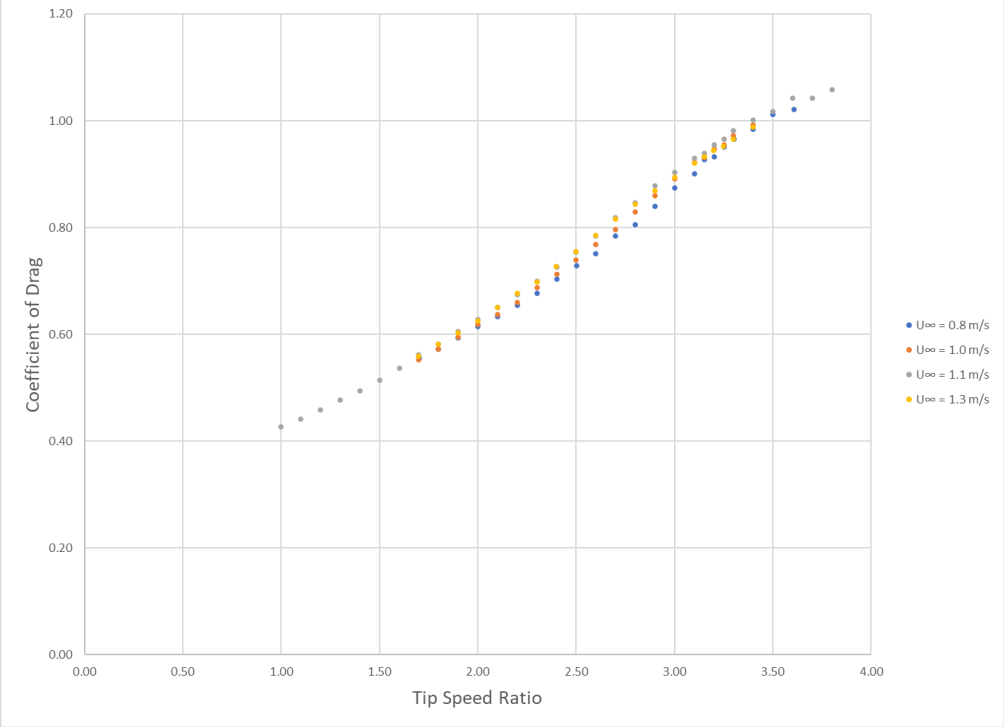

Figure 34: Average Coefficient of Drag vs. Tip Speed Ratio for glass composite helical foil turbine. Testing performed at different tow speeds. Movable strut is located at 0.900m position.

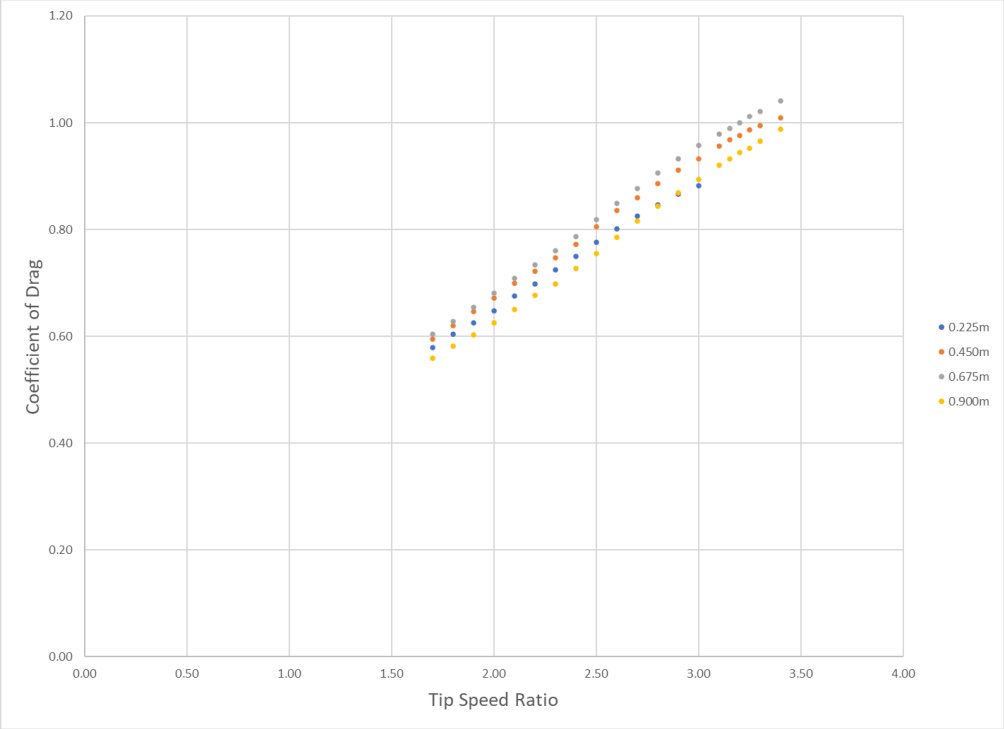

Figure 35: Average Coefficient of Drag vs. Tip Speed Ratio for glass composite helical foil turbine, for a tow speed of 1.3 m/s, and strut positions from 0.123 to 0.900 m.

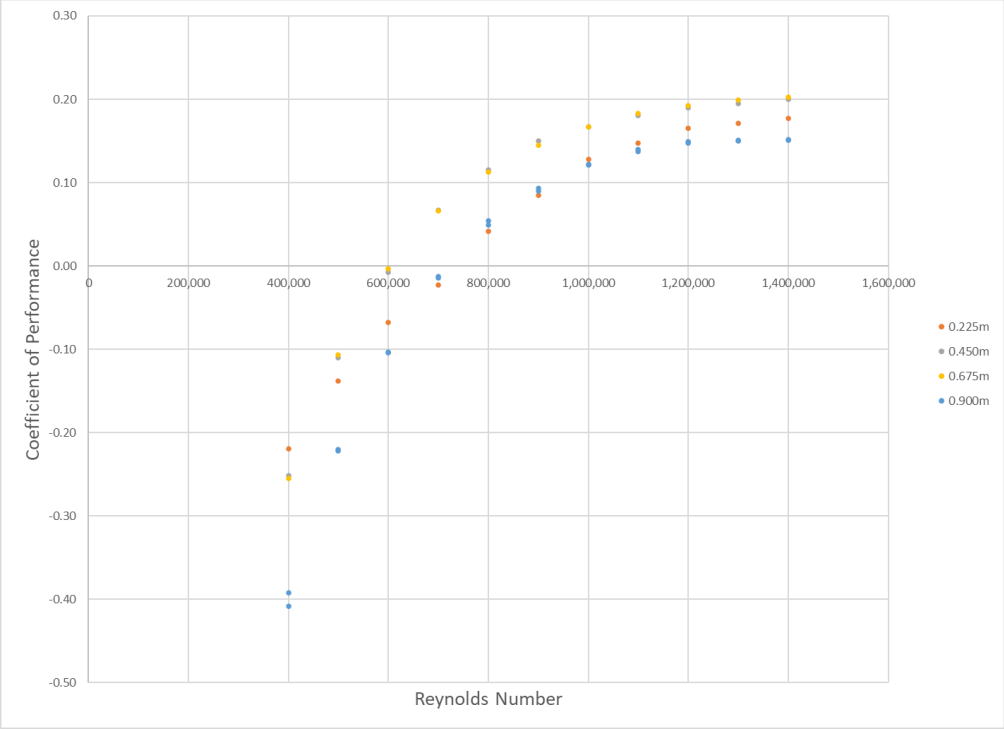

Figure 36: Average Coefficient of Performance at a Tip Ratio of 3.20 for glass composite straight foil turbine for different Reynolds Number (different tow speeds).

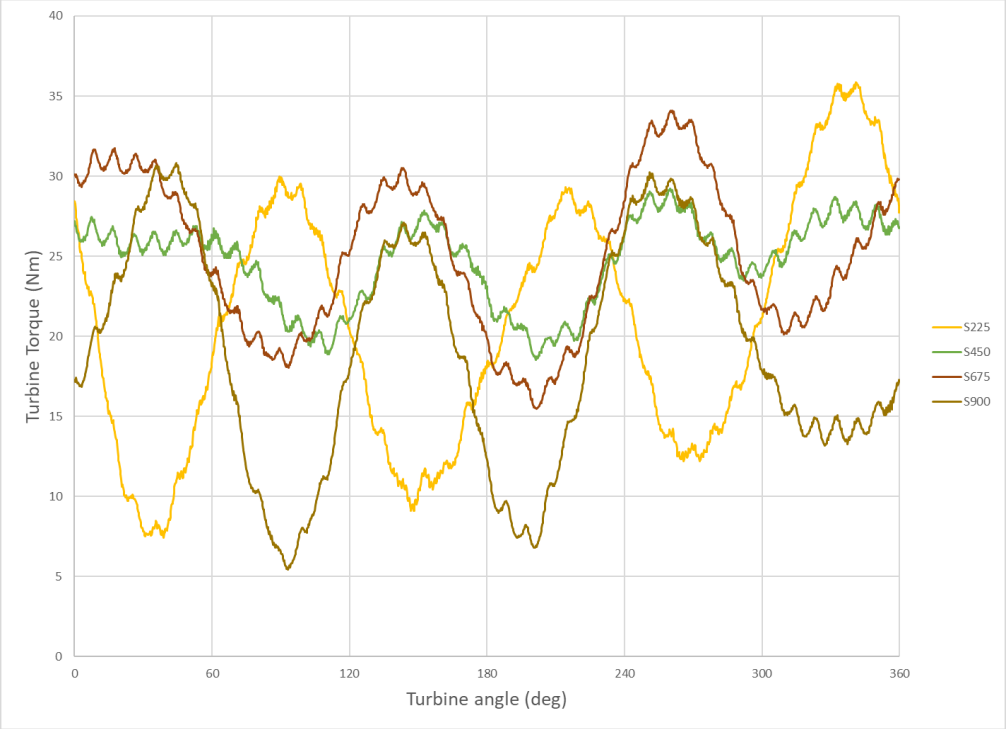

Figure 37: Turbine torque as a function of turbine angular position for glass helical foil turbines with different strut positions.

The helical turbine is highly twisted when compared with full scale ORPC turbines, with a helical angle of 135 degree/m as compared to a typical twist of 27 degree/m for a full-scale turbine. This large helical twist was chosen to provide a minimum of oscillation in turbine torque and drag during rotation for this model scale test.

1.10.2 Helical Foil Glass Composite Turbine Structural Results

Strain data for the helical glass composite foil turbine for various struts locations is shown in the following figures. The data is presented in two charts. The leftmost chart shows the strain on the outside surface of the foil along the length of the fiber sensing element as a function of turbine angular position. The rightmost chart shows the strain on the outside surface and the inside surface at a stated spanwise location on the foil as a function of turbine angular position. The pattern of strain at any given point along the span can be inferred from these two plots. Note that compared with the previous tests, the strains are higher, and that the strain sensing seems less capable with significant amount of data dropouts.

These plots show a different x-axis scale when compared to prior plots of strain, since the fiber optic sensing element was embedded parallel to the leading edge of the helical foil. The glass helical foil is longer than the glass straight foil: 1.334m as compared with 0.900m for the straight foil.

Testing was not performed for the 0.123m strut spacing as strain values were too high for the material to sustain.

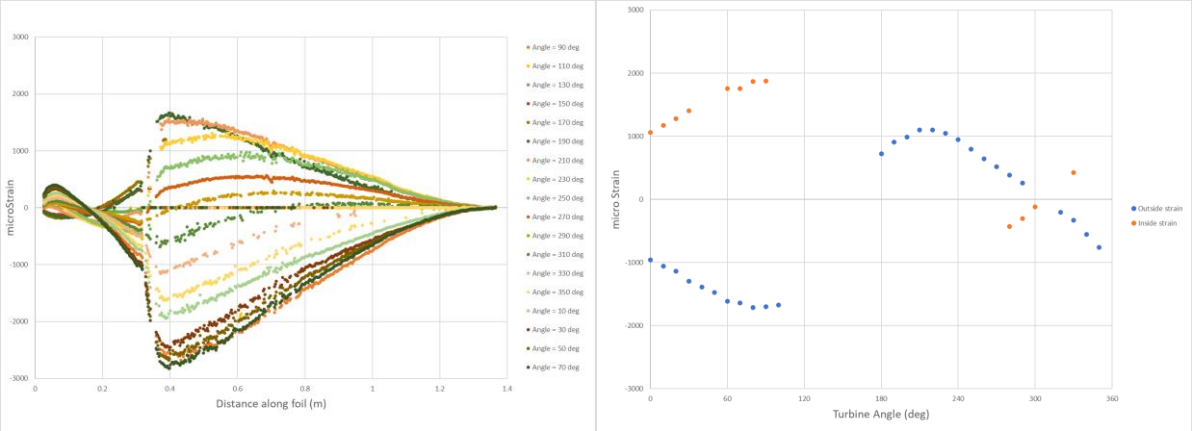

Figure 38: Strut location of 0.225m. Major strain in outermost ply of the outside surface for the helical glass composite foil along the foil span, for different turbine rotational positions (left). Major strain for the outermost plies on the outer and inner surface of the same foil as a function of turbine rotational position at location of 0.715m along gauge (right). Tip speed ratio is 3.00.

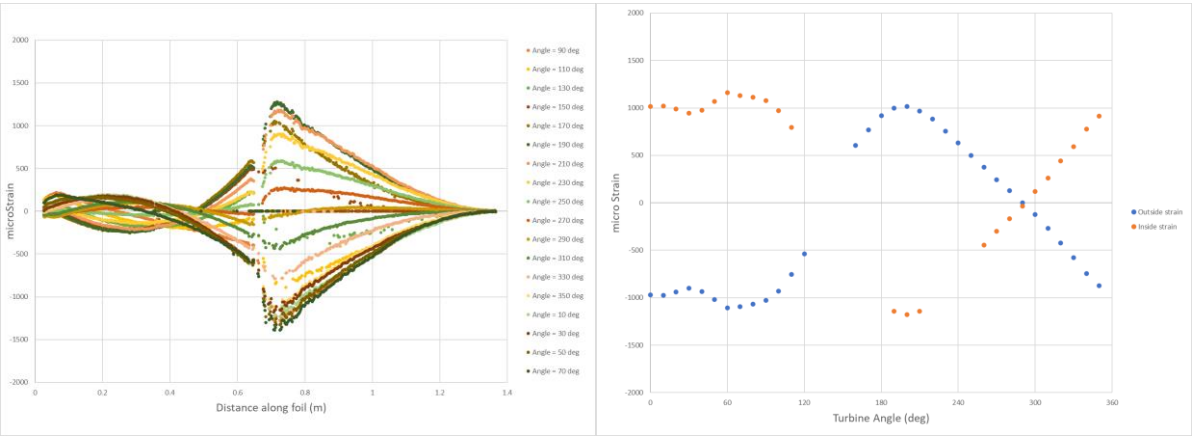

Figure 39: Strut location of 0.450m. Major strain in outermost ply of the outside surface for the helical glass composite foil along the foil span, for different turbine rotational positions (left). Major strain for the outermost plies on the outer and inner surface of the same foil as a function of turbine rotational position at location of 0.800m along gauge (right). Tip speed ratio is 3.00.

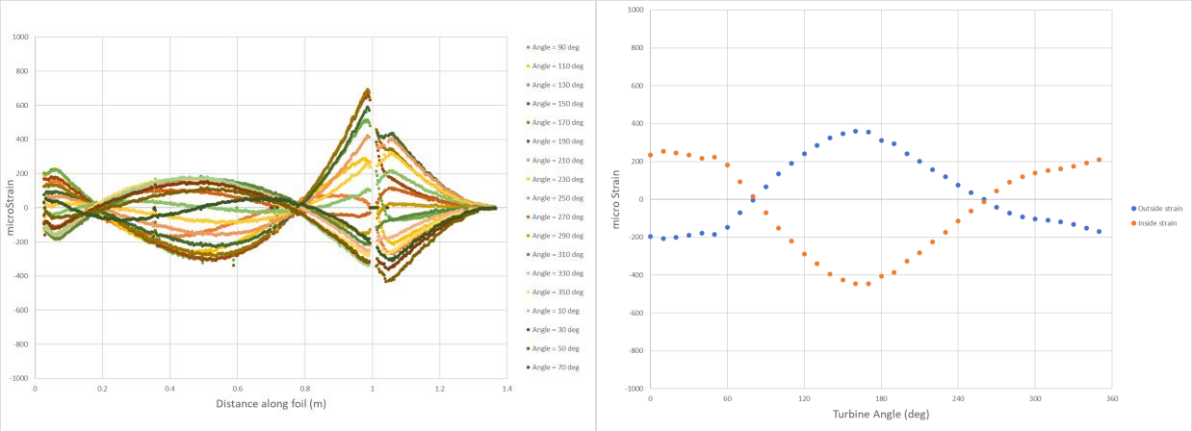

Figure 40: Strut location of 0.675m. Major strain in outermost ply of the outside surface for the helical glass composite foil along the foil span, for different turbine rotational positions (left). Major strain for the outermost plies on the outer and inner surface of the same foil as a function of turbine rotational position at location of 0.900m along gauge (right). Note change in scales compared with prior plots. Tip speed ratio is 3.00.

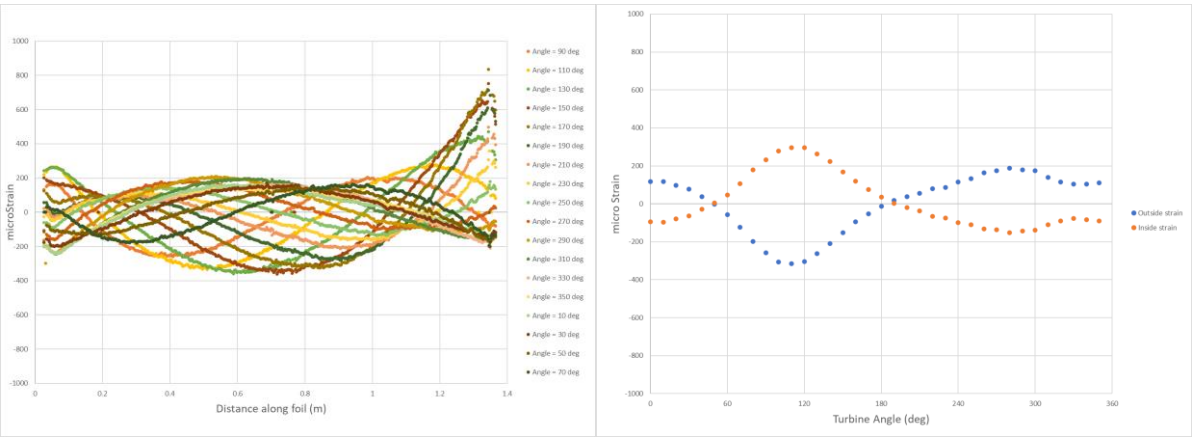

Figure 41: Strut location of 0.900m. Major strain in outermost ply of the outside surface for the helical glass composite foil along the foil span, for different turbine rotational positions (left). Major strain for the outermost plies on the outer and inner surface of the same foil as a function of turbine rotational position at location of 0.440m along the gauge (right). Note change in scale compared with prior plots. Tip speed ratio is 3.00.

1.11 Helical Foil 3D-printed Titanium Turbine Hydrodynamic Results

Tow testing was performed for the 3D printed titanium turbine. Initial tests were performed with the turbine in the as printed surface condition. The 3D printed material comprises sintered titanium particles and the as-printed part has a relatively rough surface finish of 20 to 22 µm Sa. The efficiency of the turbine in this configuration was negative.

The surface finish was improved by buffing, where the average surface roughness decreased to 6 to 13 µm Sa. The efficiency of the turbine in this configuration was positive.

For the smoother configuration the turbine was run at different Reynolds numbers to determine at which point the results became independent of Re.

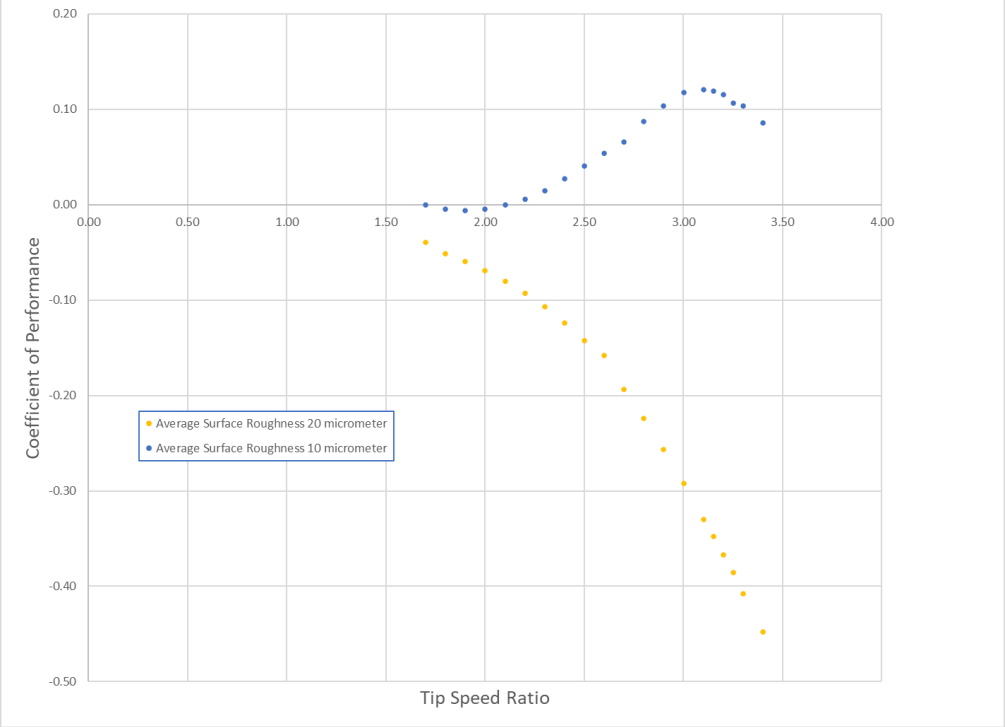

Figure 42: Average Coefficient of Performance vs. Tip Speed Ratio for 3D printed titanium helical foil turbine of different surface roughness. Testing performed at 1.3 m/s. Movable strut is located at 0.900m position.

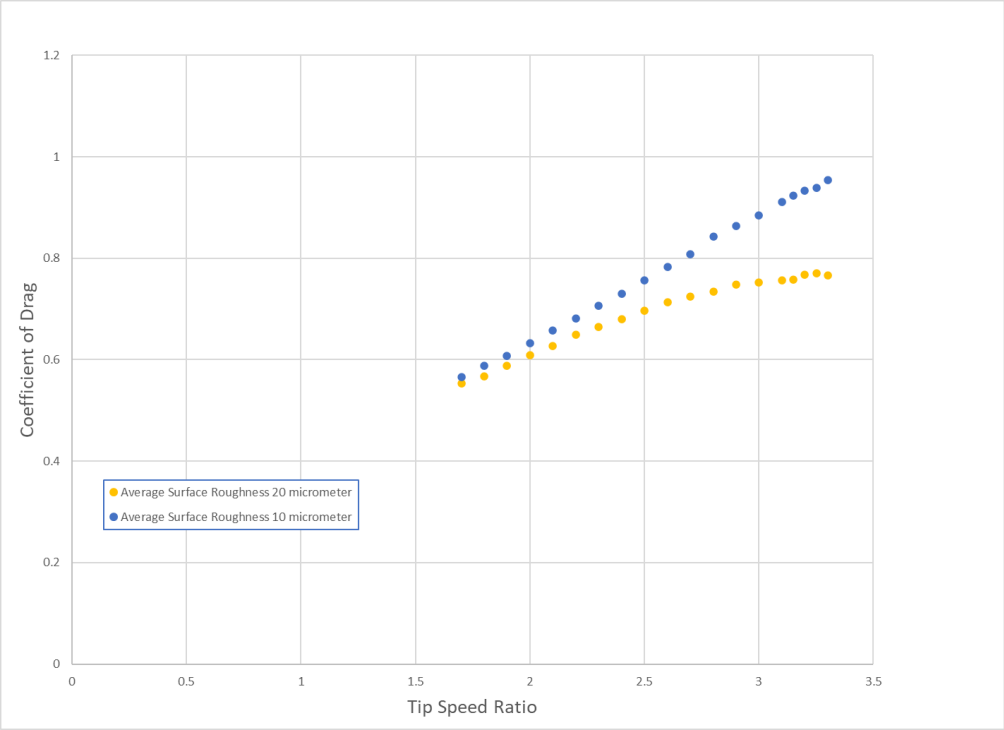

Figure 43: Average Coefficient of Drag vs. Tip Speed Ratio for 3D printed titanium helical foil turbine of different surface roughness. Testing performed at 1.3 m/s. Movable strut is located at 0.900m position.

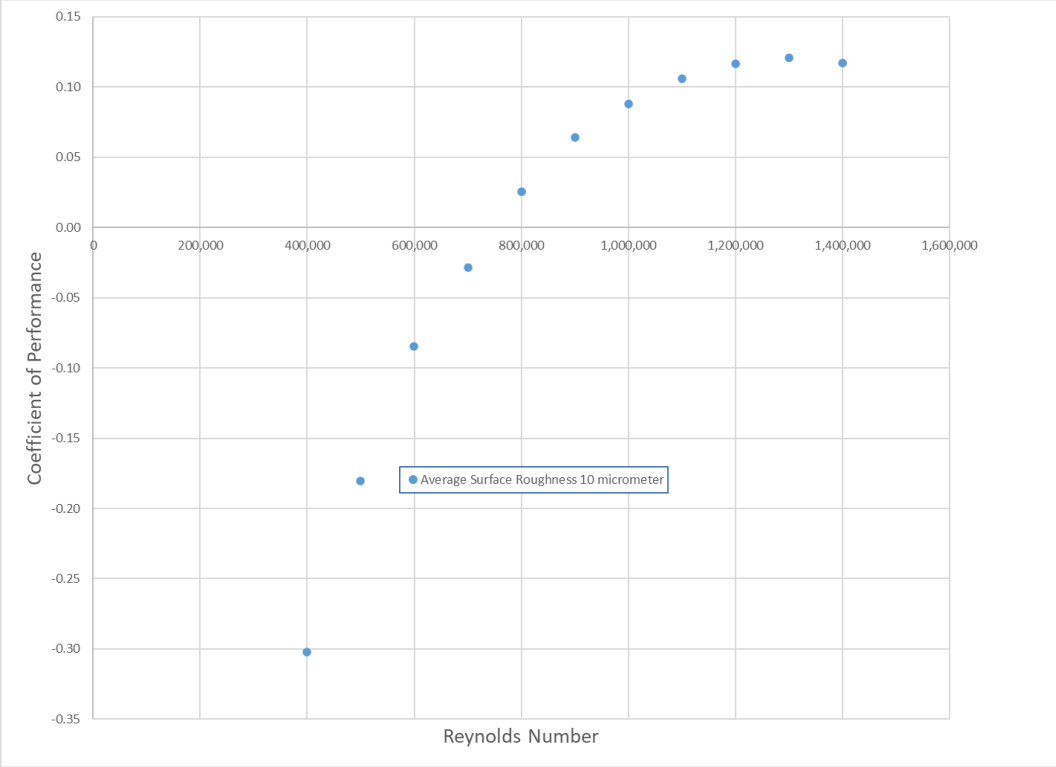

Figure 44: Average Coefficient of Performance at a Tip Ratio of 3.1 for 3D printed titanium helical foil turbine of given surface roughness for different Reynolds numbers. Testing performed at 1.3 m/s. Movable strut is located at 0.9m position.

1.12 Comparison of Data

Table 7 provides a summary of some data from the tank testing. Maximum and minimum strain values for the outer strain fiber are provided. For each of the test setups these maxima and minima will occur at different locations along the foil span, and at different turbine angular positions. These values will depend on flow speed, tip speed ratio, as well as the strut location and the material composition of the foils. A strain range is calculated from the max and min values, but this should only be used as a guide to the range of strain that a particular setup may experience, as it is possible that max and min values of strain will not occur at precisely the same location on the foil. The largest Cp is provided for each test setup.

Table 7: Summary of data from tank testing

		Max Tensile Strain (microStrain)	Max Compressive Strain (microStrain)	Strain range (max - min) (microStrain)	Max Coefficient of Performance	Tip Speed Ratio
Carbon Straight Foil	S123	769	-278	1,047	0.256	2.40
Carbon Straight Foil	S225	573	-217	790	0.273	2.40
Carbon Straight Foil	S450	257	-105	362	0.284	2.40
Carbon Straight Foil	S675	84	-96	180	0.292	2.40
Carbon Straight Foil	S900	70	-224	294	0.306	2.40
Glass Straight Foil	S123	3,265	-1,545	4,810	0.232	2.40
Glass Straight Foil	S225	2,625	-1,014	3,639	0.253	2.40
Glass Straight Foil	S450	1,170	-473	1,643	0.285	2.40
Glass Straight Foil	S675	455	-388	843	0.292	2.40
Glass Straight Foil	S900	441	-806	1,246	0.294	2.40
Glass Helical Foil	H225	4,487	-2,827	7,314	0.171	3.00
Glass Helical Foil	H450	1,281	-1,430	2,711	0.198	3.00
Glass Helical Foil	H675	697	-432	1,129	0.201	3.00
Glass Helical Foil	H900	835	-361	1,196	0.154	3.00
Titanium 3D printed Foil	H900				0.058	3.00

1.12.1 Carbon Straight Foil Data

Comments on the hydrodynamic performance data presented for the straight carbon composite foil turbine.

- Maximum Cp occurs in the region of TSR of 2.5 for all tests.
- Test results are dependent on tow tank speeds up to a tow speed of 1.1 m/s (Figure 9, Figure 13).
- Maximum value of Cp increases as the strut spacing increases (Figure 10).
- Values of Drag Coefficient are independent of strut spacing (Figure 12).
- Turbine torque as a function of turbine angle appears mostly unaffected by strut position (Figure 14).

Comments on the strain data presented for the straight carbon composite foil turbine.

- Strain magnitude generally increase as unsupported length increases.
- Strain reflects patterns generally expected from distributed loads on beams.
- Strain is symmetric between inner and outer surfaces, indicating a pure bending loading.
- Highest strain occurs at larger turbine angles for increasing tip speed ratios.

As the struts are moved, the strain range experienced by the foil changes significantly, with high strains experienced at the S123 strut location, which provides the lowest level of structural support to the foil. The strain pattern on the foil outer surface changes from a compressive to a tensile dominated strain as the struts are moved from the 0.900 through the 0.123m positions.

The hydrodynamic performance of the turbine is reduced as the stiffness of the setup is reduced.

1.12.2 Glass Straight Foil Data

Comments on the performance data presented for the straight glass composite foil turbine.

- Maximum Cp occurs in the region of TSR of 2.5 for all tests.
- Test results are dependent on tow tank speeds up to a tow speed of 1.1 m/s (Figure 21, Figure 25).
- Maximum value of Cp increases as the strut spacing increases (Figure 22).
- Values of Drag Coefficient are somewhat dependent on strut spacing (Figure 24).

- Turbine torque as a function of turbine angle is somewhat different for different strut positions (Figure 26).

Comments on the strain data presented for the straight glass composite foil turbine.

- Strain magnitude generally increase as unsupported length increases.
- Strain reflects patterns generally expected from distributed loads on beams.
- Strain is symmetric between inner and outer surfaces, indicating a pure bending loading.
- When the strain values exceed 0.1 percent strain, strain data is often dropped.

The strain pattern for the glass foils follows similar behavior to the carbon foil case, but with strain values approximately 4.6 times higher.

The hydrodynamic performance of the turbine is reduced as the stiffness of the setup is reduced as was the case for the carbon foils, but with a slightly overall smaller max Cp for all setups.

1.12.3 Glass Helical Foil Data

Comments on the performance data presented for the helical glass composite foil turbine.

- The shapes of the Cp/TSR curves for this helical turbine are fundamentally different than for the straight foil turbines. The maximum Cp value is lower and occurs at a higher TSR value.
- Maximum Cp occurs in the region of TSR of 3.1 for a flow speed of 1.3m/s (Figure 32)
- The location of the struts has a significant effect on the maximum value of Cp (Figure 33)
- Tow speed does not have a large effect on the Coefficient of Drag (Figure 34)
- Strut location has a small effect on the Coefficient of Drag (Figure 35)
- Higher tow test speeds were achievable for the helical turbine (Figure 34)
- Turbine torque patterns show differences for different strut positions (Figure 37)

Comments on the strain data presented for the helical glass composite foil turbine.

- Since the turbine is helically twisted, strain along the foil is a composite of strain at different angular locations relative to the flow. This complicates the interpretation of these data.
- It appears that strains at the movable upper strut are higher than at the lower strut.

The helical turbine is hydrodynamically very different from the straight foil turbines. Fundamental behavior has changed, with the optimum tip speed ratio shifting from 2.40 for straight foils to 3.00 for the helical turbines. The helical foil is almost 50 percent longer in length than the straight foil due to the helical twist. Strains are significantly larger.

1.12.4 Carbon Straight Foil vs. Glass Straight Foil Data

We can compare the performance of the straight foil data sets.

The glass foil strains are approximately 4.6 times higher than those for the carbon foils, as would be expected based on the materials properties of carbon and glass composites. The reduction in stiffness for the glass composite foil is perhaps more than would be expected based on the design material properties. Based on the strain values we would expect that the glass foils move ~4 times more than the carbon foils during turbine rotation.

The hydrodynamic performance reduction from carbon to glass composite foils is very small and may well be within the error bounds of the test. This indicates that while stiffness is important from a structural viewpoint, its impact on hydrodynamic performance may be less than expected.

1.12.5 Glass Helical Foil vs. Glass Straight Foil Data

The helical turbine tested is a highly twisted turbine and may as a result be introducing additional hydrodynamic effects when compared with the straight foil turbines.

Given the magnitude of the performance shift it may not be possible to make any direct comparison with straight foil performance. The large reduction in Cp for the helical glass turbine is more likely due to changes in the turbine shape than in the turbine stiffness.

The helical turbine exhibits lower average torque values than the equivalent straight foil turbine, but also exhibits much lower torque oscillations as expected. However, the torque oscillation is still not reduced to a negligible level.

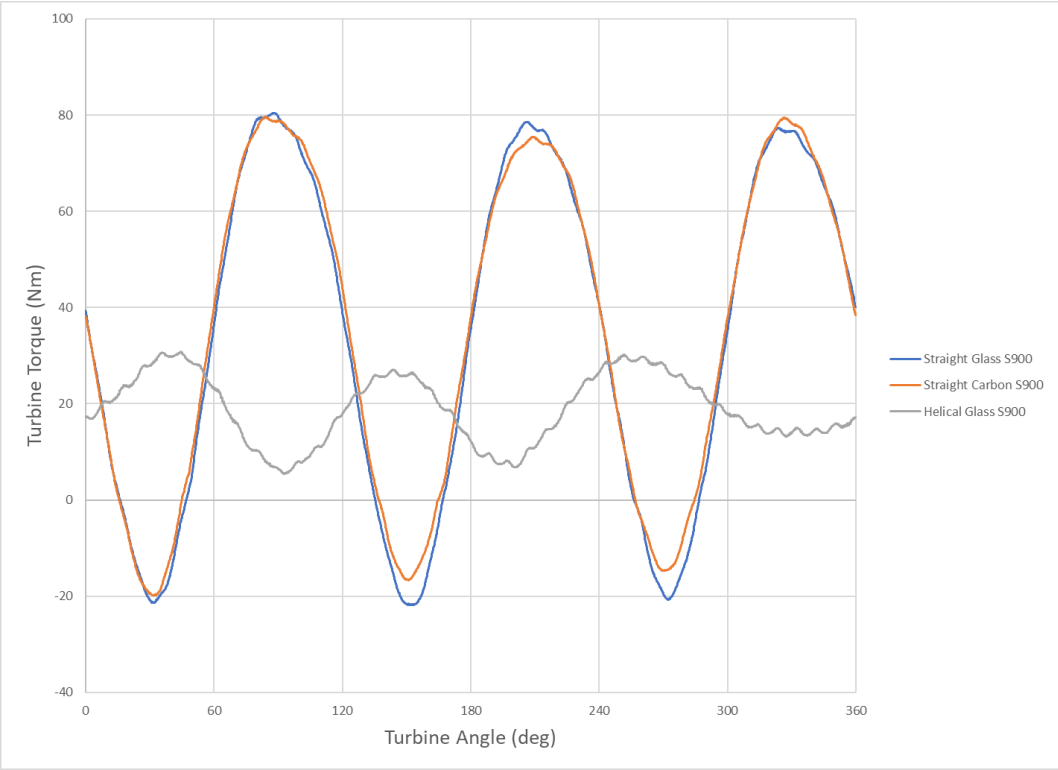

Figure 45: Turbine torque for carbon straight, glass straight, glass helical turbines as a function of turbine rotational position. Torque shown is at 1.1 m/s for the straight foils, and 1.3 m/s for the helical foils. Torque production for the helical turbine is lower than for straight foils, but also has a smaller oscillation range.

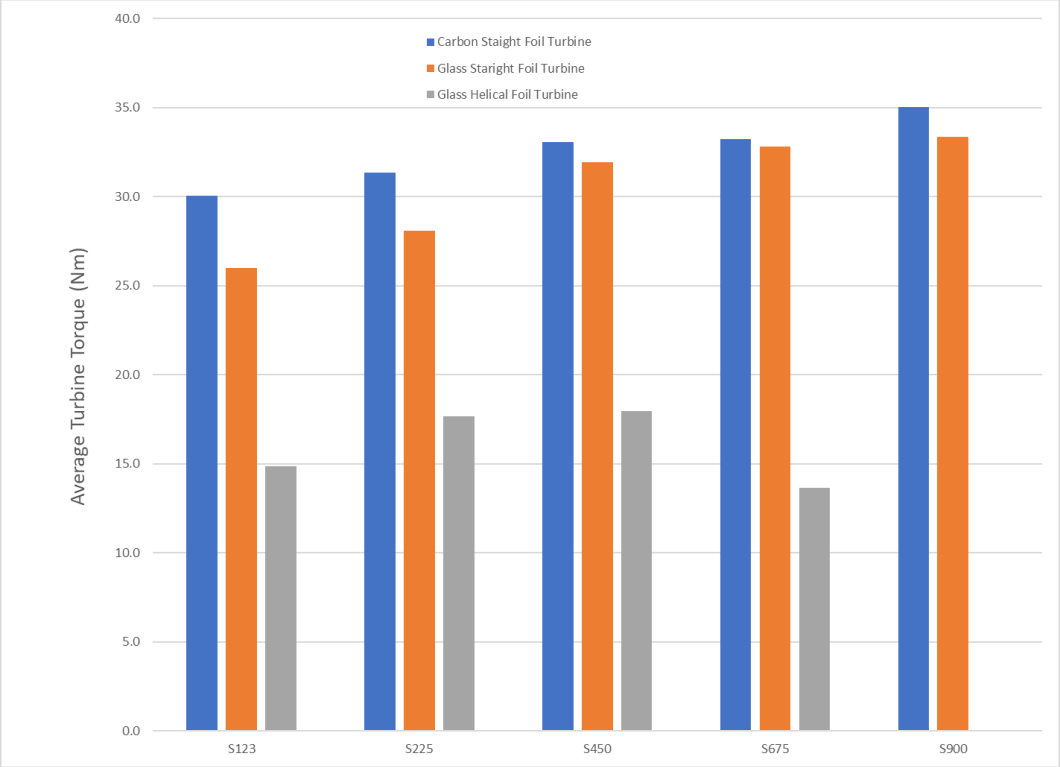

Figure 46: Average turbine torque for carbon straight, glass straight, glass helical turbines for different strut positions. In this plot the average torque for the glass helical foil turbine is scaled to a 1.1 m/s flow speed for direct comparison with the straight foil data.

1.12.6 Titanium Helical Foil vs. Glass Helical Foil Data

The Cp for the titanium helical turbine is lower than that for the glass helical turbine, even though the stiffness of the titanium turbine is greater. The major effect of surface roughness on the results (Figure 42) shows that surface finish at this model scale is more significant than stiffness of the system. Additional investigation will be required to determine relative effects.

1.13 Task 1 Summary and Milestones Status

Tow tank testing of different implementations of cross flow turbine was completed.

High quality strain and performance data was collected for the tested configurations.

Milestones were completed as follows:

Table 8: Task 1 Milestone Summary

Milestone 1.1	Test plan for scale model testing completed with best practices identified and accounted for in testing methodology. Data acquisition system (DAQ) design will define instrumentation, resolution, and accuracy requirements to validate FSI models; simulated datasets will have been post-processed to verify DAQ requirements.
Status	Complete
Deliverable	EE0008386 Deliverable 1.1 UNH experimental test plan.pdf

Milestone 1.2	Completed design for test foils. Analytical models of scale model foil performance will predict achievement project target objectives for full-scale efficiency, system performance and costs improvements.
Status	Complete
Deliverable	EE0008386 Deliverable 1.2 Design for Test Foils.final.pdf

Milestone 1.3	Scale model foils built and prepared for tank testing. Foils will have been verified to meet structural and dimensional specifications per scale test requirements.
Status	Complete
Deliverable	EE0008386 Deliverable 1.3 Scale Model Foil Build.pdf

Milestone 1.4	Testing of all turbines completed, data processed, and results summarized. Test results will be complete and validate performance predictions from analytical models to achieve project objectives for efficiency, system performance and costs.
Status	Complete
Deliverable	This final report serves as deliverable for M1.4

2.0 Task 2: Fluidic and Structural Modeling of Hydrokinetic Turbines

2.1 Task Summary

ORPC will develop fluidic and structural modeling methods which can be used to design and analyze high-deflection foils.

2.2 Low-order Fidelity Modelling

At the beginning of the project, the intent was to focus on using low order computational methods such as momentum models, panel and vortex models, and simple beam-element structural models for FSI modelling. ORPC worked to develop such low-order analytical methods to guide design of high deflection foils. These analytical methods provide one-way fluid structure analysis, taking hydrodynamic loadings and applying the loadings to structural models to estimate deflections. The work investigated multiple approaches, with varying degrees of success. Some of the analytical paths were followed but were deemed inadequate to the task or were assessed to be computationally intense with insufficient benefit. None of the low-order methods are fully capable of taking the structural deflections as inputs to hydrodynamic models.

ORPC completed this effort and determined that the project should focus instead on computational fluid dynamics methods.

2.3 Computational Fluid Dynamics

ORPC focused hydrodynamic analysis efforts on Reynolds Averaged Navier-Stokes (RANS) methodologies. A review of the various commercial codes available indicated that licensing models for use of these codes would lead to a prohibitively large computational cost. Open-source RANS codes were investigated, and OpenFOAM was selected as a CFD tool which appeared to be scalable and cost effective. The opensource nature of the code also offered the ability to modify the code if such modification was needed for a fluid-structure interaction analysis.

2.4 Structural Analysis

In keeping with the desire to use scalable, opensource tools, ORPC focused on using Calculix[2] for structural analysis. Calculix uses an Abaqus type input deck which allows for reading and editing of deck entries in the American Standard Code for Information Interchange (ASCII). As the project developed ORPC tended towards using Nastran type deck inputs instead of Abaqus.

2.5 CFD Validation

To provide validation of the CFD code, settings, and solution parameters ORPC conducted several validation exercises. An analysis of a 2D static airfoil problem was conducted. The analysis was expanded to a pitching airfoil problem. Analytical results were compared with empirical data.

2.6 2D CFD -Static Foil

A test case for a NACA0012 airfoil was used to assess performance of mesh settings and turbulence models. Meshes were generated with ORPC determined mesh parameters.

Runs were performed for a range of angles of attack. Finer time steps were required for convergence as flow approached separation.

Empirical data was obtained from Ladson[3].

A panel code analytical tool Xfoil[4], was also used for comparison purposes.

The Spalart-Almaras[5] (SA) and the k-ω SST[6] models turbulence models were assessed.

Runs were performed with and without wall functions. For the cases without wall functions, y+ values of order ~1 were used. Table 9 summarizes the results. A root mean square (RMS) error is calculated to compare the CFD predictions with the empirical data.

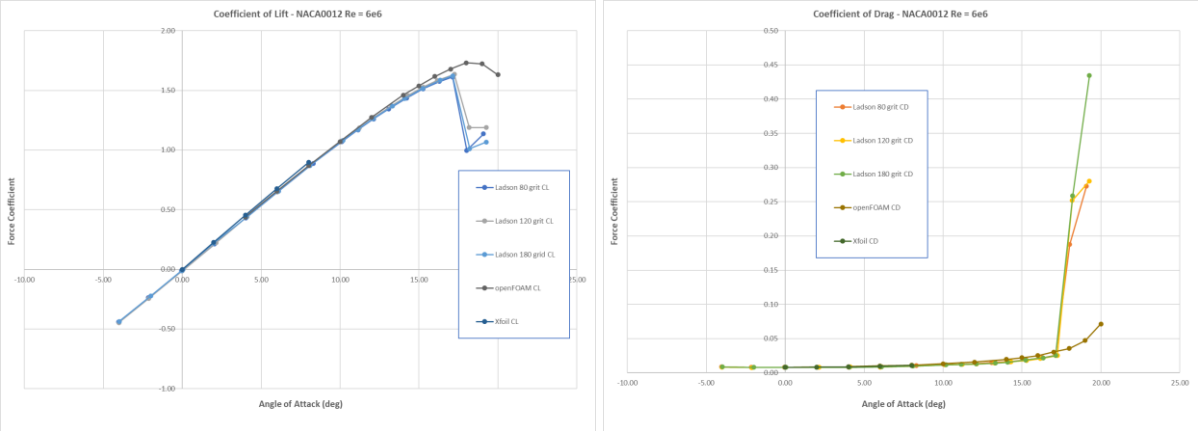

Figure 47: OpenFOAM predictions for Coefficient of Lift and Drag using Spalart-Almaras turbulence model as compared with empirical data and XFoil predictions.

[2] CALCULIX: A Three-Dimensional Structural Finite Element Program
[3] 2D NACA 0012 Airfoil Validation (nasa.gov)
[4] https://web.mit.edu/drela/Public/web/xfoil/
[5] Spalart-Allmaras Model (nasa.gov)
[6] OpenFOAM: User Guide: k-omega Shear Stress Transport (SST)

Table 9: Summary of lift and drag errors for two turbulence models in OpenFOAM for a NACA0012 case

	Root Mean Square Error			
	SA	*kω SST*	*SA - wall function*	*kω SST - wall function*
CD (0 to 16 deg)	0.003	0.009	0.028	0.008
CD (16 to 20 deg)	0.199	0.166	0.096	0.047
CL (0 to 16 deg)	0.023	0.048	0.157	0.059
CL (16 to 20 deg)	0.515	0.264	0.217	0.205

- For attached flows the SA model follows drag better.
- For attached flows the SA model follows lift better.
- For separated flows the SA performs well for drag, but oddly the wall function version of the kω-SST model performs better.
- For separated flows the wall function models appear to be marginally better, and the SA model performs worst, but agreement with empirical data is poor in either case.

2.7 2D CFD -Pitching Foil

A further refinement is to examine the ability of the RANS solver to predict behaviors from oscillating foils compared to test data[7] for pitching foils over a wide range of conditions.

The pitching function is expressed as a sinusoidal variation of pitch around a fixed pitch value. The reduced frequency parameter is used to characterize the rate of the pitch oscillation.

$$reduced\ freqency = \frac{\omega\ c}{2V}$$

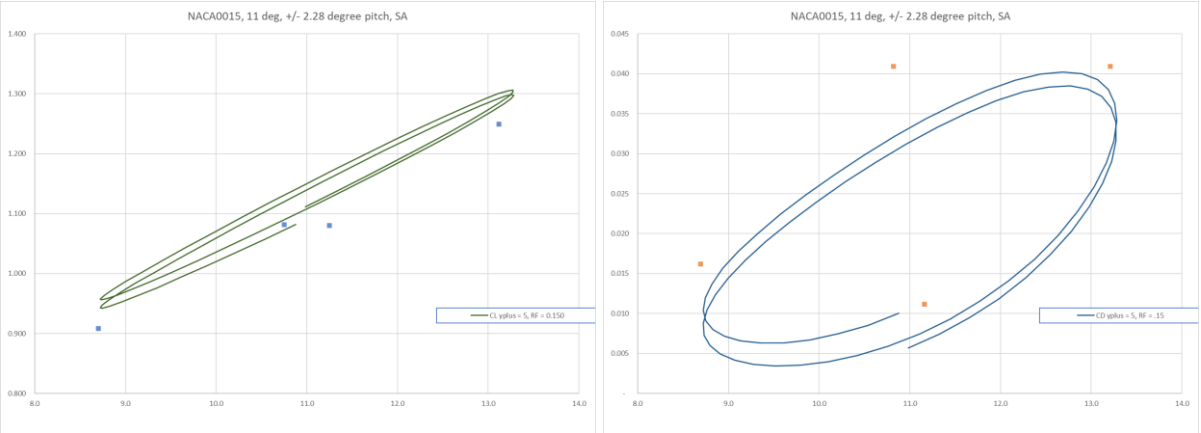

Figure 48: CD and CL for a pitching foil with 11 +/- 2 degrees, reduced frequency = 0.190, as compared with data from Piziali. NACA0015 profile.

Additional cases were run with higher values of reduced frequency.

From this work ORPC concluded:

[7] Piziali NASA TM 4632 2D and 3D Oscillating wing aerodynamics for a range of angles of attack including stall

1) SA turbulence model is easier to implement, than the kω-SST model which requires entry of multiple constants. The kω-SST does not seem to improve accuracy relative to empirical data.

2) A y+ of approx. 5 is suitable for SA model.

3) Flow separation is not well captured in OpenFOAM by either turbulence model.

4) Lift is well predicted by the OpenFOAM models.

5) Drag is often overpredicted for static OpenFOAM models, but underpredicted for the pitching model cases.

2.8 3D CFD Tests

To evaluate the settings required for a 3D CFD solution a simplified 3D mesh consisting of only the scale model turbine straight foils and the UNH tank geometry was created. This model ignores turbine shafting, struts, and the turbine model support structure in the tank.

3D CFD models were setup for each of the straight foil model cases tested in the UNH tow tank.

Two initial meshes were created: a fine mesh and a coarser mesh. For both meshes only the cells in the rotor zone were adjusted, with cells in the volume domain the same for both meshes.

A run for TSR 2.75 was completed for both meshes, with two complete final rotations for each of time steps equivalent to 8,4,2, and 1 degree.

The M1 and M3 meshes results in y+ values of order 1.

A coarser mesh, M4, was created with y+ values for the foils of order 30. Wall functions are active for this mesh.

Table 10: Mesh Density study. Rotor zone cells.

	Rotor Zone Mesh					
Mesh	Pentagon cells	Hexagon cells	Polyhedral cells	Total number of cells	Initial Layer height (mm)	Number Layers
M1	65,844	7,422,516	6,622,631	14,110,991	0.005	25
M3	44,604	5,028,156	1,620,731	6,693,491	0.010	22
M4	10,620	1,179,180	1,627,707	2,817,507	0.300	6

A comparison of time step (in degrees), Mesh density, and use of wall functions indicates that the only significant outliers are when time step is greater than 6 degrees.

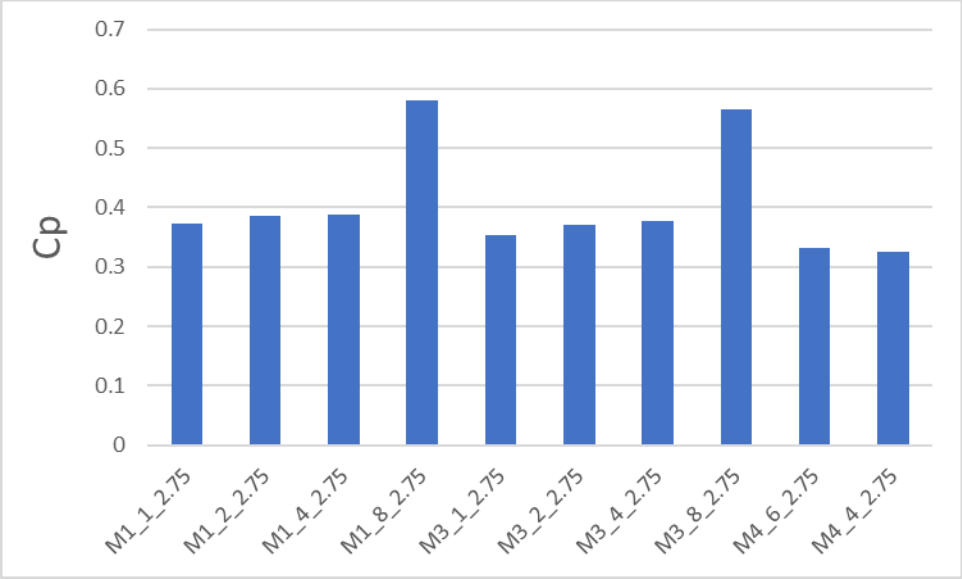

Figure 49: Sensitivity of Cp to mesh settings

A time step of less than 6 degrees is adequate.

The M1 model was run for more than 3 rotations. The average MZ value continues to reduce but only marginally after rotation 5.

Table 11: Number of rotations required for rotor torque convergence

Rotation	Average rotor torque (Nm)	% Difference from previous rotation
1	32.13	
2	21.55	67.08%
3	19.87	92.21%
4	19.34	97.35%
5	19.16	99.04%
6	19.00	99.19%

Only 5 rotations are required to establish a steady state.

2.9 3D CFD Straight Foil Turbine Meshing

Using the settings determined from the previous sections, ORPC created CFD meshes for a straight foil turbine with the movable strut located at the five different strut locations (0.123, 0.225, 0.450, 0.675, 0.900m). These meshes included the turbine strut and shaft geometry. In addition, the fixturing system for holding the scale model in the UNH tank was included in the model geometry.

These are large meshes which require substantial computational effort to solve. ORPC utilized cloud computing services to provide high performance computing (HPC) facilities for these analyses.

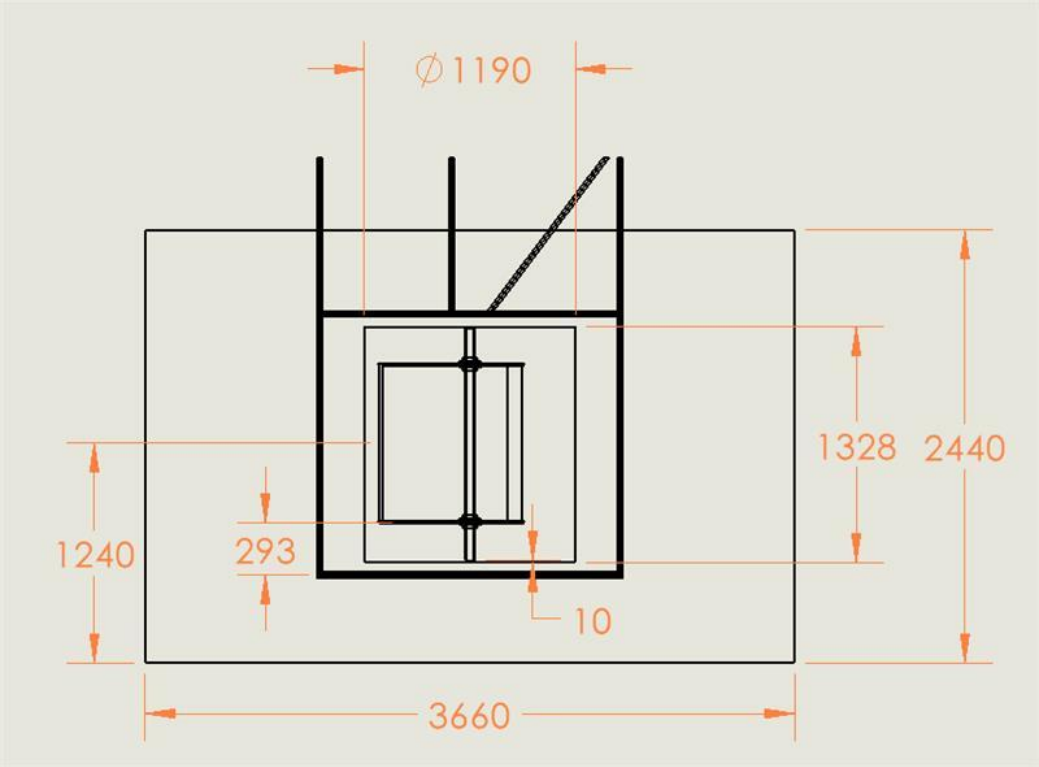

Figure 50: Cross sectional view of the test turbine setup in the UNH tow tank.

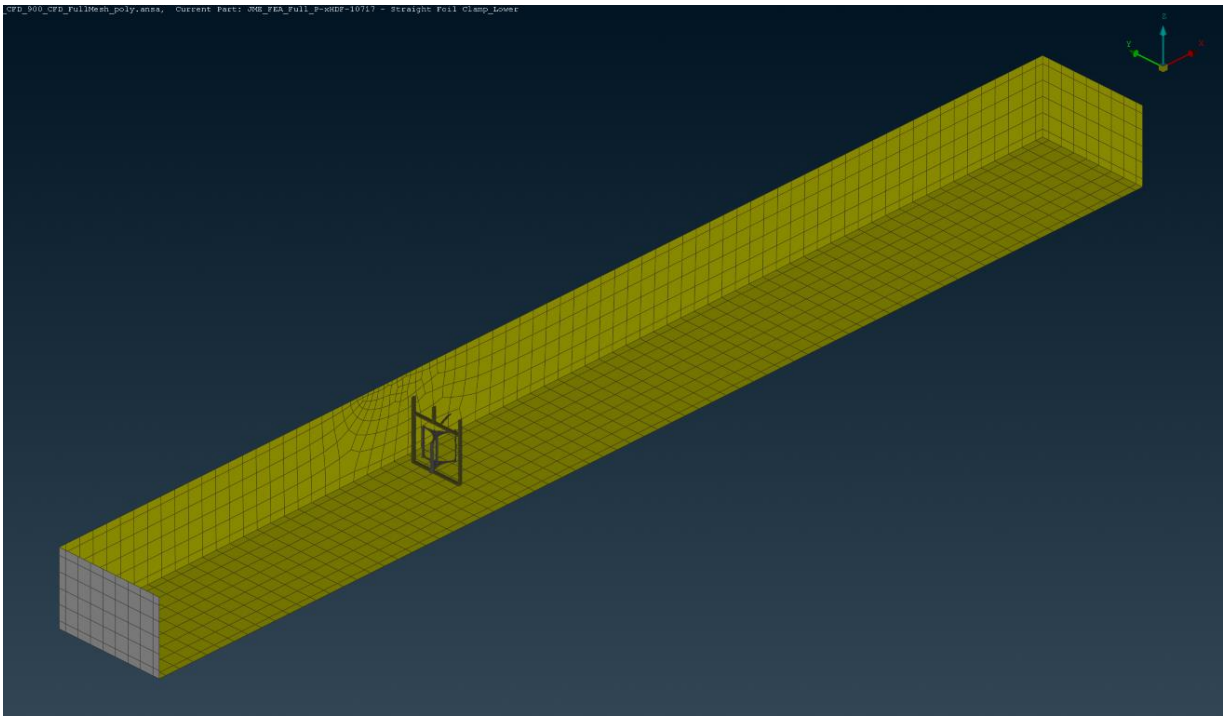

Figure 51: Isometric view of straight foil turbine domain. The dimensions of the UNH tow tank are used for the domain. The turbine is located at a fixed position in this domain and flow is in the x direction (left to right above).

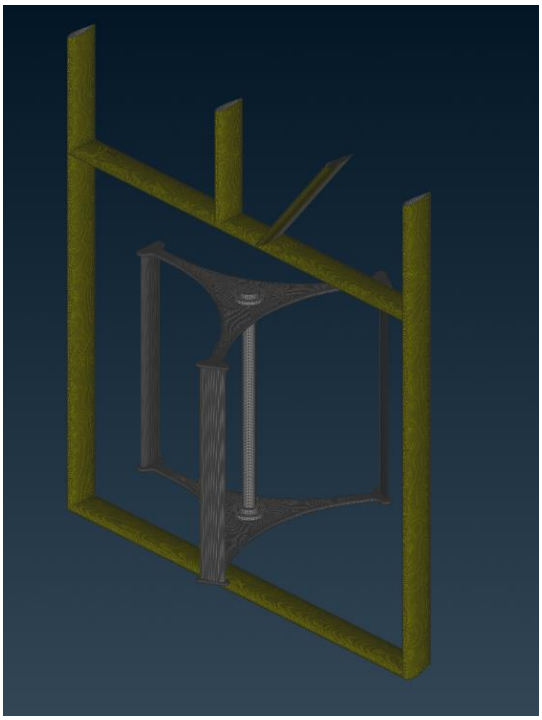

Figure 52: Isometric view of straight foil turbine rotor. The vertical and horizontal tank support structure for the turbine is shown. Some shaft connection details are not modelled to allow for separation of the static mesh and the rotating turbine rotor mesh.

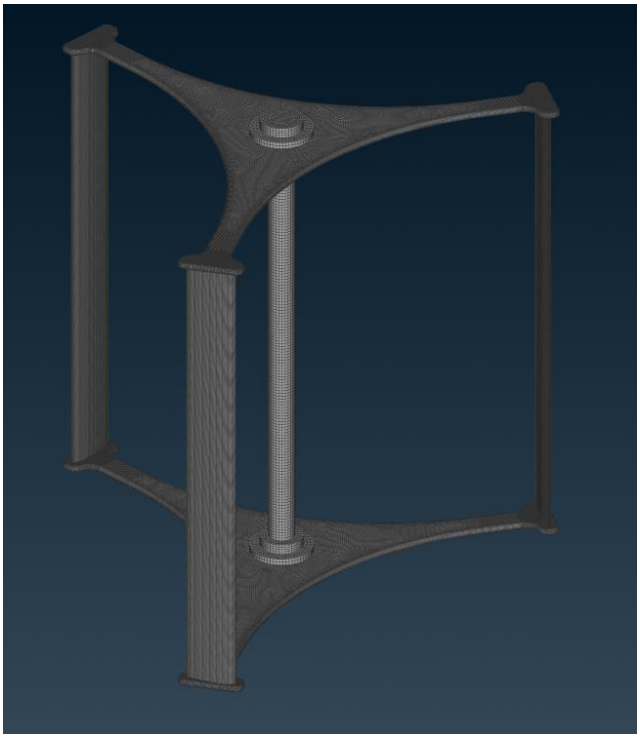

Figure 53: Isometric view of straight foil turbine surface mesh. The meshes used were quad dominant and aligned with the chord and span of the foil. The mesh is refined at the leading and trailing edges of the foil.

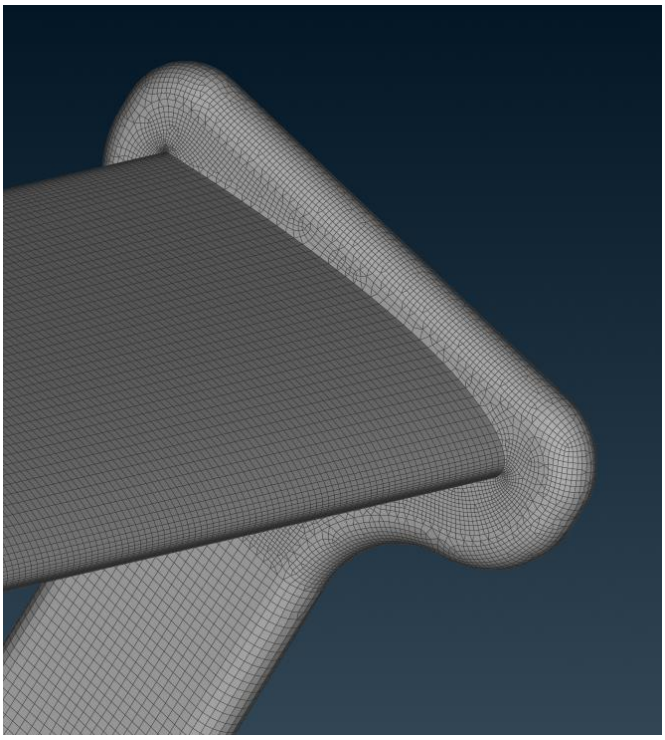

Figure 54: Detail view of surface mesh at the intersection of a strut and foil. For this area of the mesh, it was difficult to grow layers from the surface mesh due to the mesh refinement at the trailing edge, and the two perpendicular surface layer sets growing "into" each other.

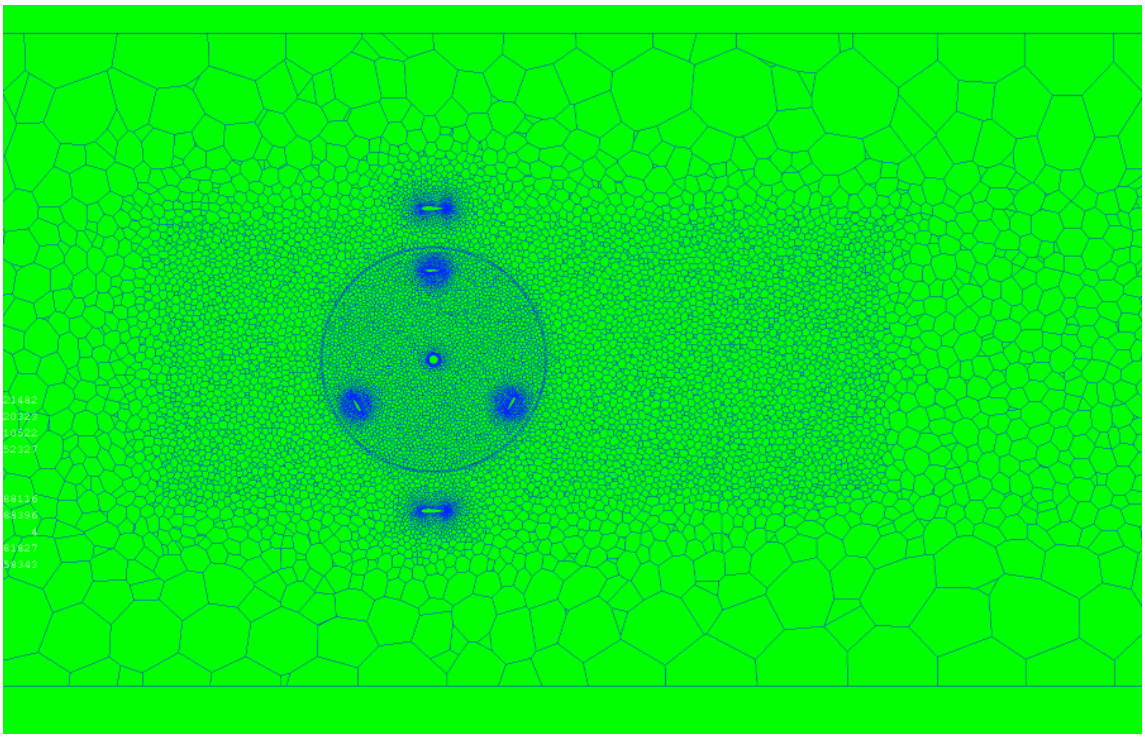

Figure 55: Cross sectional view of the rotor domain. The mesh shown is polygonal. Polygonal meshes were used where possible to reduce cell count, but in some cases, it was not possible to generate a high-quality polygonal mesh with the available tools, and hex and tetra meshes were used instead.

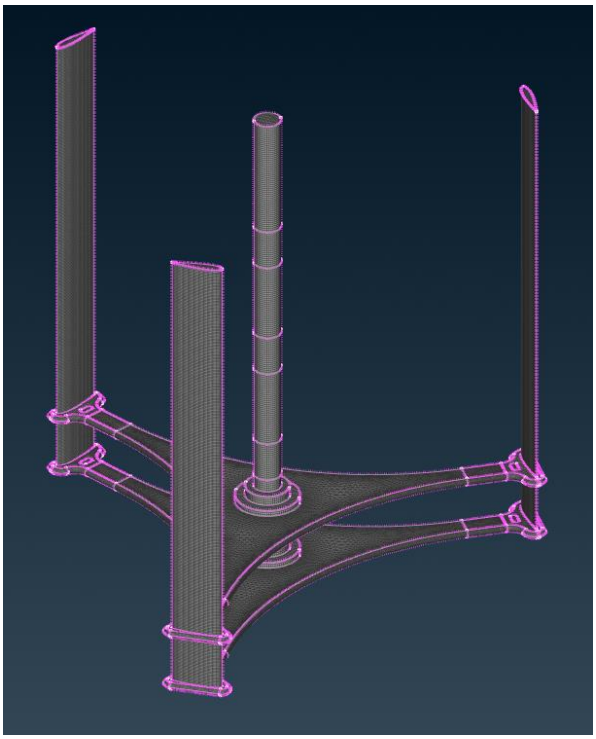

Figure 56: Isometric view of straight foil turbine domain with struts at the 0.123m location.

Table 12: Summary of straight foil mesh cell count.

Turbine	*Case*	*# Cells - Rotor Volume*	*# Cells - Rotor Volume*	*Total # cells*	*Solution CPU Hours*
Straight Foil	S123	16,667,958	3,221,903	19,889,861	6764
Straight Foil	S225	12,544,723	3,221,903	15,766,626	Continuation run
Straight Foil	S450	11,155,800	3,221,903	14,377,703	7208
Straight Foil	S675	13,117,664	3,221,903	16,339,567	5015
Straight Foil	S900	8,836,440	3,221,903	12,058,343	Continuation run

A continuation run in Table 12 indicates that the run had multiple restarts, and that an accurate calculation of CPU hours was not feasible as a result.

2.10 3D CFD Straight Foil Turbine CFD Results

Table 13 provides a high-level summary of the CFD results for the straight foil meshes. These are the results that would be expected from an infinitely stiff foil, with no foil deflection.

Table 14 provides values for moments on individual components for each case.

Table 13: Summary of CFD results for Straight Foil Meshes

Turbine	*Case*	*Strut Location (mm)*	*TSR*	*V (m/s)*	*Time Step (deg)*	*Cp*	*Cd*
Straight Foil	S123	123	2.4	1.1	4	0.295	0.950
Straight Foil	S225	225	2.4	1.1	4	0.298	0.949
Straight Foil	S450	450	2.4	1.1	4	0.298	0.952
Straight Foil	S675	675	2.4	1.1	4	0.297	0.949
Straight Foil	S900	900	2.4	1.1	4	0.320	0.969

Table 14: Moment values for straight foil CFD

Turbine	*Case*	*TSR*	*V (m/s)*	*Avg. Moment Foil 1 (Nm)*	*Avg. Moment Foil 2 (Nm)*	*Avg. Moment Foil 3 (Nm)*	*Avg. Moment Strut 1*	*Avg. Moment Strut 2*	*Avg. Moment Shaft (Nm)*
Straight Foil	S123	2.4	1.1	13.36	13.38	13.38	-3.20	-3.49	-8.04E-04
Straight Foil	S225	2.4	1.1	13.40	13.38	13.35	-3.04	-3.37	-4.28E-04
Straight Foil	S450	2.4	1.1	13.45	13.44	13.43	-3.11	-3.53	-9.11E-04
Straight Foil	S675	2.4	1.1	13.42	13.66	13.48	-3.32	-3.61	-7.60E-04
Straight Foil	S900	2.4	1.1	14.00	14.24	14.10	-3.11	-3.05	-7.61E-04

From Table 13, there is an increase in overall coefficient of performance as the struts are moved further away from each other.

From Table 14:

- The moment for each of the three foils is equal for all cases.
- The foil moment increases as the strut separation increases.
- The moment on the struts is large and negative.
- The moment on the shaft is negligible.

The parasitic moment from the struts account for a large reduction in turbine performance, reducing the Cp by approximately 6 percent points in all cases.

Figure 57 shows typical moment patterns for each of the components in a turbine as a function of turbine rotational position. Foil 1, 2, and 3 data are offset by 120 degrees as expected. Strut torque is negative. The total turbine torque pattern shows peaks of less than those of each foil, and a strong oscillatory pattern of three peaks per revolution.

Figure 58 shows pressure distribution along the span of a foil for the outer and inner surfaces. Pressures on the outer surface are positive, and pressures on the inner surface are negative. A large difference in pressure between inner and outer surfaces is desired. The cases presented are for the maximum strut separation (S900) and for the minimum strut separation (S123). In these plots there is a clear pattern at the free end of the foil which indicates tip effects for the S123 spacing, which explains some of the reduction of performance of this turbine configuration. For the S900 case there is pressure recovery at the tip due to the presence of the strut at this location.

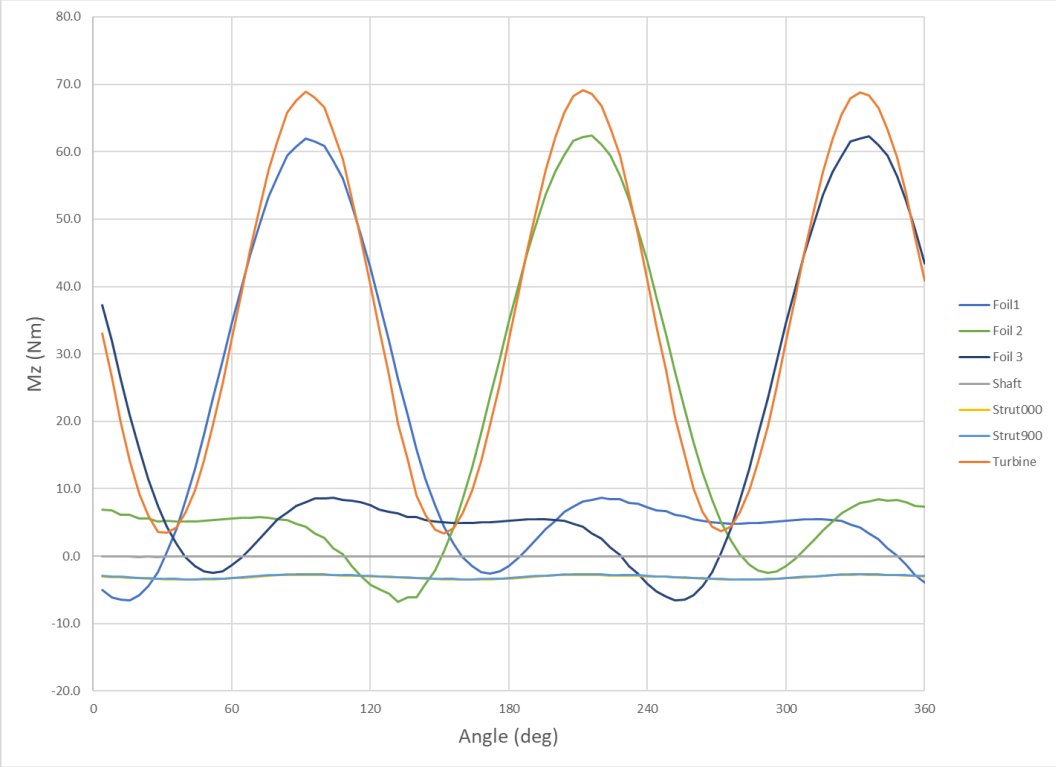

Figure 57: Straight foil case, with strut separation = 0.900m. CFD predicted moments on each component. TSR =2.40, U = 1.1 m/s.

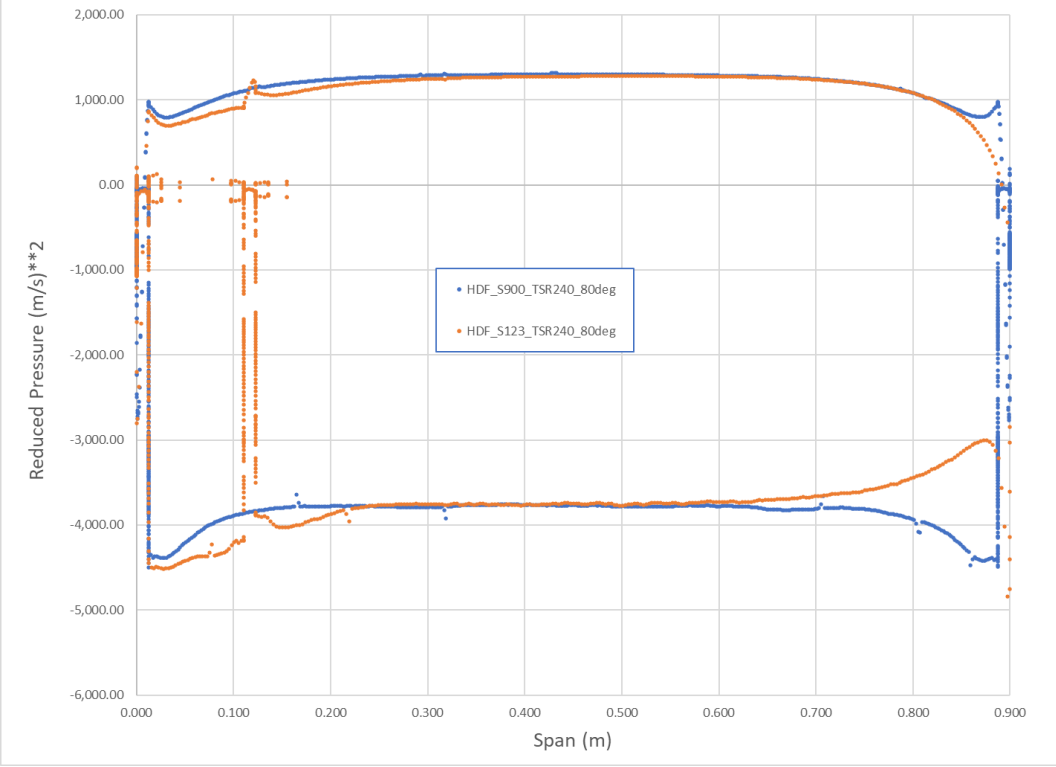

Figure 58: Pressure along the foil span for two different strut cases. TSR =2.40, U = 1.1 m/s.

2.11 3D CFD Straight Foil Turbine Comparison with Tow Tank Results

A comparison of the test data for both the carbon and glass straight foil turbines with the CFD results for an infinitely stiff straight foil turbine for different strut support cases is presented below.

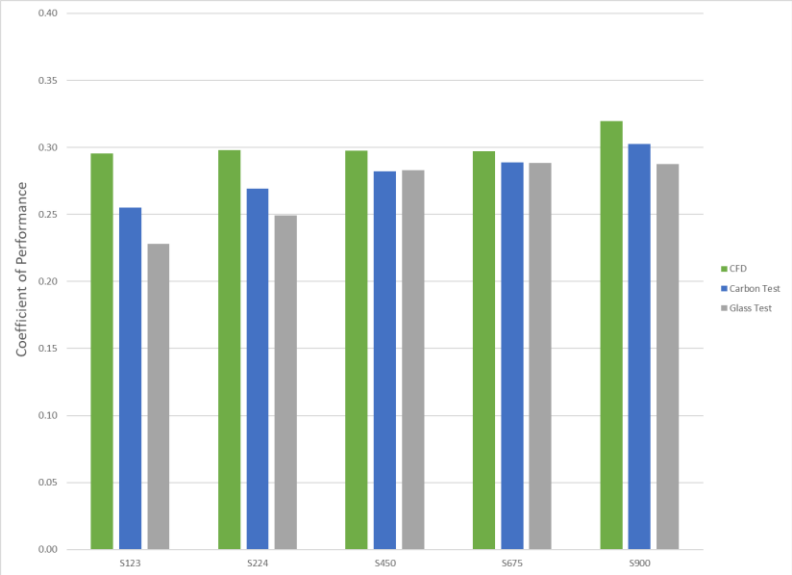

	Cp difference % - Carbon	*Cp difference % - Glass*
S123	-16%	-29%
S224	-11%	-20%
S450	-5%	-5%
S675	-3%	-3%
S900	-6%	-11%

Figure 59: Comparison of test data and CFD prediction for Coefficient of Performance: Straight Foil Turbine. TSR =2.40, U = 1.1 m/s.

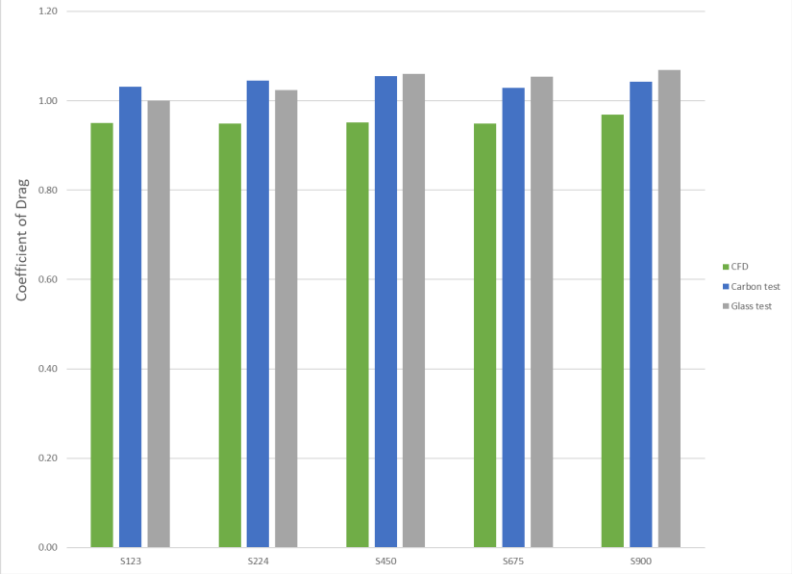

	Cd Difference % - Carbon	*Cd Difference % - Glass*
S123	8%	5%
S224	9%	7%
S450	10%	10%
S675	8%	10%
S900	7%	9%

Figure 60: Comparison of test data and CFD prediction for Coefficient of Drag: Straight Foil Turbine. TSR =2.40, U = 1.1 m/s.

Across the board the agreement between the 3D CFD results and the test data for the straight carbon foil turbine is very good. This is the case even without consideration of foil deflections. The CFD data tends to slightly overpredict Cp and underpredict Coefficient of Drag.

The agreement between the infinitely stiff results from the CFD and the glass turbine test is still very good for drag but is less so for the Cp values, with larger differences occurring for the S123 where the glass foil is most flexible.

We should acknowledge that the test data should be bounded by an error bar, which may be sufficiently large to make the carbon test data and the CFD data basically indistinguishable.

2.12 3D CFD Helical Foil Turbine Analyses

Using the same approaches as outlined above ORPC created analyses of the helical turbine tested in the tow tank. Maintaining sufficient mesh quality for 3D CFD meshes for the helical turbine shape proved more challenging than for the straight foil meshes. The case with strut separation at 0.123m was not analyzed as this case was not tested in the tow tests, due to excessively high strain.

Table 15: Helical Foil Mesh parameters

Turbine	*Case*	*# Cells - Rotor Volume*	*# Cells - Rotor Volume*	*Total # cells*	*Solution CPU Hours*
Helical Foil	H123	-	-	-	-
Helical Foil	H225	16,911,449	3,221,903	20,133,352	7,195
Helical Foil	H450	19,651,733	3,221,903	22,873,636	5,956
Helical Foil	H675	26,554,211	3,221,903	29,776,114	3,756
Helical Foil	H900	7,540,764	3,221,903	10,762,667	3,559

Parameters for the helical meshes are outlined in Table 15. The case for a strut separation of 0.900m (H900) is an outlier in terms of cell count, since this mesh is a polygonal mesh as compared to the hex and tetra meshes used for the other cases.

Table 16: Summary of CFD results for Helical Foil Meshes

Turbine	*Case*	*Strut Location (mm)*	*TSR*	*V (m/s)*	*dT (deg)*	*Cp*	*Cd*
Helical Foil	H225	225	3.0	1.3	2	*0.204*	
Helical Foil	H450	450	3.0	1.3	2	0.088	0.785
Helical Foil	H675	675	3.0	1.3	4	0.066	0.782
Helical Foil	H900	900	3.0	1.3	2	0.112	0.809

Table 17: Moment values for Helical foil CFD (red text indicates assumed values)

Turbine	*Case*	*Avg. Moment Foil 1 (Nm)*	*Avg. Moment Foil 2 (Nm)*	*Avg. Moment Foil 3 (Nm)*	*Avg. Moment Strut 1 (Nm)*	*Avg. Moment Strut 2 (Nm)*	*Avg. Moment Shaft (Nm)*
Helical Foil	H225	13.81	13.88	13.96	*-8.67*	*-7.23*	*-0.01*
Helical Foil	H450	8.31	8.74	9.08	-8.04	-6.92	-0.01
Helical Foil	H675	7.73	7.92	8.35	-8.43	-7.21	0.00
Helical Foil	H900	10.42	10.42	10.41	-9.53	-7.57	-0.01

3D CFD results for the helical turbines are summarized in Table 16 and Table 17. Some numerical issues arose with the H225 case studies, and strut forces were deemed to be unreliable for these runs. An assumption was made that the forces on the struts would be equivalent to strut forces for other cases and these values were assumed for calculation of Cp for H225.

Helical turbine cases were run at a TSR of 3.00 and a flow speed of 1.3m/s. These run conditions were informed by tank testing of the helical glass foil turbine. The Coefficient of Performance values are much lower than for the straight foil case, and there is greater variability between the cases.

Given the increase in flow speed from 1.1 to 1.3m/s we would expect to see higher values of Foil moments than were found for the straight foil cases, but this is not the case, indicating that the helical foil is performing less efficiently that then straight foil.

There is a significantly larger parasitic torque experienced by the struts for these runs, but this can be mostly explained by the increased rotational speed moving from a TSR of 2.40 and U of 1.1m/s to a TSR of 3.00 and a U of 1.3m/s. The rotational speed increases from 5.28 to 7.20 rad/sec, which would scale the drag on the struts by a factor of 2.18. Values increased by 2.12 from the straight foil CFD runs to the helical foil runs.

Shaft torques are again negligible.

The difference in behaviors between the straight and helical foils CFD runs can be ascribed to the foils alone.

Figure 61 shows the moments on a single helical foil for each of the four strut cases examined. There are indications of numerical instabilities for the H675 case, but averages are consistent with H450. H225 and H900 have similar behaviors but H225 has overall better performance, as there is no negative torque. This finding is somewhat inconsistent with all the other analyses.

Figure 62 plots the pressure trace along the inner and outer surfaces of a helical foil at one point during a turbine rotation for the H225 and H450 cases. Pressure on the outer surface is positive, and pressure on the inner surface is negative. A large difference between the inner and outer pressures is desired. The presence of the struts can be seen for both sets of traces. However, the pressure on the inner side of the foil appears to collapse over significant lengths for the H450 case. This correlates to the lower performance for this strut case. This finding is confirmed by looking at the pressure plots on the foils for these two cases, where large areas of the H450 foil do not experience low pressures (Figure 63).

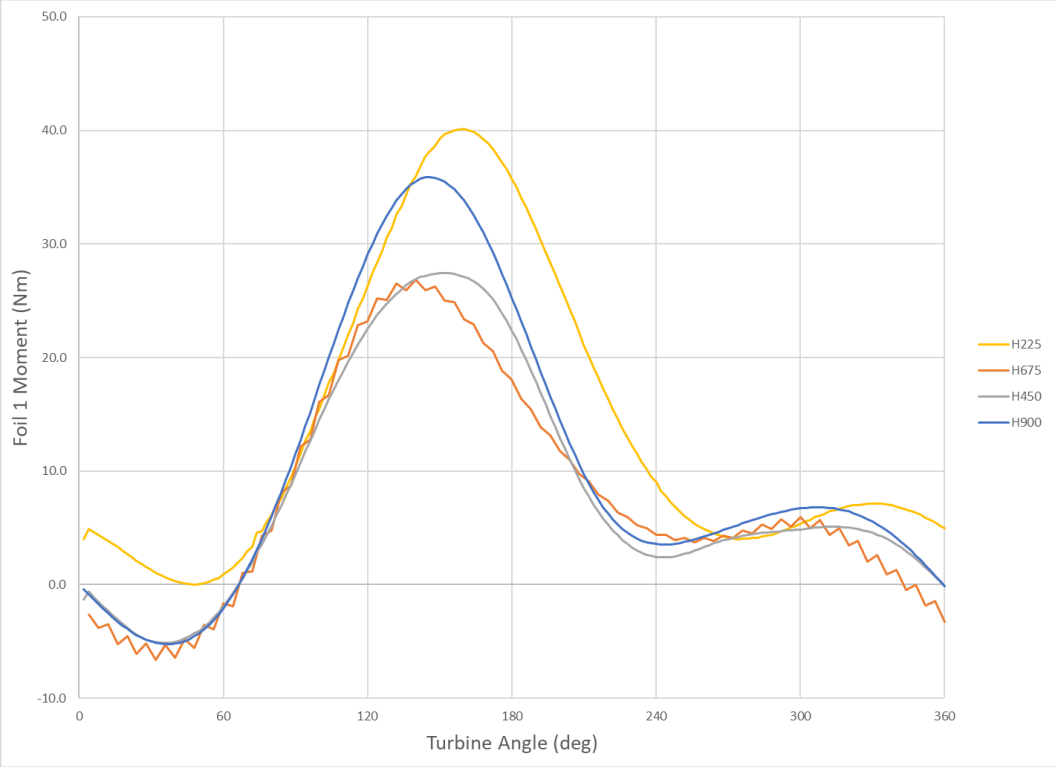

Figure 61: Foil 1 moments for helical foil cases. TSR =3.00 U = 1.3 m/s.

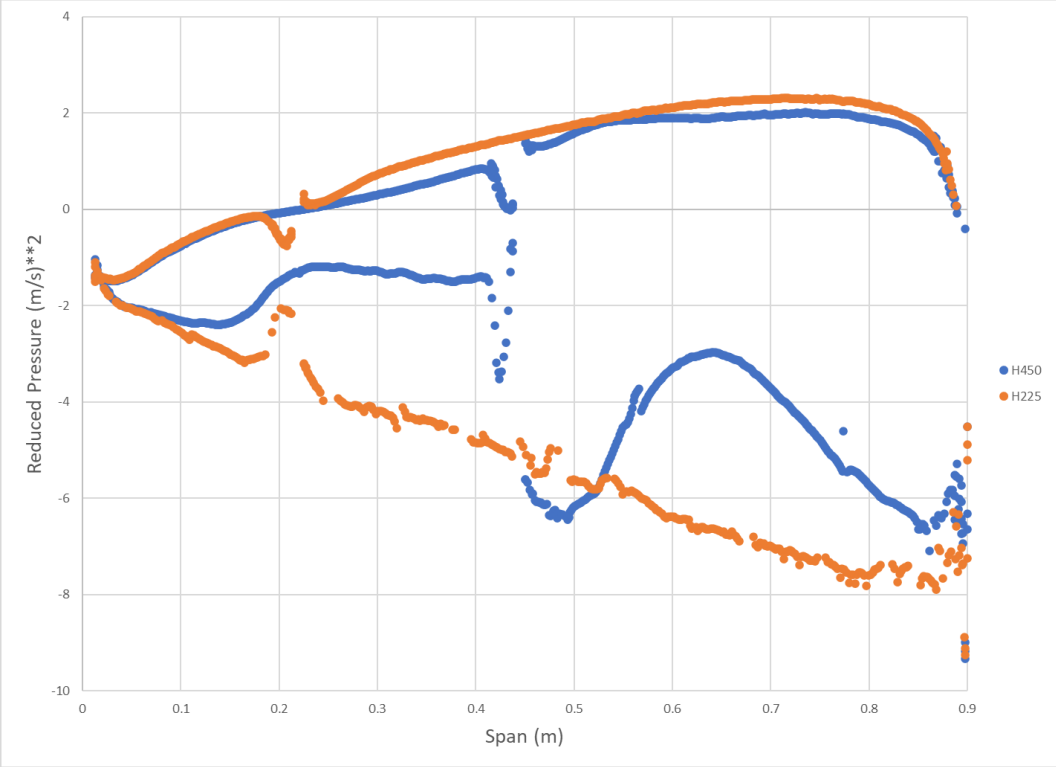

Figure 62: Pressure along the foil span for two different strut cases. TSR = 3.00, U = 1.3 m/s.

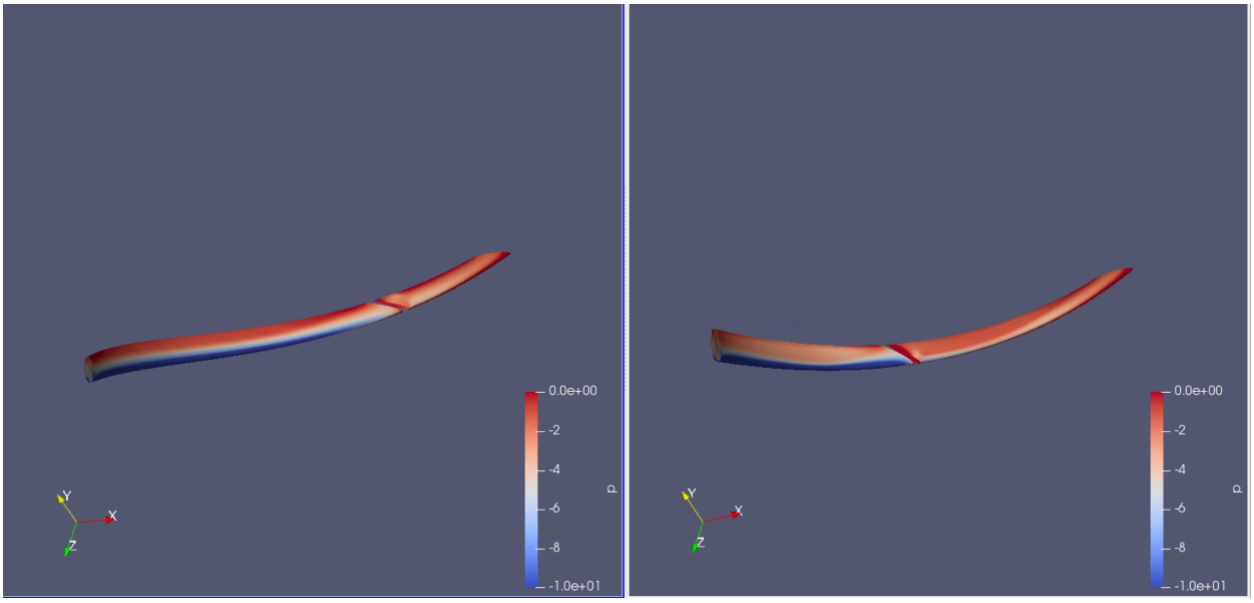

Figure 63: Pressure plots on the H225 and H450 foil.

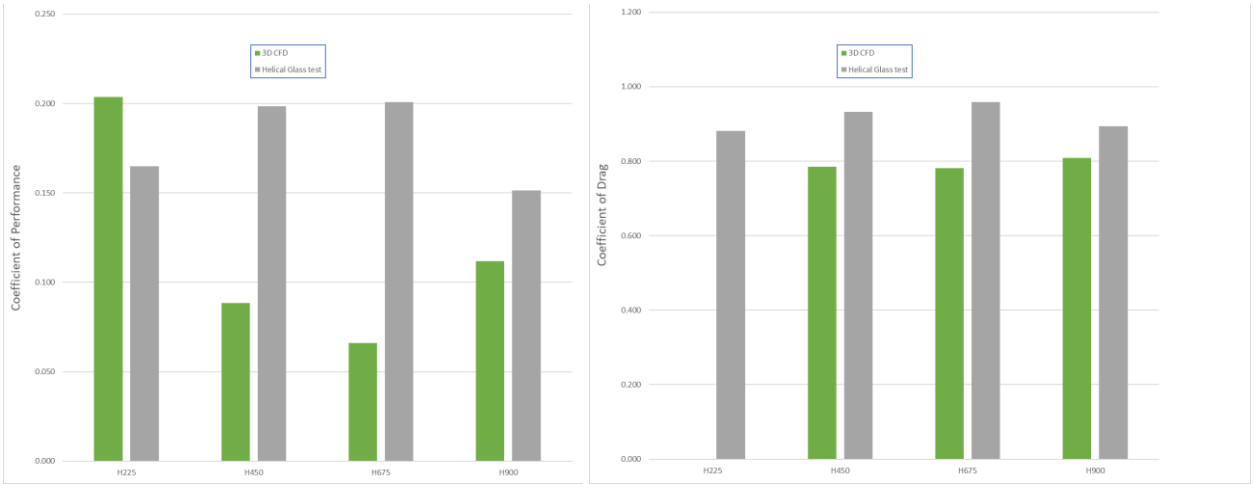

Figure 64: Comparison of test data and CFD prediction for Coefficient of Performance and Coefficient of Drag: Helical Foil Turbine. TSR =3.00, U = 1.3 m/s.

A comparison of the CFD results and the test data is provided in Figure 64. The CFD analyses for the helical cases were more difficult to construct and exhibited higher levels of numerical instabilities and overall differences between strut cases.

There is very clearly a difference in hydrodynamic behavior between the straight foil and helical foil turbines, with the helical foil turbine exhibiting a lower performance, but a higher optimum TSR value. This helical turbine design is very highly twisted, making a direct one to one comparison between straight and helical foils difficult. The CFD results are in general underpredicting performance observed in testing. A potential conclusion is that the CFD models for the helical turbines may require additional verification and validation work before being able to fully depend on their findings.

2.13 Structural Analysis

Structural analysis of the scale model turbines is required to determine deflections of the foils in operation. Results from the structural analysis can be directly compared with the in-situ strain measurements from the testing to validate both the structural and CFD models.

2.13.1 Carbon Straight Foil Structural Model

The material composition of the straight carbon foils was provided in prior sections. Structural calibrations were performed on the turbine by applying known loads and measuring both deflection and strain response. These results were used to evaluate the accuracy of a structural model of the static turbine.

Finite element models of the various turbine configurations were created using a commercial meshing tool. These models use isotropic materials for the shaft and struts, and a composite anisotropic ply level model defined for the foils. Shafts and foils are modelled as shell elements, and struts as volume elements. The strut joints are modelled with steel pins joining the strut cap to the strut and capturing the foil. Contacts between parts are modelled as bonded joints for simplicity and speed of analysis.

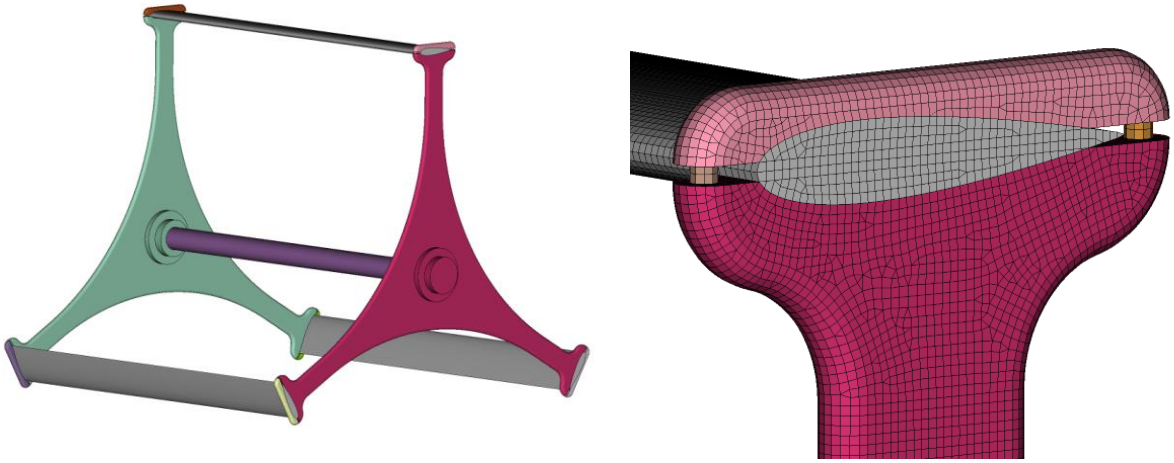

Figure 65: Typical construction of a finite element model for the S900 case.

The full laminate schedule (Table 5) is not used in the definition of the material properties of the foil, as several of the plies used are not full chord width plies. An effective ply definition was developed by modifying the full laminate schedule to replicate the observed structural response from calibration testing. The S123 case which has the lowest stiffness was the primary case used for structural model calibration since this has the highest strains and deflections. The model response was then cross-checked with the S900 case which has the lowest strains and deflections.

The reduced laminate used for structural modelling is shown in Table 18.

Table 18: Reduced laminate definition based on structural calibration testing

Layer No.	Orientation	Thickness	CPT	Width (mm)
1	0		0.586	98
2	0		0.586	95
3	45		0.586	91
4	-45		0.586	87
6	0		0.586	80
7	90		0.586	21
10	90		0.586	47
11	0		0.586	53
13	45		0.586	63
14	-45		0.586	67
15	0		0.586	70
16	0		0.586	74

Using the reduced laminate schedule, a FEA run was performed for the case with a load applied at 0.800m along the span. A comparison of strain as measured by the in-situ fiber optic sensor as compared with strain predicted by the finite element model is shown in Figure 66. Agreement is excellent across the free span of the foil. There is a difference between strain readings in the vicinity of the strut joint at 0.123m, and this is probably due to the assumption of a bonded connection between the strut and foil. This assumption greatly simplifies the numerical structural analysis and the deviation from measurement is accepted as a consequence.

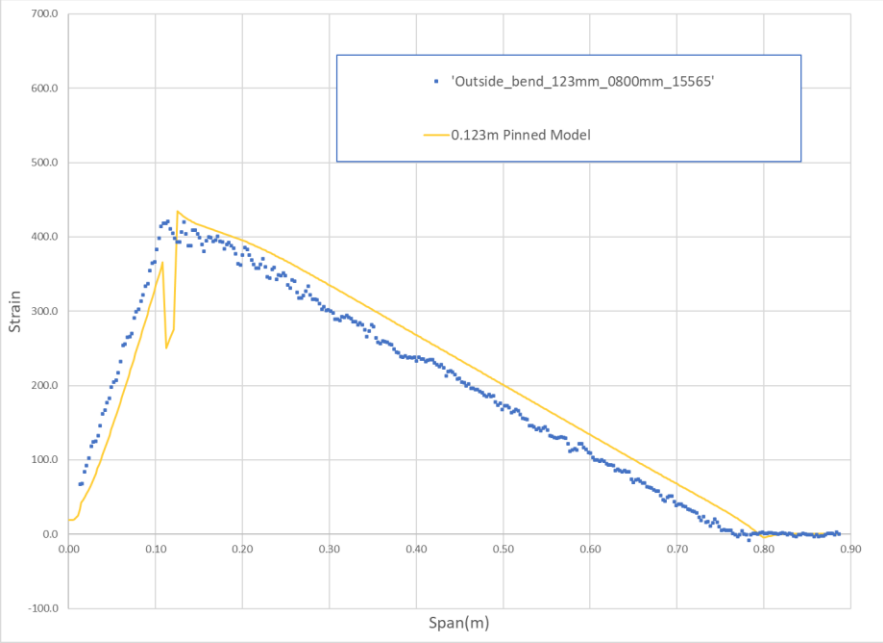

Figure 66: Calibration of carbon foil S123 structural model.

The process was repeated for the S900 case, where structural support for the carbon foil is greatest. Again, the strain pattern is well captured by the finite element model. There are discrepancies near the strut junctions, but these are considered acceptable. Note that the values of strains in the S900 case are much lower than for S123 case, and that there appears to be a fixed offset of approximately 25 µStrain between measured data and finite element results in both cases.

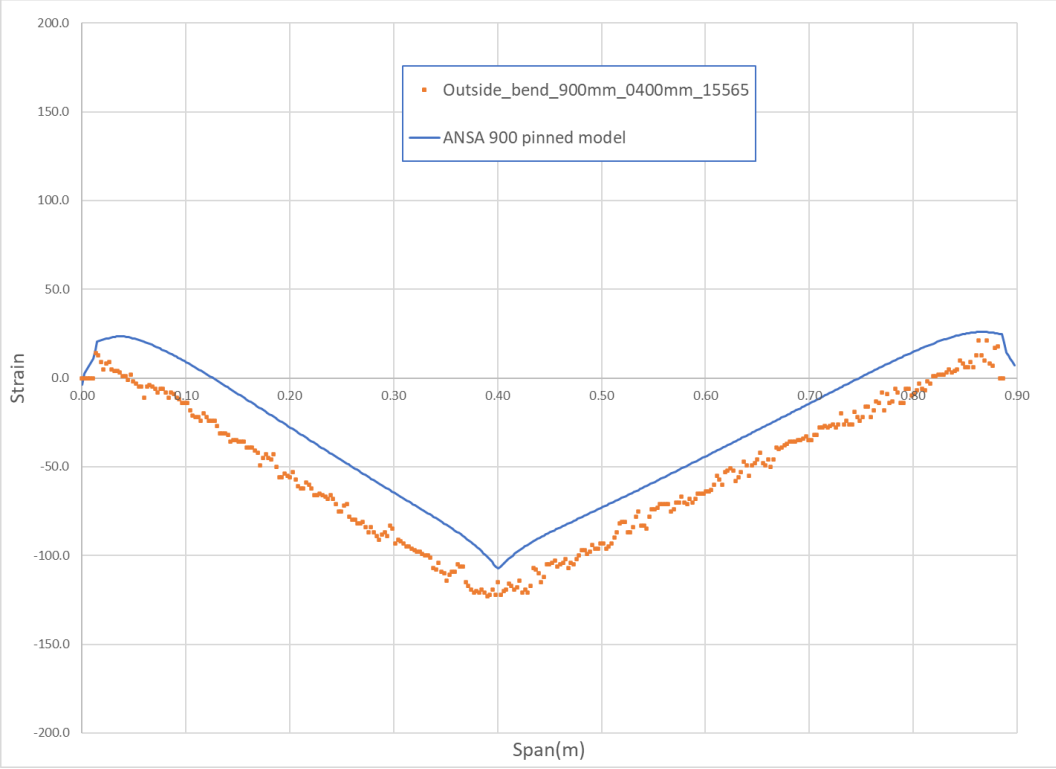

Figure 67: Calibration of carbon foil S900 structural model.

2.14 One Way Fluid Structure Interaction

To predict the strains that would be expected to occur on the turbine based on the CFD models ORPC developed a workflow process where pressures loads were extracted from the CFD models at defined points of the rotation and mapped onto the structural models of the turbines. This process may be accomplished in multiple ways, but all involved some manipulation of intermediate pressure load files.

2.14.1 Carbon Composite Straight Foil One Way Fluid Structure Interaction

To validate the methodology, ORPC focused on two cases for the straight foil turbine, S900 and S123, which represent extremes of structural stiffness. Results for the structural analysis assuming carbon foils are presented.

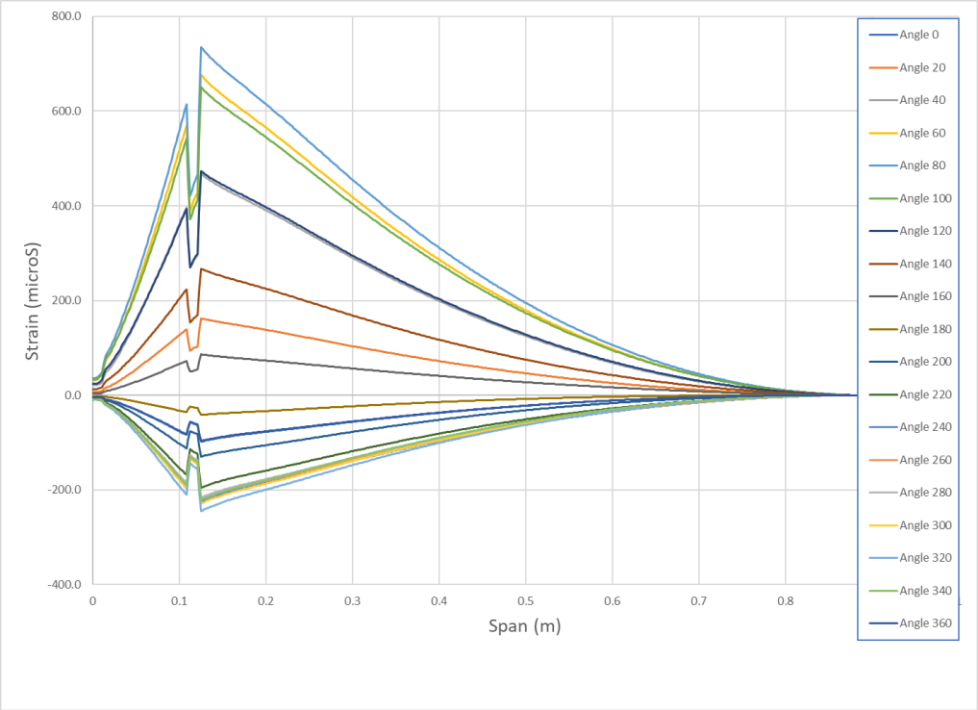

Figure 68: Spanwise strain along the outer ply of a carbon straight foil turbine (S123), as predicted from finite element structural models, with loadings provided by 3D CFD. Strut spacing – 0.123m; TSR – 2.40; U – 1.1 m/s.

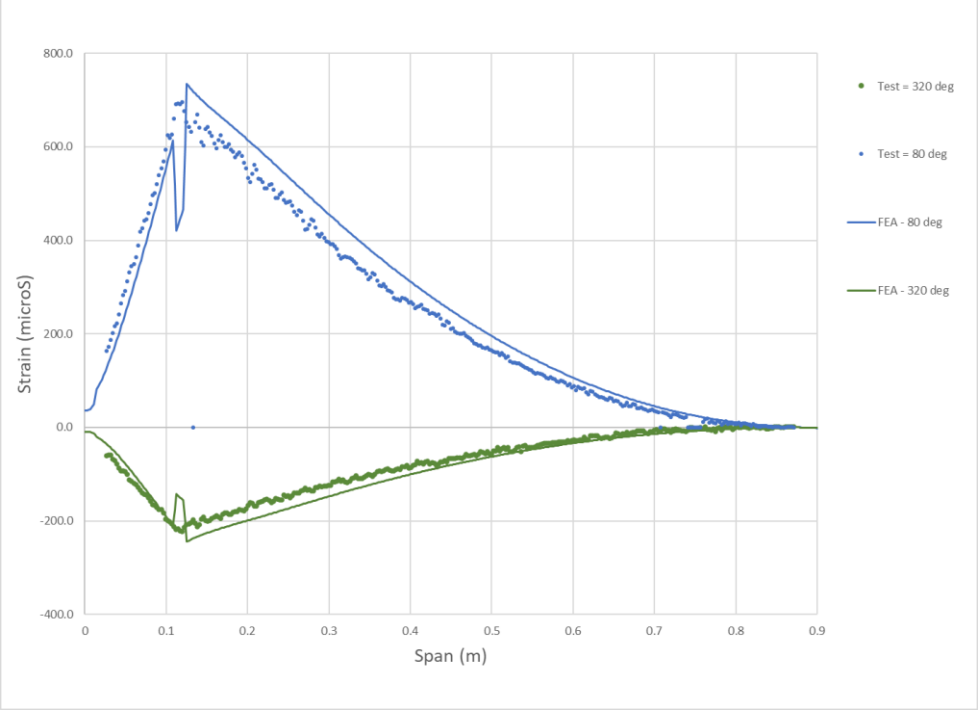

Figure 69: Spanwise strain along the outer ply of a carbon straight foil turbine (S123), as predicted from finite element structural models, with loadings provided by 3D CFD, compared with test data. Strut spacing – 0.123m; TSR – 2.40; U – 1.1 m/s. Data are presented at the turbine angles at which maximum and minimum strain are experienced within a rotation.

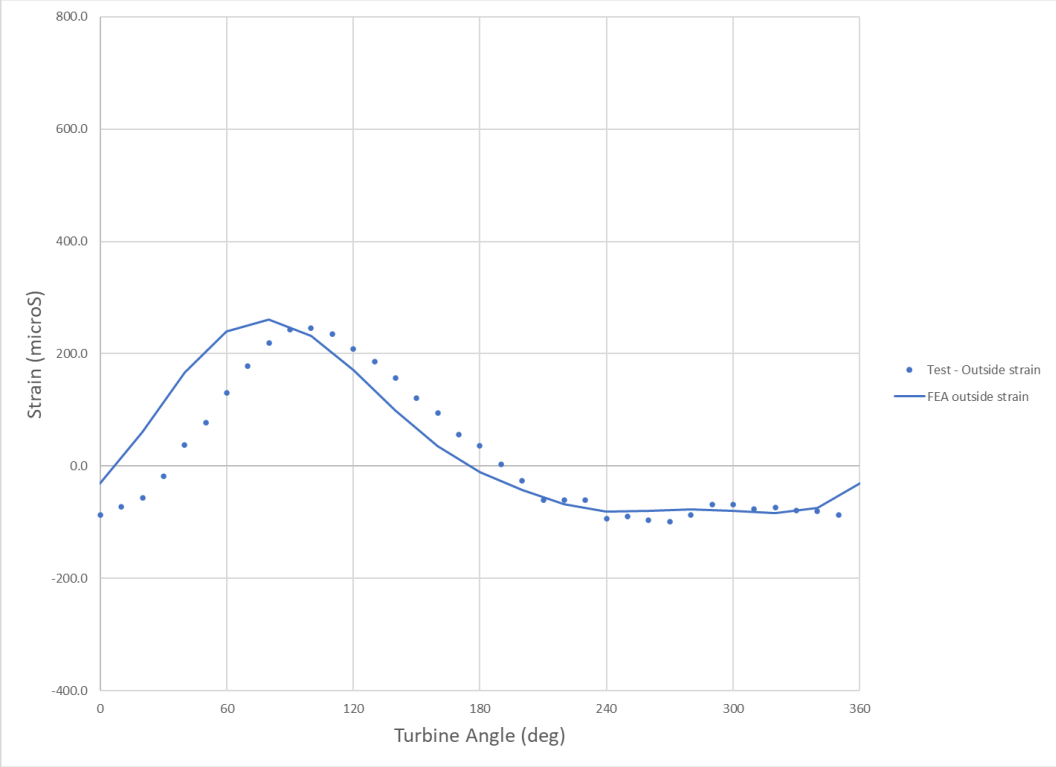

Figure 70: Strain on the outer ply of a carbon straight foil turbine (S123) at span = 0.440m, as predicted from finite element structural models, with loadings provided by 3D CFD, compared with test data. Strut spacing – 0.123m; TSR – 2.40; U – 1.1 m/s. Data are presented as a function of turbine rotation angle.

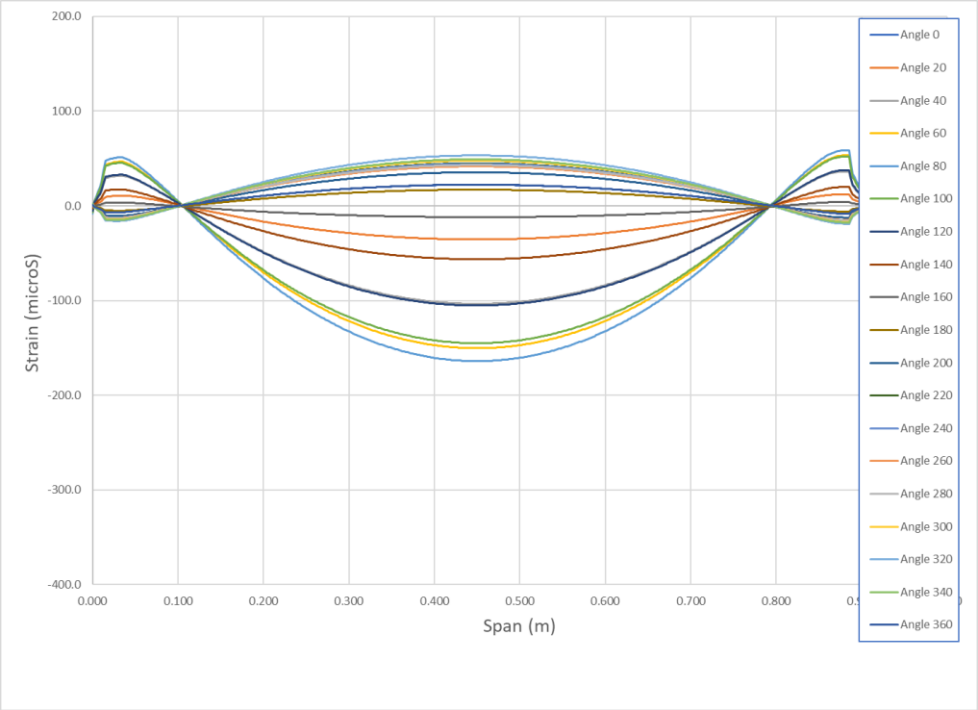

Figure 71: Spanwise strain along the outer ply of a carbon straight foil turbine (S900), as predicted from finite element structural models, with loadings provided by 3D CFD. Strut spacing – 0.123m; TSR – 2.40; U – 1.1 m/s.

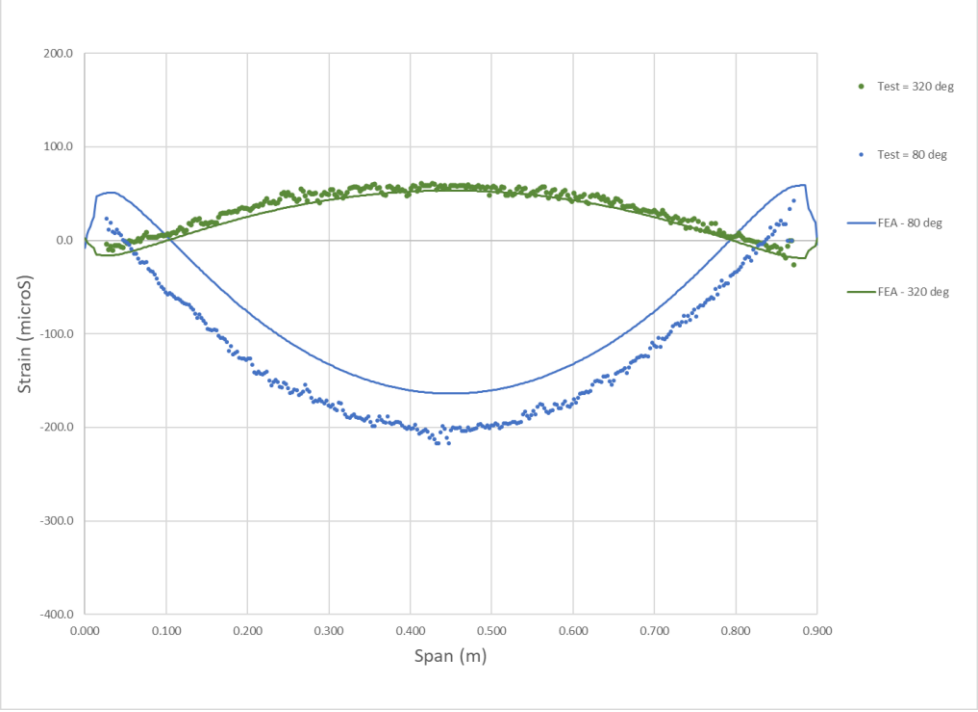

Figure 72: Spanwise strain along the outer ply of a carbon straight foil turbine (S900), as predicted from finite element structural models, with loadings provided by 3D CFD, compared with test data. Strut spacing – 0.123m; TSR – 2.40; U – 1.1 m/s. Data are presented at the turbine angles at which maximum and minimum strain are experienced within a rotation.

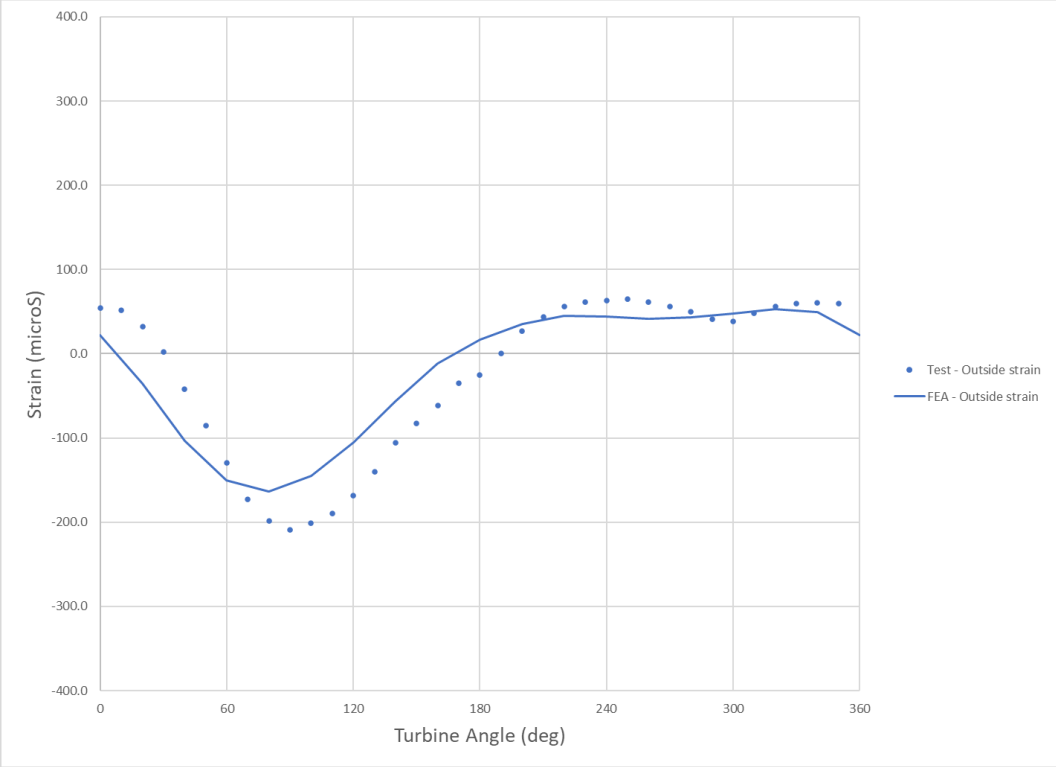

Figure 73: Strain on the outer ply of a carbon straight foil turbine (S900) at span = 0.439m, as predicted from finite element structural models, with loadings provided by 3D CFD, compared with test data. Strut spacing – 0.123m; TSR – 2.40; U – 1.1 m/s. Data are presented as a function of turbine rotation angle.

2.14.2 Glass Composite Straight Foil One Way Fluid Structure Interaction

A similar exercise was conducted for the glass composite straight foil turbine. Material properties for the glass composite were established by calibrating the model against the measured structural response.

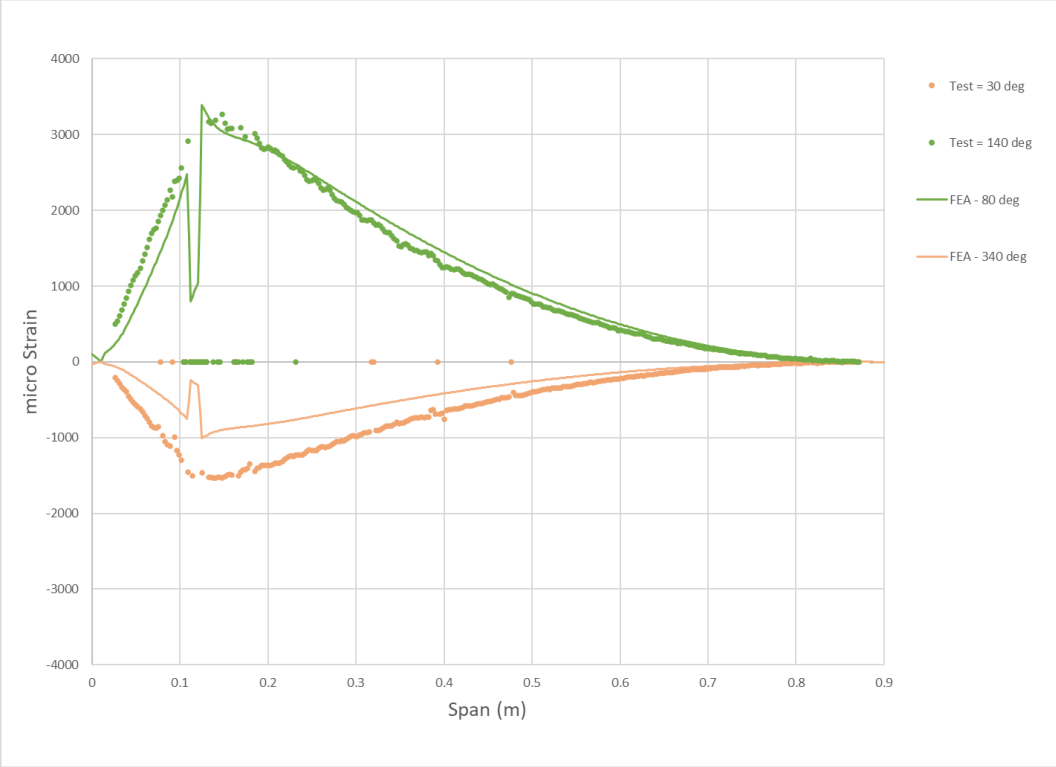

Figure 74: Spanwise strain along the outer ply of a glass straight foil turbine (S123), as predicted from finite element structural models, with loadings provided by 3D CFD, compared with test data. Strut spacing – 0.123m; TSR – 2.40; U – 1.1 m/s. Data are presented at the turbine angles at which maximum and minimum strain are experienced within a rotation. The strain presented is for the maximum and minimum cases from the test data and from the FEA run. Note that while the values of strain agree very well, there is a discrepancy in the angle at which they occur.

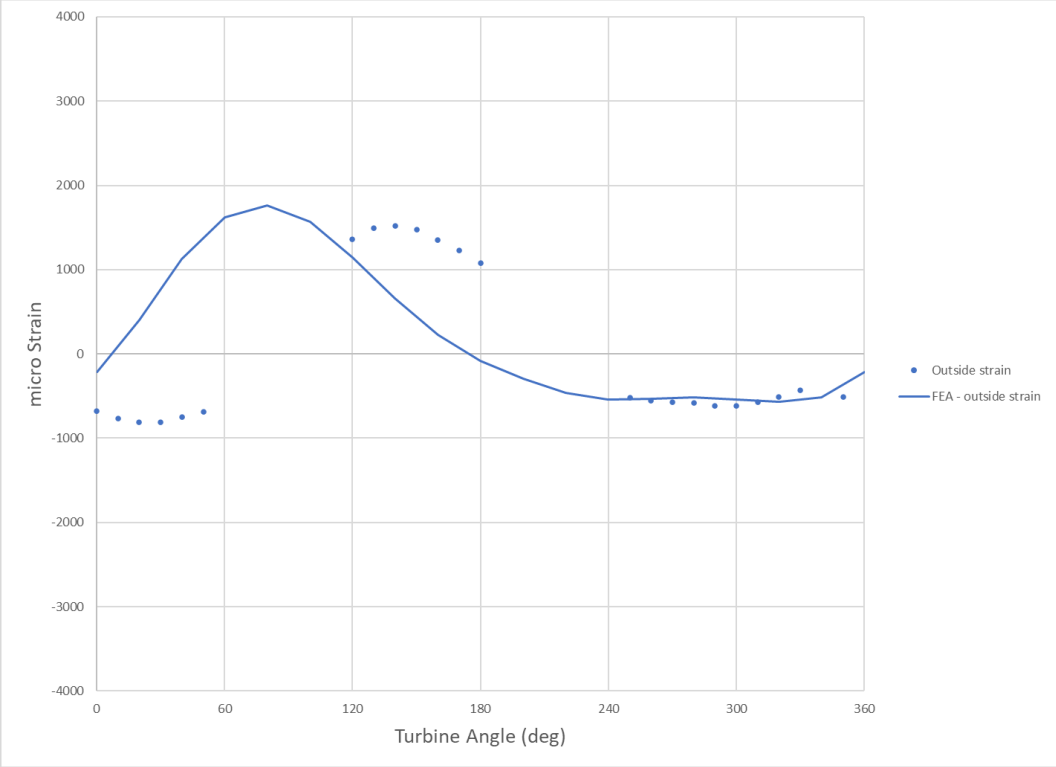

Figure 75: Strain on the outer ply of a glass straight foil turbine (S123) at span = 0.440m, as predicted from finite element structural models, with loadings provided by 3D CFD, compared with test data. Strut spacing – 0.123m; TSR – 2.40; U – 1.1 m/s. Data are presented as a function of turbine rotation angle. Note that there appears to be a phase shift occurring between the test data and FEA results.

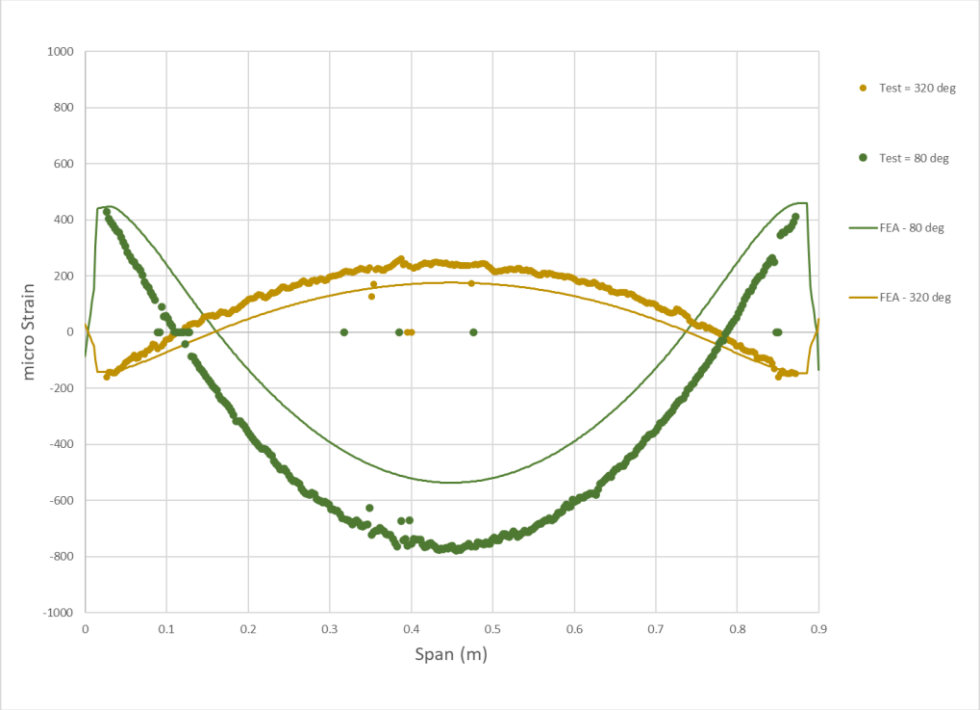

Figure 76: Spanwise strain along the outer ply of a glass straight foil turbine (S900), as predicted from finite element structural models, with loadings provided by 3D CFD. Strut spacing – 0.123m; TSR – 2.40; U – 1.1 m/s.

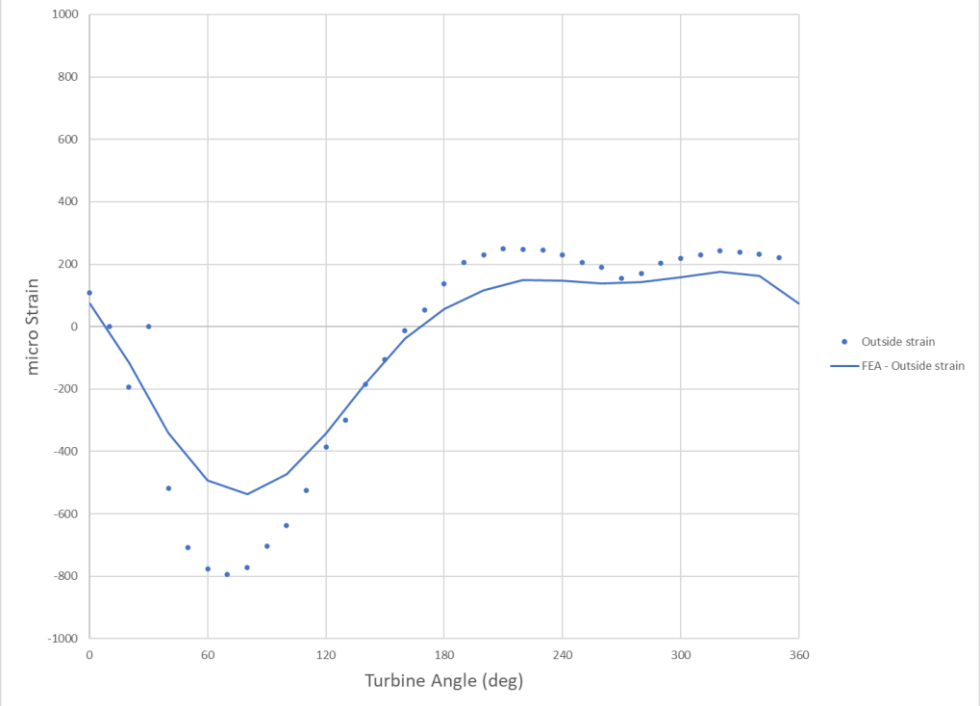

Figure 77: Strain on the outer ply of a glass straight foil turbine (S900) at span = 0.439m, as predicted from finite element structural models, with loadings provided by 3D CFD, compared with test data. Strut spacing – 0.123m; TSR – 2.40; U – 1.1 m/s. Data are presented as a function of turbine rotation angle. Note that there is a slight disagreement in magnitude of strain, but that the correlation for turbine angle is good, indicating only a slight phase shift.

2.14.3 Glass Composite Helical Foil One Way Fluid Structure Interaction

The methodology was evaluated using the helical glass composite turbine test data.

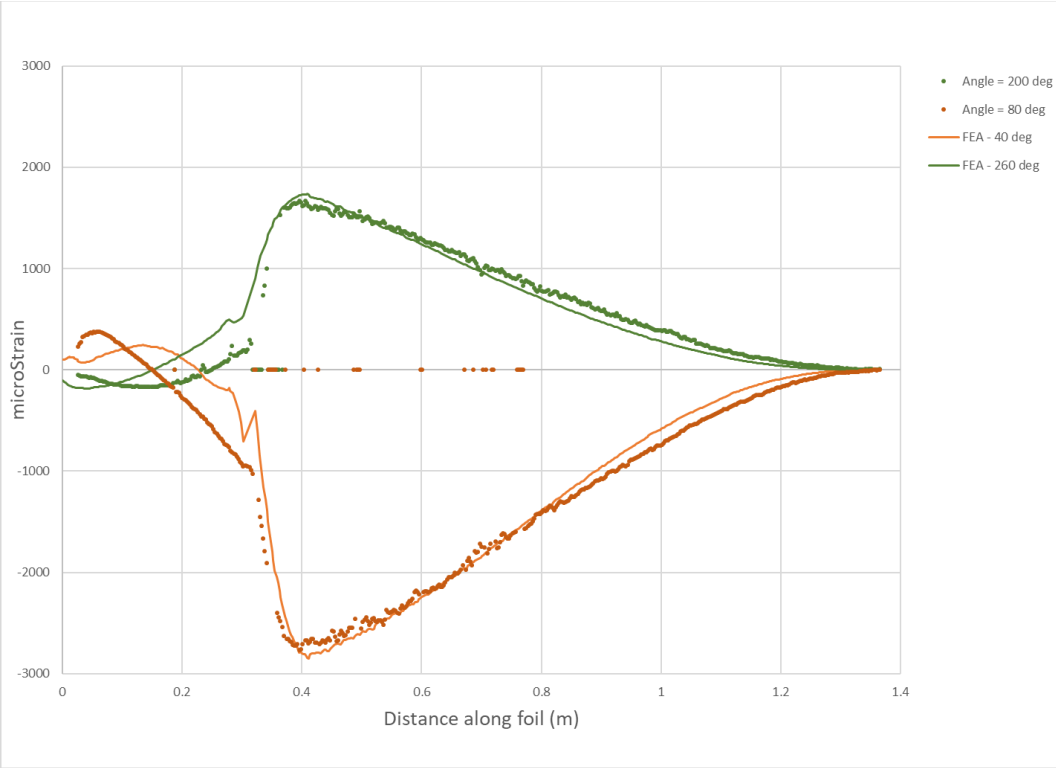

Figure 78: Spanwise strain along the outer ply of a carbon helical foil turbine (S225), as predicted from finite element structural models, with loadings provided by 3D CFD, compared with test data. Strut spacing – 0.225m; TSR – 3.00 U – 1.3 m/s. Data are presented at the turbine angles at which maximum and minimum strain are experienced within a rotation, and as with the S123 glass case there is a discrepancy between the turbine angle values, indicating a phase shifting of test data relative to FEA results. Note that the x-axis scale is the distance along the helical foil, instead of the turbine span.

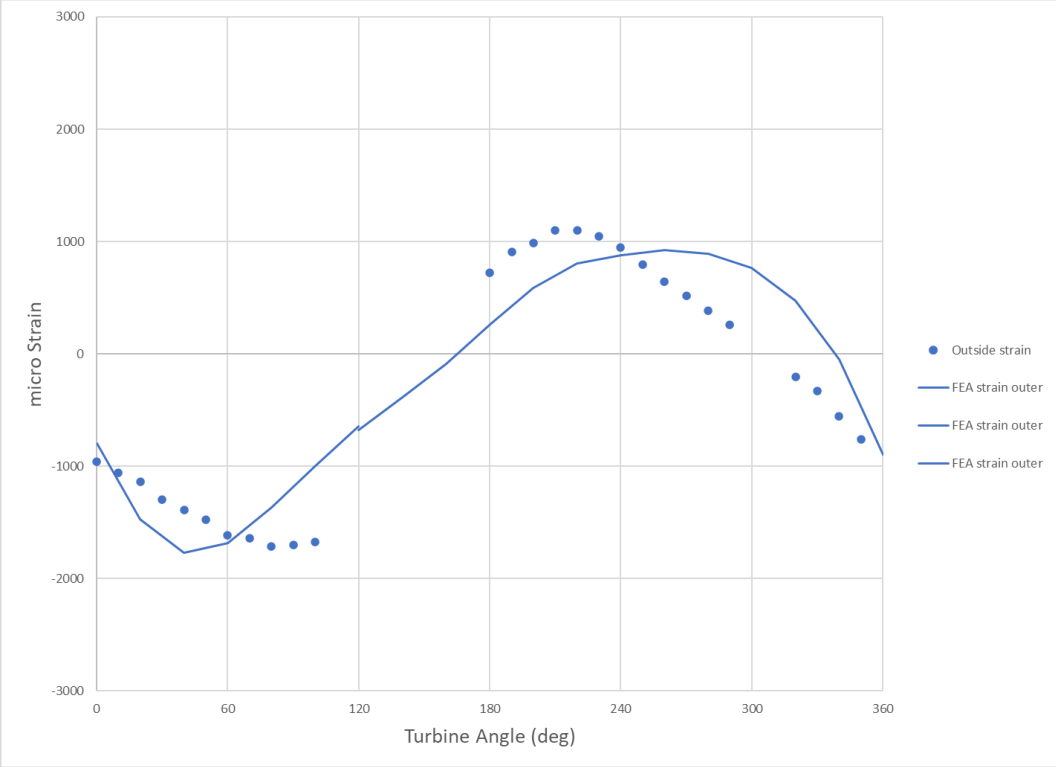

Figure 79: Strain on the outer ply of a glass helical foil turbine (S225) at location = 0.714m, as predicted from finite element structural models, with loadings provided by 3D CFD, compared with test data. Strut spacing – 0.225m; TSR – 3.00; U – 1.3 m/s. Data are presented as a function of turbine rotation angle. Note that there appears to be a phase shift occurring between the test data and FEA results. The FEA strain results are a composite of three different curves.

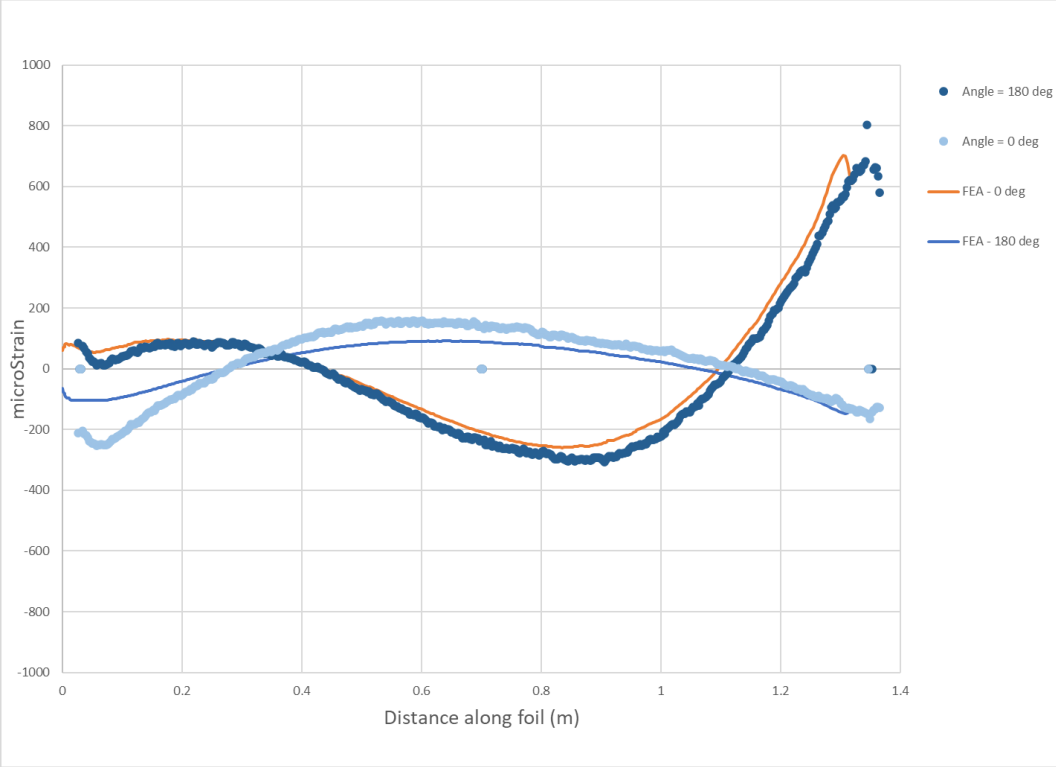

Figure 80: Spanwise strain along the outer ply of a carbon helical foil turbine (S900), as predicted from finite element structural models, with loadings provided by 3D CFD, compared with test data. Strut spacing – 0.900m; TSR – 3.00 U – 1.3 m/s. Data are presented at the turbine angles of 0 degrees and 180 degrees. There is very good agreement between strain magnitude, strain pattern, and turbine angle for this case.

2.14.4 Commentary on One-way FSI Methodology

- The one-way FSI methodology is relatively easy to implement, with an easy to replicate workflow
- Results will depend on the accuracy of the CFD predictions
- Structural responses for stiff structural cases (carbon composite or S900, H900 glass composite) show very good agreement between the measured and predicted strain levels in the outer ply of the composites
- As the stiffness of the structure decreases, moving to S225 glass composites, or H225 helical glass composites the one-way FSI methodology can predict maximum and minimum strain values well, but may not be fully capturing a phase shift in when these values occur during the rotation
- To further asses this finding will require additional validation runs to be completed to establish that the angular position of the turbine as defined in the test work is sufficiently precise to draw any such conclusions.

2.15 Two-way FSI Methodology

ORPC performed work to implement a fully coupled two-way FSI model using multiple approaches. This work was performed in two separate tranches: 1) evaluating commercial software for this work, and 2) developing additional modules for opensource modelling.

2.15.1 FSI Using Commercial Software

ORPC contracted with a third party to use commercial software tools for a full scale ORPC turbine with the intent of developing a model which could then be compared with ORPC's own internal development tools. The contractor started with the intention to use a modal analysis approach embedded in a well-developed commercial code, which offered the promise of reducing the computational effort required to solve the FSI problem. The modal vibrations modes of the turbine were provided as inputs to a CFD model. However, implementation of this approach did not proceed as smoothly as expected, due in part to unfamiliarity with the approach. It was determined that a more standard structural-CFD coupling method would be preferred, and a switch was made to a second commercial code.

The CFD model setup and structural model setup proceeded smoothly. However, the joint coupling of these analyses illustrated numerical issues with the fluid-structure coupling that prevented obtaining a solution in a reasonable time. Consultation with the software supplier confirmed that the approach was fundamentally sound, but that for this problem the combination of mesh size requirements, mesh morphing, FSI mapping, interface tracking and paralleling the solution across multiple cores, leads to a very slow solution process.

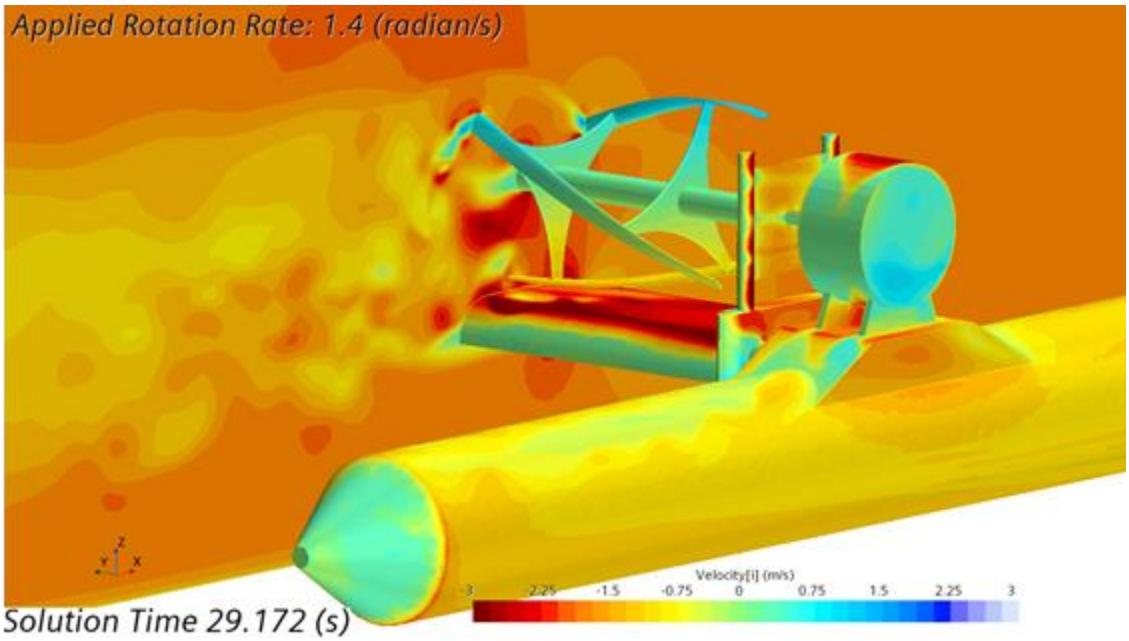

Figure 81: CFD model for full scale turbine. Commercial codes were evaluated to assess whether there could solve this FSI problem within reasonable resource.

Based on these findings ORPC determined that use of the commercial codes was not practicable at that time and ceased work on this avenue of investigation. It should be noted that these commercial codes are under continuous development, and they may well be capable soon.

2.15.2 FSI Using Opensource Software

Continuing with ORPC's view that opensource software would provide good scalability for the crossflow turbine problem, ORPC investigated the use of OpenFOAM coupled with Calculix, using PreCICE.

Several issues were encountered with OpenFOAM which required writing of a new class structure for dynamic meshes. Simulations are performed using moving deforming mesh in transient mode, where the deformation of the external boundary is calculated separately. In conventional simulations of rotating machinery, motion of rotating mesh components is achieved using algebraic mesh deformation, where point position is calculated from the rotational speed. In cases of fluid-solid interaction, boundary deformation on solid walls is prescribed based on the solid mechanics solution, while motion of internal points needs to be calculated based on boundary deformation. Internal point motion is calculated using a Laplacian-based mesh deformation solver, with external deformation acting as a boundary conditions.

The objective of this software development project was to handle a transient simulation of rotating machinery with fluid-solid interaction using simultaneous algebraic mesh deformation for the rotation and Laplacian-based mesh deformation solver for wall deflection. To achieve this, a combined dynamic mesh class needed to be assembled.

This dynamic mesh class was constructed and validated. A simple test case of a single rotating foil was created to evaluate the workflow and the full two-way FSI coupling. The test case was assembled and run on a local machine with multiple cores. The code function but as expected the solution time was long, and a fully converged case was not obtained on local machines.

The test case was ported to several different High Performance Computing cloud services, and the codes built according to the same procedures used for building the codes on a local machine. When the code was tested on a single compute node the code functioned as was observed with the local machine, in that results were obtained but compute times were large. Next, the code was trialed on multiple compute nodes/cores on the HPC systems. However, at this stage links between the dynamic libraries for the PreCICE coupler and Calculix could not be established between the multiple compute nodes, meaning that parallelization was not achieved. Given that parallel computing was not achieved with this FSI methodology, it was not feasible to run test cases using the methodology as sufficient compute resources were not available.

(Note: at the time of writing of this report, the issue related to linking of different dynamic libraries across multiple cores appears to have been solved, and such FSI modelling now appears feasible, if computationally intense).

2.16 Task Summary and Milestone status

Using data from UNH's test work, ORPC:

- Validated a 2D Computational Fluid Dynamics methodology with OpenFOAM
- Validated a 3D Computational Fluid Dynamics methodology with OpenFOAM
- Used the 3D CFD models to predict performance from the tank testing
- Developed a low-order approach to FSI modeling, but determined that this approach would provide insufficient accuracy for the effort required
- Developed a one-way FSI methodology from CFD to structural models
- Demonstrated that the one-way FSI methodology is very good in terms of predicting structural response for a crossflow turbine, especially for cases where stiffness of the turbine is high

- Evaluated several commercial software codes for crossflow FSI analysis and determined that they were not capable of addressing the problem yet, indicating that the crossflow turbine problem is a complex one
- Developed a fully coupled FSI methodology using open-source tools
- ORPC was not able to evaluate the fully coupled FSI methods due to an inability to port the codes to multi-node HPC systems.

An original goal of the project was to develop a fully validated two-way Fluid Structure Interaction protocol. Such a methodology has been developed but not fully validated in this work. With such a methodology there will be substantial computational effort and expense required. A simplified version of this methodology involving one-way FSI mapping was developed and validated under this work and proved to be sufficiently accurate and computationally achievable for the purposes of design and is presented here as the preferred implementation.

Table 19: Task 2 Milestone Summary

Milestone 2.1	Documented development of low-order FSI techniques suitable for use in early-stage design. Methodologies will have been validated for qualitative accuracy of representative model sets.
Status	Complete.
Deliverable	EE0008386 Deliverable 2.1 Design Tool Overview.final.pdf

Milestone 2.2	Completion of a full case set up for FSI investigation of crossflow turbines using OpenFOAM, with performance predictions indicating achievement of project objectives for efficiency, system performance and costs.
Status	Complete.
Deliverable	Final report serves as text deliverable Additional deliverables include: Computational Fluid Dynamic OpenFOAM models of straight and helical foil test turbines • HDF_TSR240_S123_4deg • HDF _TSR240_S225_4deg • HDF _TSR240_S450_4deg • HDF _TSR240_S675_4deg • HDF _TSR240_S900_4deg • HDF_H225_TSR300_2deg • HDF_H450_TSR300_2deg • HDF_H675_TSR300_4deg • HDF_H900_TSR300_4_2_1deg One-way FSI models (Nastran files) of straight and helical foil test turbines • HDF_FEA_123_glass_carbon • HDF_FEA_450_glass_carbon • HDF_FEA_900_glass_carbon • HDF_H225_TSR300 • HDF_H900_TSR300

3.0 Task 3: System Integration

3.1 Task Summary

ORPC will apply the FSI tools to a commercial ORPC turbine design.

As the basis for design exploration using the FSI tools developed in Task 2, ORPC selected the RivGen 2.1 turbine variant. This turbine has been previously deployed in multiple applications, and while there are differences in mechanical joint design between the variants, the basic hydrodynamic shape has been well established, and operational experience with the design obtained in open-water tests.

Table 20: RivGen 2.1 Turbine Design

Span (m)	5.00
Diameter (m)	1.80
Turbine area	9.00
Max. Operational speed (m/s)	3.50
Rated Speed (2.25)	2.25
Rated Turbine Power (kW)	20.0
Number of Foils	3
Number of Struts	3

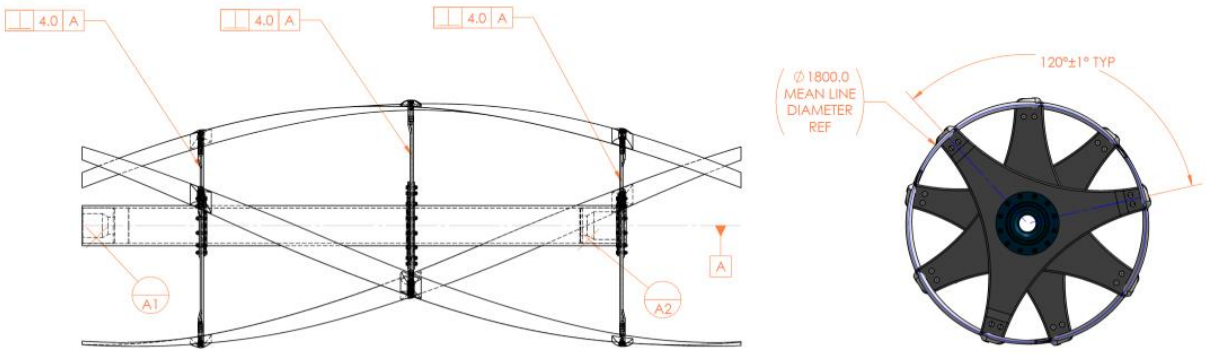

Figure 82: RivGen 2.1 Turbine

The RivGen 2.1 turbine consists of three carbon fiber foils of varying chord and profile along the span. These foils are mounted to a steel shaft via three glass composite struts. The turbine is mounted on different frameworks and supports depending on the application. For the purposes of this work, these additional supports, fairings, or structure will not be investigated, and the focus will be on the turbine performance in an open flow domain.

Prior performance predictions with commercial CFD codes matched well with measured in-field performance. The previous models referenced here accounted for degree of blockage and free-surface effects, which improves crossflow turbine performance.

All 3D RivGen CFD runs were performed under the following environmental conditions, with a Spalart-Almaras turbulence model, and a y+ value of O (1).

- Inflow speed, U = 2.0 m/s
- Water temperature = 5°C
- Water density = 999.95 kg/m^3
- Water kinematic viscosity = 1.56e-6 (m^2/s)
- Tip speed ratio = 2.50

3.2 RivGen 2.1 3D CFD

For the purposes of this work a 3D CFD model of the RivGen turbine was constructed in an open domain. No additional fairings or structures were considered. Free surface effects were not considered.

The turbine surface is split into several named patches for the purposes of tracking loads on each of the named section.

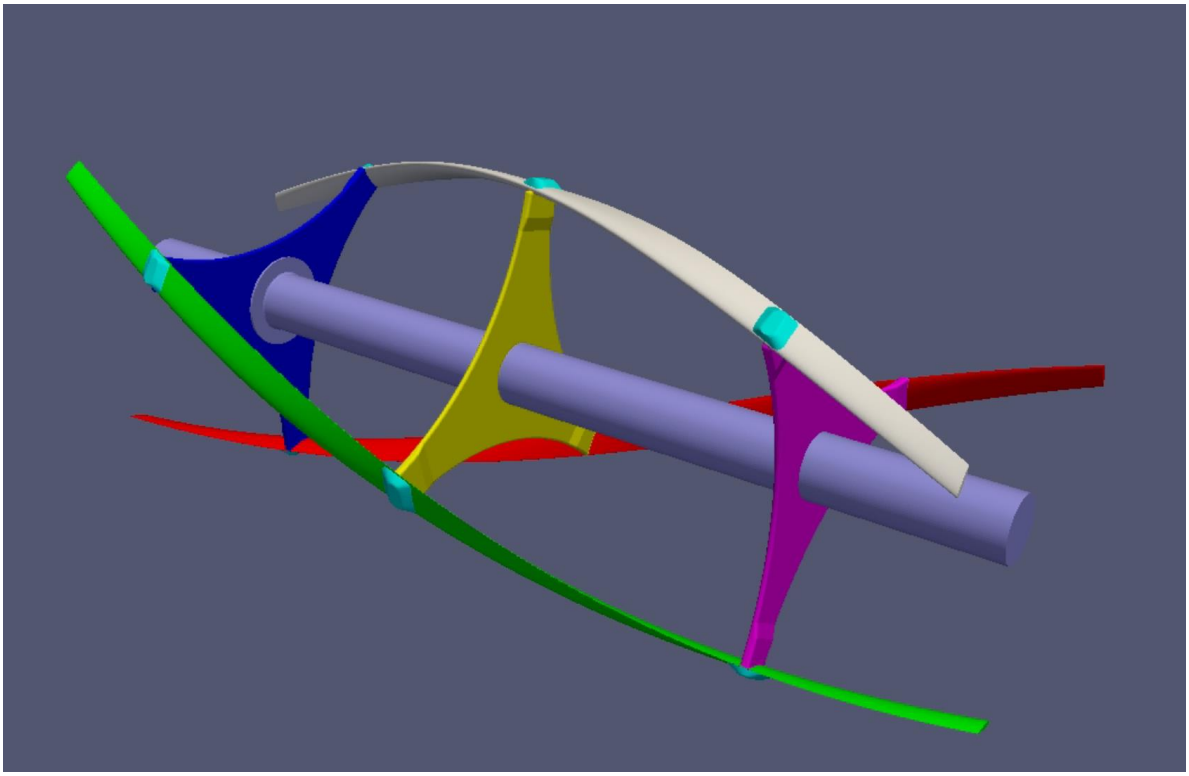

Figure 83: Geometry for RivGen RV2.1 case setup

The named patches are:

- Foil1 - white
- Foil2 - red
- Foil3 - green
- Strut1 – dark blue
- Strut2 - yellow
- Strut3 – pink

- Shaft – purple
- BackingPlates – light blue

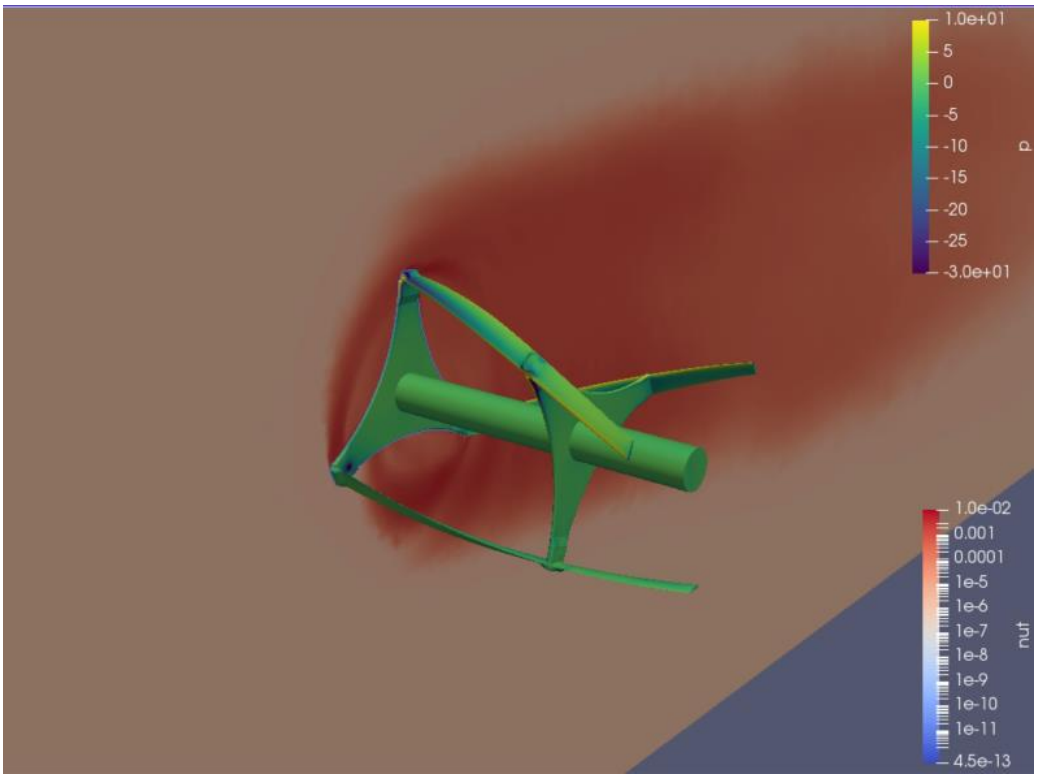

Figure 84: Turbulent viscosity at a slice, and pressure on the turbines. RV2.1 case.

3.2.1 RivGen 2.1 3D CFD – End Struts

Additional simple end struts were attached to each of the foils to provide structural support.

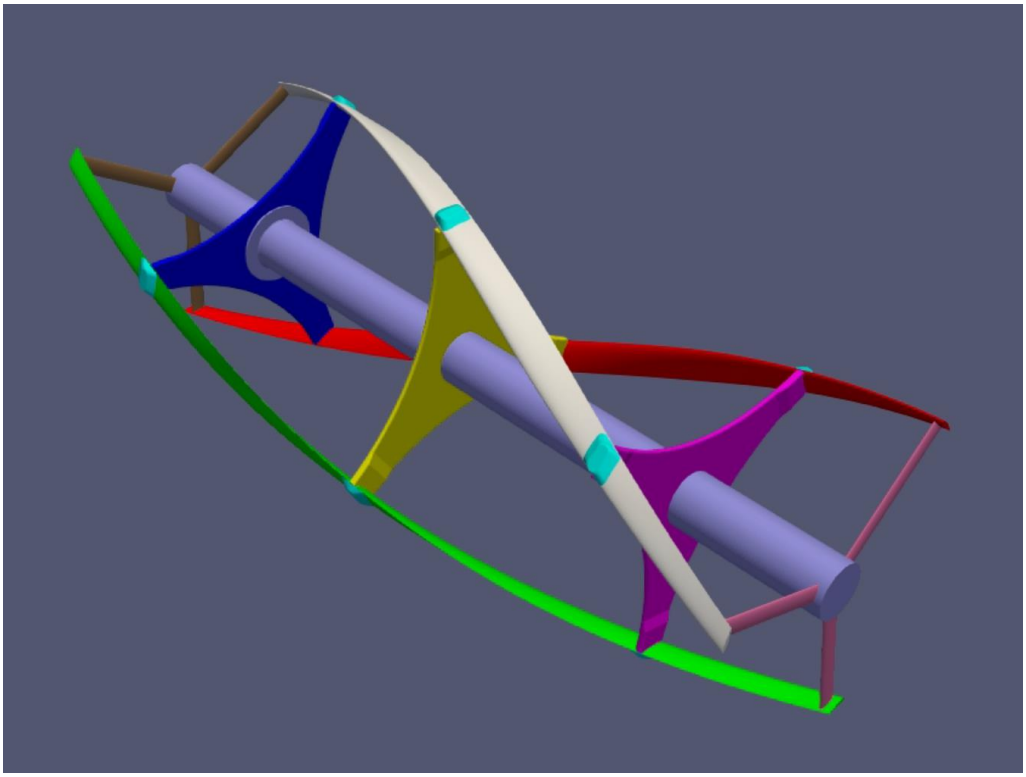

Figure 85: Geometry for RivGen RV2.1 with simple end struts added

The named patches are

- Foil1 - white
- Foil2 - red
- Foil3 - green
- Strut1 – dark blue
- Strut2 - yellow
- Strut3 – pink
- Shaft – purple
- BackingPlates – light blue
- Endstrut1 – brown
- Endstrut2 - pink

3.2.2 RivGen 2.1 3D CFD – Wing Struts

A more refined wing strut section was added to the basic RivGen 2.1 model and analyzed.

The named patches are

- Foil1 - white
- Foil2 - red
- Foil3 - green
- Strut1 – dark blue
- Strut2 - yellow
- Strut3 – pink

- Shaft – purple
- BackingPlates – light blue

Note that the foil definition includes the end wing strut.

3.3 Comparison of 3D CFD Results

Simple mesh statistics and solution run times are provided in Table 21.

A high-level summary of performance is provided in Table 22.

A part-by-part breakdown of performance is provided in Table 23. Values are presented as the coefficient of performance for each patch, with a positive value indicating power production, and a negative value indicating power loss. Within each run we observe some variation in foil-to-foil torque, but consistent values of power dissipation from each of the struts, and the backing plates. For the RV2.1 case the struts and backing plates account for a reduction in CP of 6.4 percentage points.

Table 21: Mesh summary for 3D CFD RivGen models

Turbine	*# Cells - Rotor Volume*	*# Cells - Tank Volume*	*Total # cells*	*Solution CPU Hours*
RV2.1	69,025,517	936,198	69,961,715	15,495
RV2.1_End_Strut	50,903,795	2,824,639	53,728,434	11,434
RV2.1_Wing_Strut	90,553,434	2,153,740	92,707,174	17,575

Table 22: 3D CFD results for full scale turbines, at TSR = 2.50.

Turbine	*TSR*	*V (m/s)*	*dT (deg)*	*Cp*	*Cd*
RV2.1	2.5	2.0	2	0.250	0.933
RV2.1_End_Strut	2.5	2.0	2	0.269	0.967
RV2.1_Wing_Strut	2.5	2.0	2	0.267	0.960

Table 23: 3D Coefficient of performance values for each of the components at TSR = 2.50

Turbine	*Foil 1*	*Foil 2*	*Foil 3*	*Strut 1*	*Strut 2*	*Strut 3*	*Backing Plates*	*Shaft*	*End Strut 1*	*End Strut 2*
RV2.1	10.2%	10.9%	10.4%	-1.6%	-1.6%	-1.6%	-1.6%	0.0%		
RV2.1_End_Strut	11.2%	11.3%	11.2%	-1.5%	-1.5%	-1.5%	-1.6%	0.0%	-0.3%	-0.3%
RV2.1_Wing_Strut	11.4%	10.9%	11.0%	-1.6%	-1.6%	-1.6%	-1.7%	0.0%		

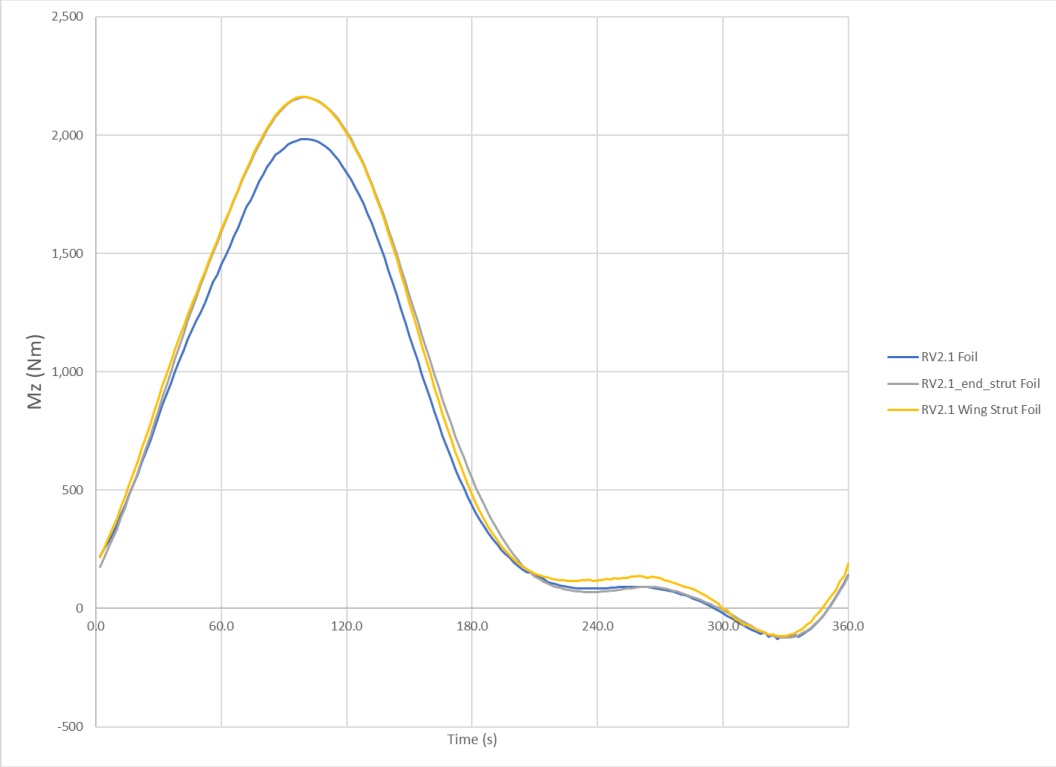

Figure 86: Foil 1 moments for 3D CFD RivGen cases with various end strut modifications

From Figure 86 we see that the difference in performance of the foils between the two end strut cases is minimal. Based on this we will continue with the wing strut foil case for structural analysis.

3.4 RivGen RV2.1 Structural Analysis

A baseline structural analysis model was constructed using pressure outputs from the 3D OpenFOAM analyses.

The design process will use the Load and Resistance Factor Design (LRFD) method as outlined in the DNVGL-ST-0164 standard for design of tidal turbines. For the design case the pressure loads from the CFD analysis must be scaled to the design flow speed, and additional load factors applied. The load cases are the Ultimate Limit State (ULS) and the Fatigue Limit State (FLS).

Table 24: Ultimate Limit State (ULS) Design Load Factor

CFD Speed	2.0	
CFD density	999.95	
Design Speed	3.5	RivGen Specifications
Environmental Factor	1.25	DNVGL-ST-0164, Section 6.2
ULS Load Factor, Normal	1.35	DNVGL-ST-0164, Table 6-1
Load Factor	*1.6875*	

The turbine is constructed of 39 carbon fiber prepreg plies.

As used in the following analysis, the laminate is a full thickness laminate over the full turbine foil surface. The foil laminate is 11.7mm thick.

The structural model was constructed and analyzed by the methods developed under Task 2. As before, checks confirmed that the applied pressure loads were correctly mapped onto a structural model, by plotting the reaction loads from the structural model along with the same loads derived from the CFD model. Excellent agreement was obtained.

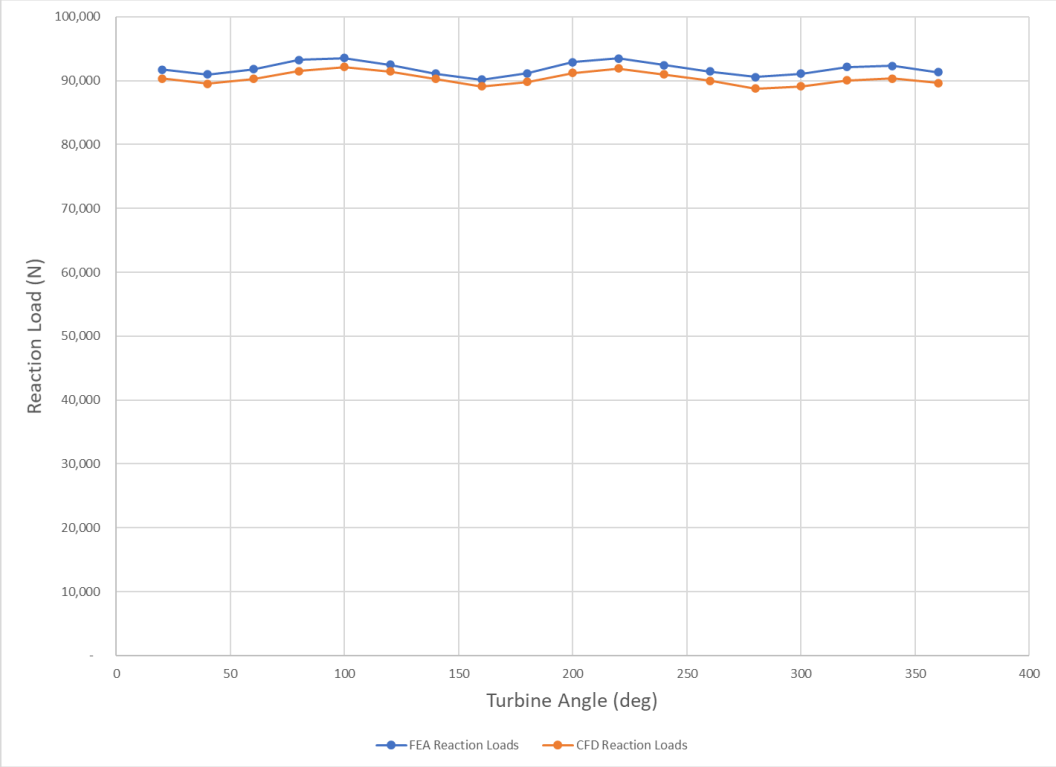

Figure 87: RivGen 2.1 structural model reaction loads and CFD model loads

Typical deflection patterns are shown for a point in the rotation in Figure 88. The foil tips experience the largest deflection of approximately 60mm, during a rotation.

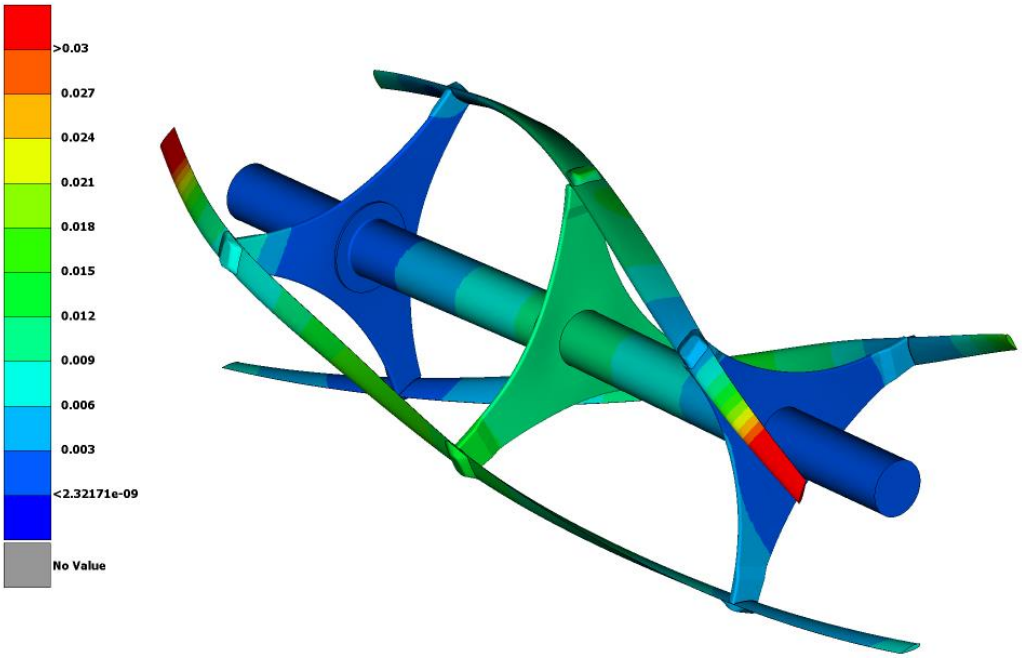

Figure 88: RivGen 2.1 structural deflection plot at a turbine angle of 0 deg.

Strain in the outer ply of a foil is shown (Figure 89). There is a clear peak in strain at the strut with the forward projecting foil segment, with local strain concentrations around the junction of the backing plates and the foil.

DNVGL recommended strain levels for carbon fiber prepreg in fatigue are shown as straight lines in Figure 89, but are intended only as a guide to allowable strain, since the strains predicted for the model are for the ULS case and not the FLS case.

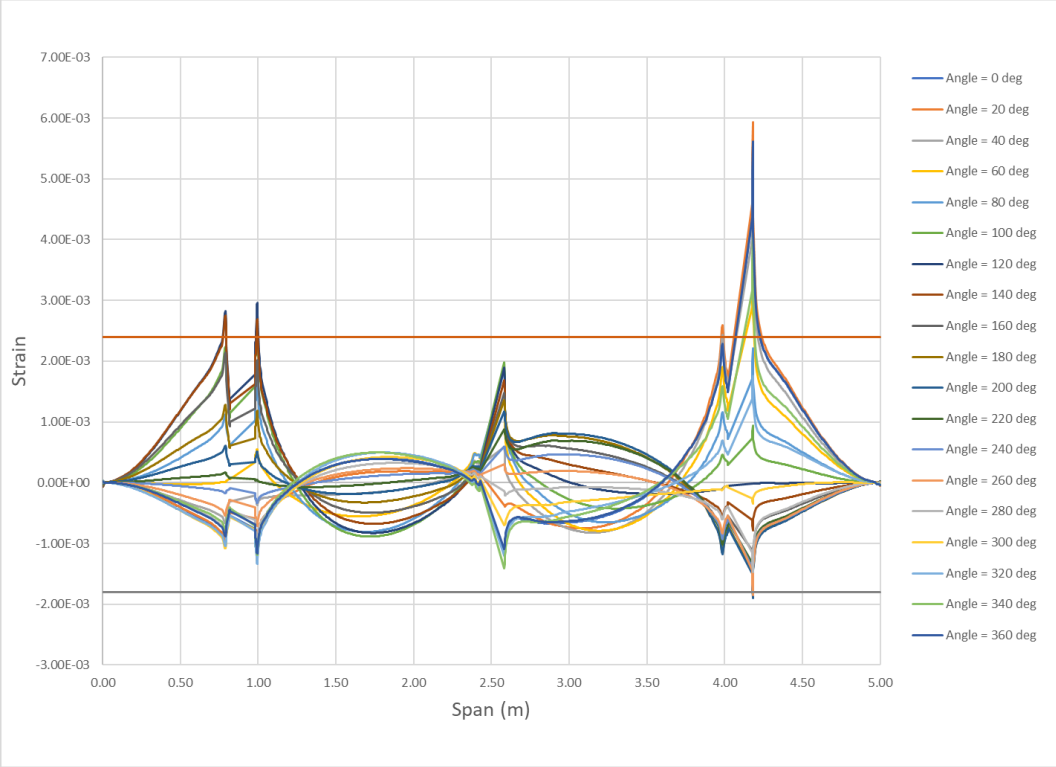

Figure 89: RivGen 2.1 E11 strain in the foil outer ply. Upper and lower allowable design strain limits are shown as straight lines.

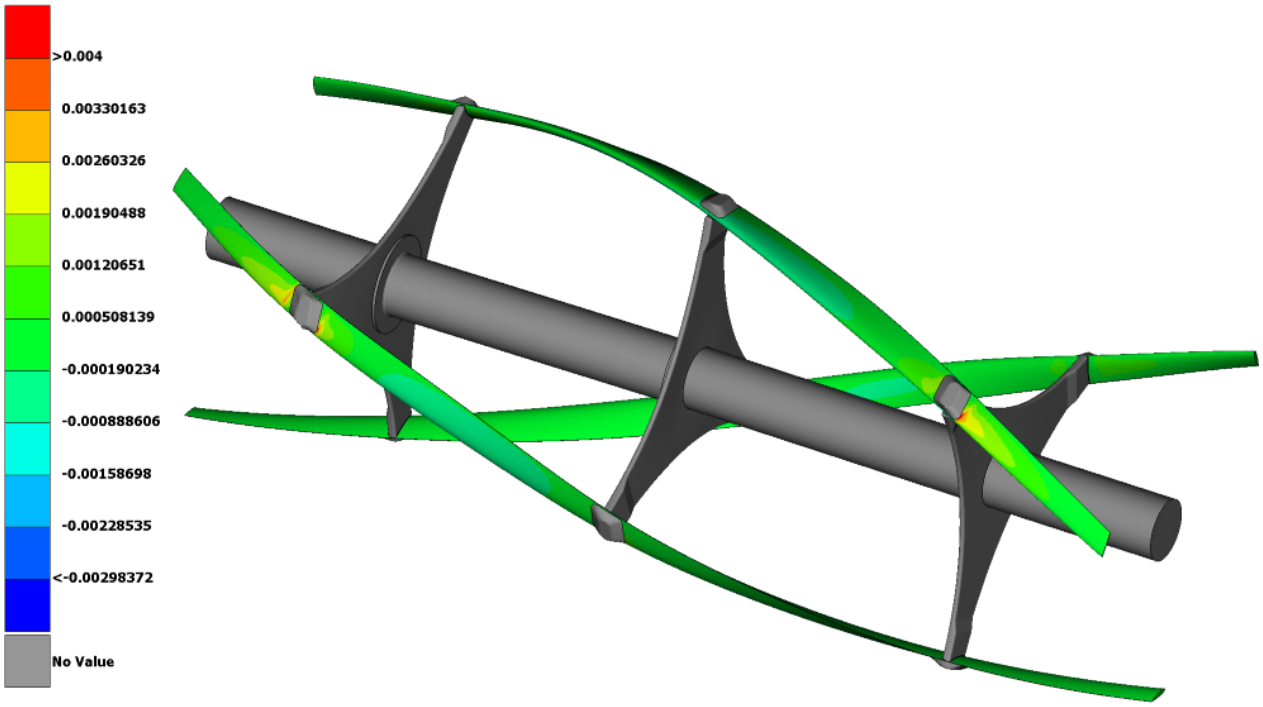

Figure 90: RivGen 2.1 E11 strain in the turbine foil outer plies.

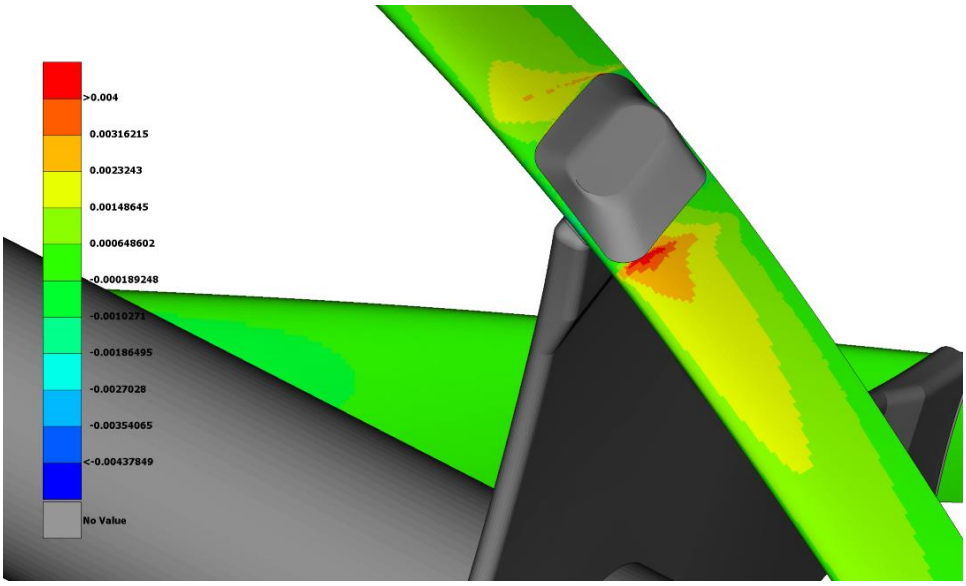

Figure 91: RivGen 2.1 E11 strain in at the Strut 3 joint

3.5 RivGen – New Design

A goal of this work is to reduce the LCOE for the system. This can be achieved in several ways, including increasing the efficiency of the system, or by reducing the capital cost of the system. In this work we focus on increasing the efficiency of the system while maintaining an acceptable level of structural integrity.

Two separate design options were investigated. In the first option, we change the base RV2.1 design to remove the two outermost radial struts and replace them with end struts. This leads to an improved Cp at a TSR of 2.50, of 31.1 percent as compared with the baseline performance of 25.0 percent. The performance increase is due to a reduction in drag from the removal of the struts, and an overall improvement in foil performance by reducing the tip losses. This change, as will be seen, will lead to a large increase in foil deflection, and an increased level of strain in the foil.

The second option consists of removing only the central mid strut and leaving the remaining four radial supports in place. This will provide more structural support. This leads to an improved Cp at a TSR of 2.50, of 28.9 percent as compared with the baseline performance of 25.0 percent.

Table 25: RivGen Design Options – Summary of performance

Turbine	*Cp*	*Foil 1*	*Foil 2*	*Foil 3*	*Strut 1*	*Strut 2*	*Strut 3*	*Backing Plates*	*Shaft*
Option 1	**31.1%**	11.4%	10.9%	11.0%		-1.6%		-0.6%	0.0%
Option 2	**28.9%**	11.4%	10.9%	11.0%	-1.6%		-1.6%	-1.1%	0.0%

3.5.1 RivGen – New Design – Structural Analysis

Using the methods developed and validated under Task 2, we developed structural models of options presented above.

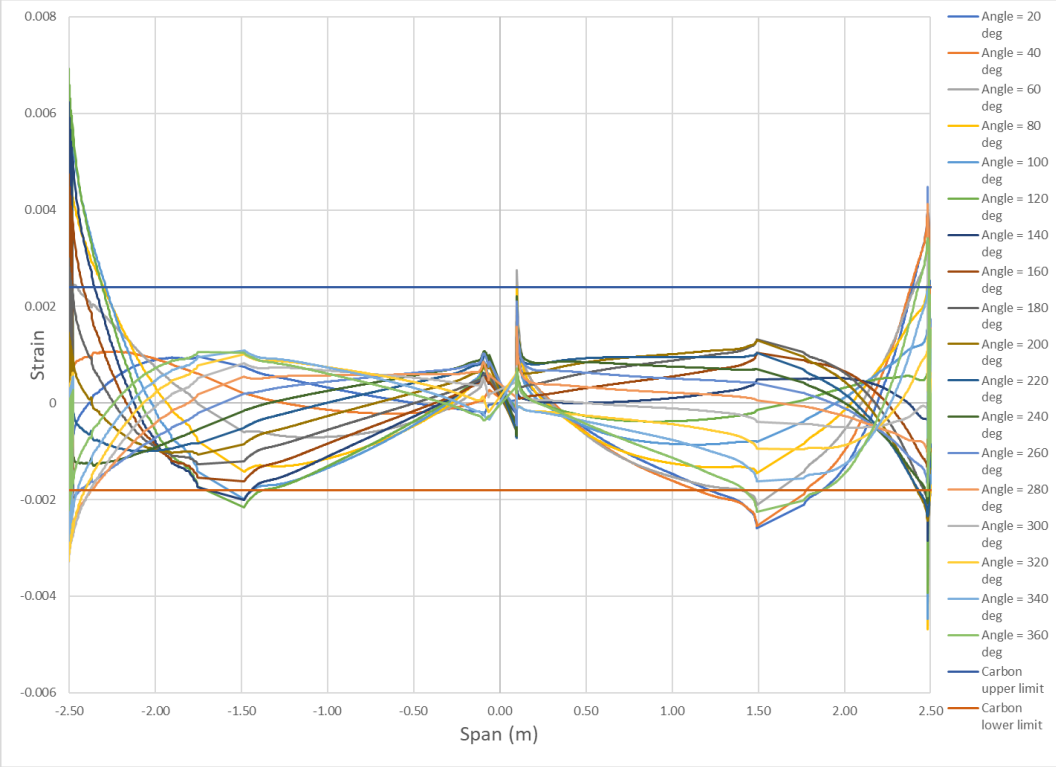

Figure 92: RivGen Design Option 1: Two struts removed, and end strut added. Strain on the outer ply. Upper and lower allowable design strain limits are shown as straight lines.

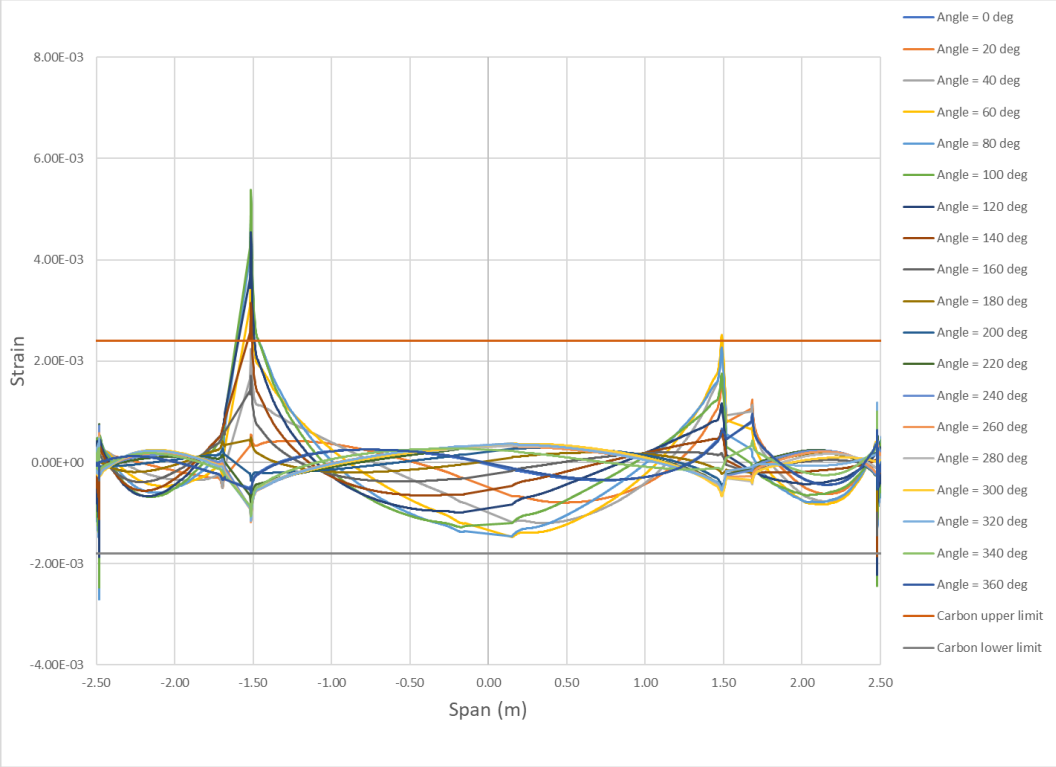

Figure 93: RivGen Design Option 2: Central strut removed, and end strut added. Strain on the outer ply. Upper and lower allowable design strain limits are shown as straight lines.

3.5.2 RivGen – New Design – Comparison of Structural Results

To evaluate the differences between the structural arrangements, we present the structural analysis response in a summary format.

The maximum deflection experienced by the turbine during a rotation for each of the three cases considered is presented in Figure 94.

A measure of the strain experienced by the turbine is calculated by the RMS sum of the strains in ply 1 of the foil and is presented as a function of turbine angle in Figure 95.

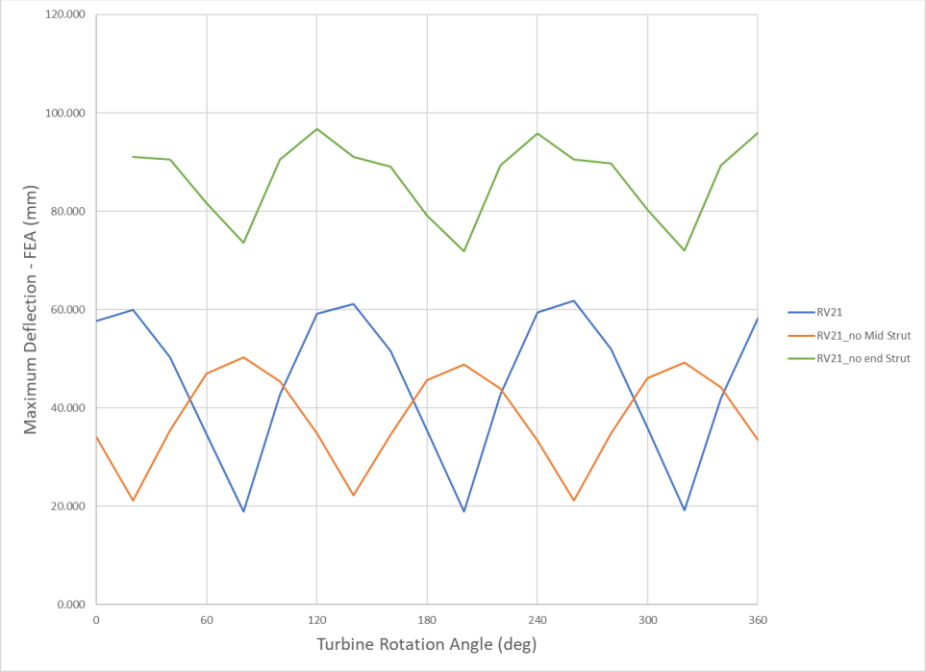

Figure 94: Maximum deflection experienced by the turbine as a function of rotation angle for the RivGen 2.1 baseline and for two design options. For Option 1 the deflections experienced by the turbine are larger than for the baseline. For Option 2 the deflections experienced are smaller.

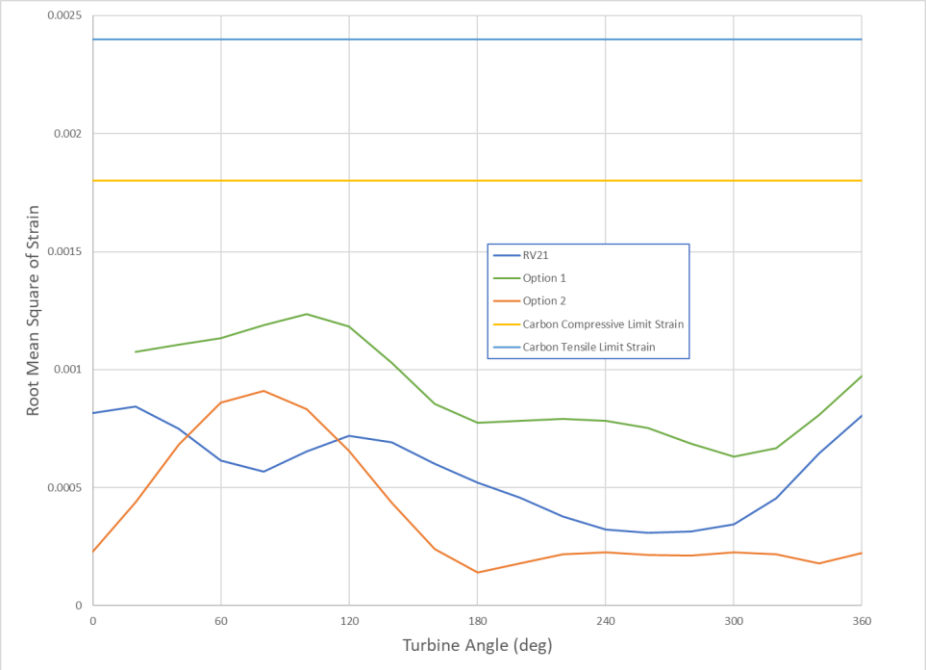

Figure 95: Root Mean Square strain experienced by the turbine as a function of rotation angle for the RivGen 2.1 baseline and for two design options. For Option 1 the strains experienced by the turbine are larger than for the baseline. For Option 2 the strains experienced are smaller.

3.5.3 RivGen – New Design – Discussion

The Option 1 design case, with two radial struts removed and replaced with wing tip struts, provides a higher level of performance than Option 2, with just the central strut removed. As expected, the deflections experienced by Option 1 are higher than for Option 2, or for the baseline. The test work performed in Task 1 indicates that this increased deflection should not significantly affect efficiency and is therefore considered acceptable. The average increase in deflection for Option 1 over the baseline case is 1.94 times.

Option 1 does experience a higher level of effective strain than either Option 1 or the RV2.1 baseline. The strain appears to be within acceptable limits (Figure 95).

The Option 1 design case provides an improved efficiency of 31.1 percent at a tip speed ratio of 2.50, as compared with the baseline RivGen 2.1 efficiency of 25.0 percent at the same TSR.

The improvement in efficiency is 24 percent.

3.5.4 New Design – LCOE Impact

The study used as a baseline for the project was a RivGen turbine. This turbine is identical to the turbines used in ORPC's TidGen® Power System. The increases in performance developed as part of this project will carry directly over to the TidGen Power System.

The increase in efficiency by 24 percent leads to an increase in AEP of 24 percent.

The increased AEP will lead to a reduction in LCOE of 19 percent.

Table 26: LCOE summary

	Baseline TidGen 4-Turbine TGU	**High Deflection Foil TidGen 4-Turbine TGU**	**% Change**
Turbine Efficiency	42.0%	52.20%	24.3%
AEP (MWhr)	538.5	669.2	24.3%
LCOE ($/kWhr)	0.67	0.54	-19.5%

Table 27: Task 3 Milestone summary

Milestone 3.1	Complete the design of a new rotor for an ORPC Power System utilizing high-deflection foil technology. Design will achieve project objectives for efficiency, system performance and costs, verified through analytical models and production cost estimates.
Status	Complete.
Deliverable	Final report serves as text deliverable for system integration report. Additional deliverables include: Computational Fluid Dynamic OpenFOAM models • RV21_TSR250_y1 • RV21_TSR250_y1_strutend • RV21_TSR250_y1_WingStrut One-way FSI models (Nastran files) • RV21_TSR250

	• RV21_WingStrut

Milestone 3.2	Update LCOE to account for impacts of high-deflection foil technology. LCOE analysis will achieve project target reductions.
Status	Complete.
Deliverable	EE0008386 LCOE Content Model.xls

3.6 Future Work

The CFD analysis of an extremely twisted helical turbine indicates that there are computational instabilities which were not expected. Additional CFD work should be conducted to investigate the necessary solution parameters for this geometry. It should be noted that the typical amount of helical twist in an ORPC turbine is far less than that used in the tow test program.

The structural analysis indicates that the baseline laminate design is conservative, and that material savings may be made by reducing the laminate thickness. This would further increase deflections and strains experienced by the turbine, but based on the findings of the test work, this should not adversely affect efficiency significantly. A program of structural optimization should be carried out by ORPC to further refine the turbine design.

The methodologies developed here will be carried over to more complex geometries to include ducting, fairings, and other incidental support structures that often exist within crossflow turbines.

4.0 Task 4: Project Reporting & Management

4.1 Task Summary

ORPC will direct and manage the Project and Project partners under the supervision of the Principal Investigator, providing all reports and deliverables from the Project to the DOE.

Cost, schedule, and technical performance was managed throughout the Project following Project Management Institute standards. Quarterly reports were submitted during the performance periods. At the beginning of the project, project management plans and intellectual property management plans were developed and agreed upon by all project partners to establish baselines and formalize the processes by which the project will be managed, as well as to define intellectual property agreements. Communication and project change management processes were defined. Risk management for project and technical risks were performed and risk management strategies were executed and updated throughout the Project.

Dissemination of technical work will occur in the form of conference papers. Component and LCOE content models are uploaded to the DOE MHKDR.

A final report describing project progress, system/component performance, lessons learned, opportunities identified for further improvement of LCOE, and next steps in technology development is provided.

Table 28: Task 4 Milestone Summary

Milestone 4.1	Complete Project Management and Intellectual Property Plans. Plans will verify resource availability to achieve project budget and schedule requirements.
Status	Complete
Deliverable	EE0008386 Deliverable 4.1 Project Management Plan.pdf EE0008386 Deliverable 4.1 Project Management Plan_DashPM_released_08.07.19.xlsm

Milestone 4.2	Completed Risk Management Plan and Risk Register. Plan will verify that project development path will adequately address technical risks for computational modeling, testing and final design.
Status	Complete
Deliverable	EE0008386 Deliverable 4.2 ORPC Risk Management Plan FOA-0001663 Design of High Deflection Foils.pdf EE0008386 ORPC Risk-Register_DE-FOA-0001663 Design of High Deflection Foils 6_22_2019.xls

Milestone 4.3	Provide presentation outlining basis for project technical objectives
Status	Complete
Deliverable	EE0008386 Deliverable 4.3 Presentation

Milestone 4.4	Project finding Dissemination via Peer Review Technical Paper
Status	In progress
Deliverable	At the time of writing of this final report, publications have not yet been submitted for publication. It is planned that two to three peer reviewed publications will be published based on this work by the PhD graduate student at UNH responsible for the test work performed.

Milestone 4.5	Component and LCOE Content Models uploaded to MHK Data Repository
Status	Complete
Deliverable	EE0008386 LCOE Content Model.xls

Milestone 4.6	Final Reports and presentations complete, with all project objectives for efficiency, system performance and costs achieved.
Status	Completed
Deliverable	Final report serves as text deliverable

5.0 Lessons Learned

The project provided an excellent opportunity to develop analytical approaches for assessing performance of hydrokinetic turbines, and for validating these approaches with a high-quality data set from scale model testing. Some key lessons learned include:

The strain data collection methodology used in this work is an excellent technique for collecting in-situ strain measurements for hydrokinetic turbine testing. However, the system is delicate and would not be suitable for use in an open water environment without improvements in robustness. When strain values become very large data quality is adversely affected.

Structural response from the scale model tests indicates that for all test cases strain is symmetric between inner and outer surfaces, indicating a pure bending loading, and strain reflects patterns generally expected from distributed loads on beams. Strain magnitude increases as unsupported length increases.

The hydrodynamic performance reduction from carbon to glass composite foils is small and may well be within the error bounds of the test. This indicates that while stiffness is important from a structural viewpoint, its impact on hydrodynamic performance may be less than expected.

Hydrodynamic performance of turbines is reduced as the stiffness of the turbine is reduced by reducing strut spacing.

The shapes of the Cp/TSR curves for the helical turbine tested are fundamentally different than for the straight foil turbines. The maximum Cp value is lower and occurs at a higher TSR value. The helical turbine is hydrodynamically very different from the straight foil turbines. Fundamental behavior has changed, with the optimum tip speed ratio shifting from 2.40 for straight foils to 3.00 for the helical turbines. The helical foil is almost 50 percent longer in length than the straight foil due to the helical twist and strains are significantly larger. It should be noted that the typical amount of helical twist in an ORPC turbine is far less than that used in the tow test program.

Surface roughness for the scale models can have a significant effect on performance.

ORPC worked to develop low-order analytical methods to guide design of high deflection foils. These were deemed inadequate to the task or were assessed to be computationally intense with insufficient benefit. None of low-order methods are fully capable of taking the structural deflections as inputs to hydrodynamic models.

From a comparison of CFD analysis and test data we find that across the board the agreement between the 3D CFD results and the test data for the straight carbon and glass foil turbine is very good.

An original goal of the project was to develop a fully validated two-way FSI protocol. With such a methodology there will be substantial computational effort and expense required. A simplified version of this methodology involving one-way FSI mapping was developed and validated under this work and proved to be sufficiently accurate and computationally achievable for the purposes of design and is presented here as the preferred implementation. This one-way FSI methodology is relatively easy to implement, with an easy to replicate workflow.

6.0 Products

6.1 Publications

At the time of writing of this final report, publications are planned but not yet submitted. These publications will form the basis for a PhD thesis program to be completed by the University of New Hampshire graduate student who performed all turbine testing.

A first publication is intended for the 2022 International Conference on Ocean Energy and will cover data collection and analysis for the straight foil testing from different materials and strut locations.

A second publication will address testing of helical foil turbines and is expected to be published in 2023.

A third publication (2023) is expected which will cover analytical methods developed under this work.

At the time of writing, the Ph.D. program is expected to require an additional two years of research by the student, during which time it is expected that they will author three peer reviewed technical papers, and a Pd.D. thesis.

6.2 Inventions

No inventions were developed during this project.